UNIVERSITY OF KWAZULU-NATAL
INYUVESI YAKWAZULU-NATALI

AEROSOL CHARACTERISTICS OVER DIFFERENT REGIONS OF SOUTHERN AFRICA - USING SUNPHOTOMETER AND SATELLITE MEASUREMENTS

By

JOSEPH AYODELE ADESINA

A thesis submitted in fulfilment of the academic

requirements for the degree of

Doctor of Philosophy

in the School of Chemistry and Physics,

University of KwaZulu-Natal,

Durban

SUPERVISIOR: PROFESSOR VENKATARAMAN SIVAKUMAR

JANUARY, 2015

ABSTRACT

Aerosols and cloud play a major role in understanding and interpreting the varying earth's energy budget. It is necessary to characterize these atmospheric particles by their sizes, chemical composition, water content etc. Aerosols can both cause heating and cooling depending on what they are made of; dust will generally tend to scatter leading to cooling effect while some species of black carbon will absorb sunlight thereby causing a heating effect. In order to assess their impact on global climate, a multiple measurement approach is necessary and specifically, we need long and short term ground-based measurements in clean and polluted environment and long term satellite measurements. In this thesis, we have used aerosol measurements from CIMEL Sunphotometer (part of the world-wide network; Aerosol Robotic Network: AERONET) over, Pretoria (25.75º S, 28.28º E) and Skukuza (24.9^{o} S, 31.5^{o} E) in South Africa, and satellite data from Moderate Resolution Imaging Spectroradiometer (MODIS) and Multiangle Imaging Spectroradiometer (MISR).

Pretoria is situated in industrial region with adequate influence of urban/industrial aerosols while Skukuza is an agricultural based region with frequent burning of agricultural waste to clear the harvest during the late winter, spring and summer seasons. Thus, the study over industrial and agricultural regions explores more understanding about the regional radiative forcing in relation to aerosol loading and meteorology. MODIS satellite data was utilized for addressing long term trend in aerosol loading and cloud interaction studies over different locations of South Africa where no ground based sunphotometer data are available. Using six months sunphotometer data (July–December 2012), aerosol characteristics over Gorongosa were studied with particular attention to how aerosol loading evolves during the biomass burning season (spring) including pre- and post-months. The results revealed that the monthly mean aerosol optical depth (AOD_{500}) was at maximum in September and minimum in November. The study also investigated biomass burning and forest fire occurrences in Mozambique using MODIS active fire data.

Using a year sunphotometer data (January – December 2012) obtained from Pretoria's (CSIR_DPPS) AERONET site, aerosol was characterized by its optical, microphysical and radiative properties. The study explored meteorological effects on aerosol loading and aerosol direct radiative forcing over Pretoria. Maximum value of aerosol optical depth (AOD_{500}) was found during February (summer) and August (winter) while the atmospheric forcing was found to be independent of seasonal variation in AOD. Besides, AOD, Angstrom exponent (AE; α440-870), columnar water vapor (CWV), volume size distribution (VSD), single scattering albedo (SSA) and aerosol radiative forcing (ARF) were computed and their variations with their climatic implications were studied. Using the ground-based instrument of AERONET at Skukuza, we performed validation of MISR and MODIS (Terra and Aqua)

level 3 AOD products using the data retrieved for the year 2010. We also carried out regression analysis on these satellite products using 10 years of dataset (2004-2013) to evaluate their performance at a hinterland and coastland stations with two distinct environments in SA. The validation showed that MISR was better correlated with sunphotometer having a coefficient of determination (R^2=0.94), Aqua MODIS (R^2=0.77) and Terra MODIS (R^2=0.68). The long term regression analysis at the two selected locations showed MODIS products underestimating MISR. At the hinterland, MISR showed an increasing trend while MODIS products showed a decreasing trend over the study period but at the coastland MISR and Terra MODIS showed a negative trend while Aqua MODIS showed a positive trend. When the two MODIS products were compared, they were better correlated at the coastland (R^2=0.66) than hinterland (R^2=0.59) and when compared based on seasonal variation, they were better correlated in the winter season in both locations than any other season. The Ozone Monitoring Instrument (OMI) Ultra-Violet Aerosol Index (UVAI) which was used to monitor the absorption aerosol index showed an increasing trend over the two locations with 0.0089/yr hinterland and 0.0022/yr at coastland.

In the present thesis, we also used data obtained from the Terra satellite onboard of the MODIS to investigate the spatial and temporal relationship between AOD and cloud parameters namely, water vapor (WV), cloud optical depth (COD), cloud fraction (CF), cloud top pressure (CTP) and cloud top temperature (CTT) based on 5 years (January 2008 - December 2012) of dataset over six locations in South Africa. AOD has high values during spring (September to November) but low values in winter (June to August) in all locations. In terms of temporal variation AOD was lowest at Bloemfontein 0.06±0.04 followed by Cape Town 0.08±0.02, then Potchefstroom 0.09±0.05, Pretoria and Skukuza had 0.11±0.05 each and Durban 0.13±0.05. The mean AE values for each location show a general prevalence of fine particles for most parts of the year. Our analysis of AOD and WV showed both quantities only co-vary at the beginning of the year but later in the year they tend to have opposite trend over all the locations. AOD and CF showed negative correlation for most of the locations while AOD and COD were positive over three of the locations. AOD and CTT, CTP showed similar variations in almost all the locations. The co-variation of CTT and CTP may be due to large scale meteorological variation.

PREFACE

The work described by this thesis was carried out at the University of KwaZulu-Natal, School of Chemistry and Physics, Durban, from August 2012 until January 2015, under the supervision of Professor Venkataraman Sivakumar.

This thesis is entirely, unless specifically contradicted in the text, the work of the author and has not been previously submitted, in whole or in part, to any other tertiary institution. Where use has been made of the work of others, it is duly acknowledged in the text.

Signed: _____ Joseph Ayodele Adesina

Date: _____

As the candidate's supervisor I have/have not approved this thesis/dissertation for submission.

Signed:_____ Professor Venkataraman Sivakumar

Date: _____

DECLARATION 1 - PLAGIARISM

I, Joseph Ayodele Adesina, declare that

1. The research reported in this thesis, except where otherwise indicated, is my original research.

2. This thesis has not been submitted for any degree or examination at any other university.

3. This thesis does not contain other persons' data, pictures, graphs or other information, unless specifically acknowledged as being sourced from other persons.

4. This thesis does not contain other persons' writing, unless specifically acknowledged as being sourced from other researchers. Where other written sources have been quoted, then:

> a. Their words have been rewritten but the general information attributed to them has been referenced.
>
> b. Where their exact words have been used, then their writing has been placed in italics and inside quotation marks, and referenced.

5. This thesis does not contain text, graphics or tables copied and pasted from the Internet, unless specifically acknowledged, and the source being detailed in the thesis and in the References sections.

Signed: _____

DECLARATION 2 – PUBLICATIONS

Journal

Adesina, A. J., Kumar, K. R., Sivakumar, V. (2014), Variability in aerosol optical properties and radiative forcing over Gorongosa (18.97^{o}S, 34.35^{o}E) in Mozambique. *Meteorology and Atmospheric Physics*, 1-12. (Impact factor 1.245)

Adesina, A. J., Kumar, K. R., Sivakumar, V., Griffith, D. (2014), Direct radiative forcing of urban aerosols over Pretoria (25.75° S, 28.28° E) using AERONET Sunphotometer data: First scientific results and environmental impact. *Journal of Environmental Sciences*, 2459-2474 (Impact factor 2.465)

Adesina, A. J., Kumar, K. R., Sivakumar, V. (2015), Assessment of satellite derived aerosol optical depth over two contrasting regions in South Africa: Trend estimation and characteristics of absorption aerosols(To be submitted).

Adesina, A. J., Kumar, K. R., Sivakumar, V. (2015), Spatio-temporal heterogeneity in AOD and its impact on cloud properties over major cities in South Africa as retrieved from MODIS (To be submitted).

Contributions by the author : All the above four articles used for this thesis were originally written by the author. Dr Raghavendra served as the corresponding author and read over the articles making corrections and contributions where necessary. My supervisor Professor Sivakumar has discussed the result, read and made suggestions before they are sent to the press or used in this thesis. Griffith is the principal Inestigator of the AERONET instrument at CSIR Pretoria and so rightly a co-author of the paper that bears his name.

Co-authored publicatons and have not been included as part of this Thesis

Kumar, K. R., Sivakumar, V., Reddy, R., Gopal, K. R., &**Adesina, A. J**. (2013). Inferring wavelength dependence of AOD and Ångström exponent over a sub-tropical station in South Africa using AERONET data: Influence of meteorology, long-range transport and curvature effect. *Science of The Total Environment, 461*, 397-408.

Kumar, K. R., Sivakumar, V., Reddy, R. R., Gopal, K. R., &**Adesina, A. J**. (2014). Identification and Classification of Different Aerosol Types over a Subtropical Rural Site in Mpumalanga, South Africa: Seasonal Variations as Retrieved from the AERONET Sunphotometer. *Aerosol and Air Quality Research, 14*(1), 108-123.

Kumar, K. R., Sivakumar, V., Yin, Y., Reddy, R., Kang, N., Diao, Y., . . . Yu, **Adesina, A. J**. (2014). Long-term (2003–2013) climatological trends and variations in aerosol optical parameters retrieved from MODIS over three stations in South Africa. *Atmospheric Environment, 95*, 400-408.

Kumar, K. R., Sivakumar, V., Yin, Y.,……**Adesina, A. J.**, (2015). Aerosol climatology over Durban in South Africa retreived from MODIS, MISR and OMI (2003-2013): Comparison of AOD and heteorogeneity in aerosol types and sources. *IJPRS Journal of Photogrammetry and Remote Sensing* (Revision Submitted, Informally acceped).

ARTICLES IN PEER-REVIEWED NATIONAL/INTERNATIONAL CONFERENCE PROCEEDINGS

Kumar, K. R., **Adesina, A. J**., Sivakumar, V. (2013),*Aerosol radiative forcing from spectral solar attenuation measurements due to aerosol loading using AERONET over Pretoria in South Africa.* Paper presented at the Emerging Research Areas and 2013 International Conference on Microelectronics, Communications and Renewable Energy (AICERA/ICMiCR), 2013 Annual International Conference on.

Adesina, A. J., V. Sivakumar, Raghavendra K. Kumar, Stuart J. Piketh, Jyotsna Singh (2014) Aerosol properties over an urban site, Johannesburg measured from Sunphotometer Proc. of 30th Annual conference of South African society for atmosphere science, ISBN 978 0 620 62777 1, Potchefstroom (South Africa), 17-20.

Adesina, A. J.,Kumar, K. R., & Sivakumar, V (2013),Aerosol optical properties over Pretoria, South Africa during spring time measured from Cimel Sunphotometer. Proc. of 29th Annual conference of South African society for atmosphere science, ISBN 978 0 620 56626 1, 26-27 September 2013, Durban (South Africa), 20-22.

Kumar, K. R. , Sivakumar, V &**Adesina, A. J.** (2013), Long term variations in MODIS derived aerosol optical depth and fine mode fraction at three different environments in South Africa Proc. of 29th Annual conference of South African society for atmosphere science, ISBN 978 0 620 56626 1,26-27 September 2013, Durban (South Africa), 16-19.

Kumar, K. R. , Sivakumar, V &**Adesina, A. J.** (2013),Aerosol-cloud interactions as inferred from MODIS over an urban coastal site, Durban – A preliminary study Proc. of 29th Annual conference of South African society for atmosphere science, ISBN 978 0 620 56626 1, 26-27 September 2013, Durban (South Africa), 159-161.

Signed: _____

ACKNOWLEDGEMENT

Though the work presented in this thesis is a product of many sleepless nights and countless busy days yet not without the help, guide and encouragement of many people. It will be an impossible task to acknowledge all those who have directly or indirectly contributed to the successful completion of this work, for those who may not find their names here, they should please try to understand that it is not because they are unimportant and I thereby request that kindly bear with me.

First I want to thank my heavenly Father who is the giver of life and wisdom. When He created the world, He gave man the task to search out what He has created and for these many ages man is still working at discovering what He made at the beginning. Unto Him alone be the glory and honor and majesty now and ever.

I want to say thank you to my supervisor Prof SivakumarVenkataraman for his moral and academic support. He inspired me to learn to use Matlab which has proved to be an invaluable instrument in my research work. He is very approachable and supported my journey to workshops and conferences and assisted in my residence fees during holiday. I owe so much to him for the assistance and guidance received under his tutelage and I pray for success in his life career.

Dr. Raghavendra has contributed so much to my success as a doctoral student; when he was a post-doc with us he was assigned to assist me understand the field of study before he left for China. He helped to lay the foundation upon which I now build. He served as the corresponding author and collaborated as co-author for the two journals which formed part of the thesis. He also read every work whether conference or journal article. He has contributed so much to this thesis both in reading and making useful suggestions. A larger percentage of my chapter one was gleaned from his work. I say thank you.

I had some challenges carrying out validation of satellite instruments using ground-based instrument even after reading, so I decided to send a mail to Dr. Charles Ichoku of NASA who not only replied but created time to see me during the Aerosol conference held in USA. He was able to guide me through and also gave useful materials related to the work. I say thanks so much. Dr. Jyostna Singh gave many useful advices in the course of writing. My colleague Dr. Olakunle Ogunjobi assisted in the formatting of the final document.

Dr. Aderemi Adewumi of Computer Science UKZN was helpful in securing admission for the PhD and he also offered assistance whenever I seek help from him. Mr. Micheal

Olusanya and his family played a great role in every aspect; he initiated the admission process and freely helped to cushion the effect of lack of funding for the program, may the Lord almighty reward him for this. Mr. Thlala Kolo stood as a guarantor when I was processing the visa and also help financially. Prof. Olaleru Johnson, Prof. Oyediran Olukayode, Prof. Agulana Christopher, Dr. Adegoke Ayodeji, Dr. Otunla Abiodun, Dr. Sofidiya Toyin, Dr. Aderemi Olaoluwa, Dr. Akugbe Arasomwan, Jerry Ogunniyi, Ayobami Akinyelu, Luke Joel, Andile Mbhele and a host of others gave words of encouragement and assisted in some unique ways.

Finally, I like to thank my wife Olayinka for her sacrifice and support; she did endure all things cheerfully to the very end. I cannot express my thank enough for helping me to be in the best state of mind to pursue this research work. Once again thank you all.

CONTENTS

CHAPTER ONE

1.0 INTRODUCTION

Aerosols consist of solid and/or liquid particles that are suspended in the air. They are present everywhere in the air being seen as dust, smoke or haze. The concentration in the air arises from both natural and human origin. Globally, natural sources such as dust and sea salt predominates. In local or regional levels, industrialized and highly populated regions can be dominated by aerosols of anthropogenic origin such as different combustion sources and intense biomass burning.

1.1 Atmospheric aerosol

When the term "Atmospheric aerosol" is being used; it encompasses an extensive range of particle types with different compositions, shapes, sizes and optical properties. The amount of aerosol in the atmosphere sometimes called aerosol loading can be quantified either by mass concentration or an optical measure known as aerosol optical depth (AOD). AOD is a dimensionless quantity, the integral of the product of particle number concentration and particle extinction cross-section (which accounts for individual particle scattering plus absorption), along a path length through the atmosphere, usually measured vertically.

Anthropogenic aerosols contribution to the global aerosol mass concentration is in the neighborhood of 10 – 20% range while the natural aerosols take almost 81% but contributing just about 25% to aerosol optical depth (Andreae, 1995; Satheesh & Krishna Moorthy, 2005).

Aerosol research interest areas include health, climate and visibility due to diversify effects in the aforementioned areas (Jacobson, 2001). In relation to Earth's climate their effect occur in three fundamental ways: (i) they cause the scattering and absorption of short-wave radiation and absorb long-wave radiation, this is termed aerosol direct effect'(Haywood & Boucher, 2000); (ii) they act as cloud condensation nuclei, increasing the number and reducing the size of cloud droplets, thus affecting the albedo termed the 'first aerosol indirect effect'(Charlson et al., 1992; Kaskaoutis & Kambezidis, 2006); (iii) through the first indirect effect, they reduce the precipitation efficiency of clouds, thus increasing their lifetime termed the 'second aerosol indirect effect',(Lohmann & Feichter, 2005); (iv) aerosol containing absorbing material contributes to the heating of the atmosphere thereby reducing relative humidity and consequently decreased low clouds cover which is termed 'aerosol semi direct effect'(Johnson et al., 2004). Aerosol size distribution as related to coagulation, condensation and gas-to-particle conversion processes is found to change with the ageing of aerosols (Reid & Hobbs, 1998).

Aerosols are generally classified into three size categories: (i) Ultra-fine/Nucleation/ Aitken mode (0.001 – 0.1 μm radius), (ii) Accumulation mode (0.1 – 1.0 μm radius) and (iii) Coarse mode (> 1.0 μm radius). Nucleation and accumulation are terms connected with the production processes of aerosols in those particular modes. The Aitken or Nucleation mode aerosols formed by gas-to-particle conversion are the most predominant in terms of number though they constitute the smallest percentage of the total aerosol loading due to their smaller size. The process involved in the accumulation mode is usually either by coagulation of smaller particles or by heterogeneous condensation of gas vapor onto existing smaller

nucleation mode particles. Coarse mode aerosols are as a result of mechanical processes such as wind-blown dust; sea-salt aerosols produced by breaking of sea waves. Once aerosols are ejected into the atmosphere they are borne along with air currents until they are finally removed from the atmosphere. Their mass, size and acceleration determines how long they will stay in the atmosphere which is normally being referred to as their residence time. The residence time depends on their average life time and prevailing meteorological conditions, this normally will be for a few days to a week (Raes et al., 2000). The removal of aerosols from the atmosphere can be through wash-out by rain called 'wet deposition' or direct uptake known as 'dry deposition'.

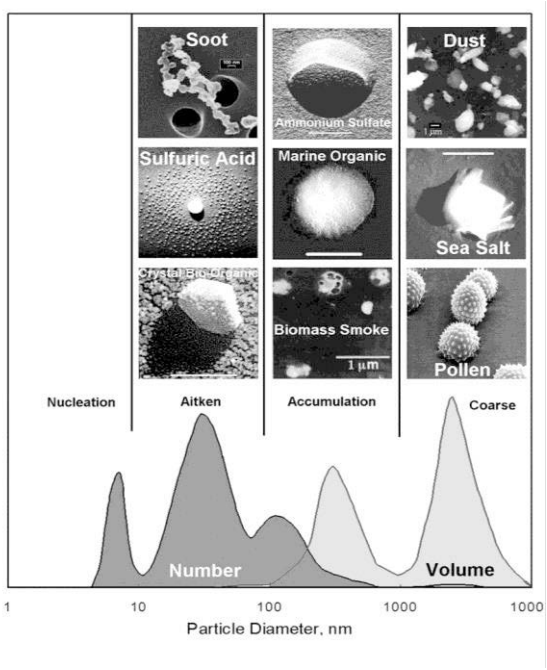

Fig 1: Showing the Aitken mode – 0.01-0.1 µm, Accumulation mode – 0.1-1 µm, Coarse mode - >1 µm and sometimes, the elusive nucleation mode <0.01 µm [Source: SASAS Conference 2013].

When aerosols are ejected into the stratosphere, they do not get removed easily like the tropospheric ones, they sometimes remain for years.

1.2 Classification of aerosols

Aerosols also sometimes called particulate matter (PM) or by synonymous terms such as Suspended Particulate Matter (SPM), Total Suspended Particulate (TSP) or Total Suspended Particulate Matter (TSPM). They are broadly classified into two according to

a. Natural aerosols and

b. Anthropogenic aerosols

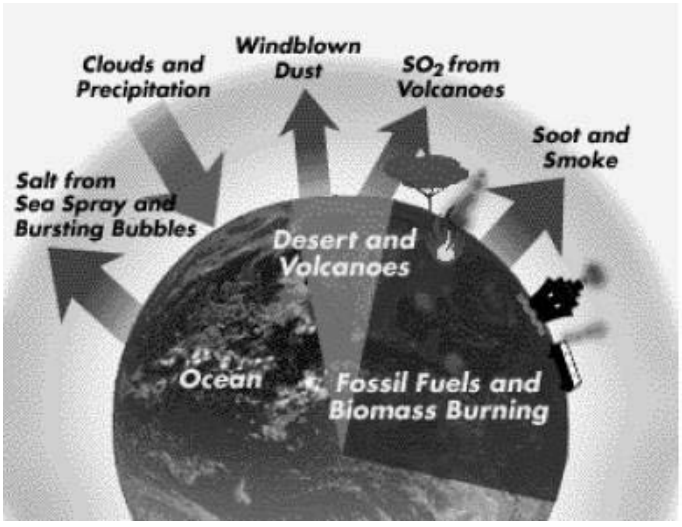

Fig 2: Showing the various tropospheric aerosols sources in the atmosphere [Source: SASAS Conference, 2013].

1.2.1 Natural aerosols

Natural aerosols originate from natural occurrences such as dust storms, sea spray, volcanoes, and forest and grassland fires.

1. Marine aerosols

These are either formed mechanically by the sea waves or by gas-to-particle conversion process of precursor gases over the marine atmosphere. These oceanic origin aerosols are

estimated to form 30% of total aerosol loading (Prospero et al., 1983). Those that are formed by mechanical process are termed sea-salt aerosols while those by gas-to-particle are non-sea-salt aerosols e.g dimethyl sulphide (Charlson et al., 1987; Hoppel, 1979).

2. Mineral dust aerosols

These are very common in desert areas where there exist either a low or sparse vegetative cover. Surface winds over these areas often inject the dry soils into the atmosphere (Tegen & Fung, 1994) and at other times they can result from human activities such as construction, agriculture, transportation and deforestation. Their lifetime is affected by their size. In dealing with these types of aerosols, their radiative effect can only be quantified when their microphysical properties are known.

3. Volcanic aerosols

During a volcanic eruption dust and gaseous sulphur are emitted. The sulphur thus produced is more efficient in producing sulphate aerosols (about 4.5 times) than those of anthropogenic origin because they have lower deposition rate (Benkovitz et al., 1994; Graf et al., 1997).

1.2.2 Anthropogenic Aerosols

Anthropogenic aerosols come from man-made activities such as industrial emissions, vehicular emissions and burnings from biomass and fossil fuels.

1. Sulphates

Sulphates are produced from activities such as oil refining and smelting, coal and oil combustion and though they are mainly submicron particles, they are capable of being conveyed from their sources to long distances (Winchester and Bi, 1984). SO_2 can be quantified as 72% from fossil fuel burning, about 2% from biomass burning, about 19% from

dimethyl sulphide emission by phytoplankton and about 7% from volcanoes (Haywood & Boucher, 2000). They can indirectly influence the optical properties of clouds by forming cloud condensation nuclei because they are hydrophilic (Takemura et al., 2000). Sulphate aerosol has a direct radiative forcing of about -0.4 ±0.2 Wm^{-2}.

2. Nitrates

They are formed by the oxides of Nitrogen like NO_2, N_2O, N_2O_4 and volatile acids of nitrogen which originates from biomass burning, fertilizers, bacterial actions on soil and vehicular exhaust (Hidy, 1984). The most predominant type is the ammonium nitrate (Pruppacher & Klett, 1978). Nitrate aerosol has direct RF of about -0.10 ±0.10 Wm^{-2} although this is subject to further investigations.

3. Carbonaceous aerosols (soot)

This is a formation arising from a complex mixture of organic carbon (OC) and elemental carbon (EC). Organic carbon (OC) and black carbon (BC) comes from incomplete combustion of carbonaceous materials. They are the most important sunlight absorbing aerosol in the atmosphere and they also serve as catalyst in some chemical reaction in the atmosphere (Gundel et al., 1989; Reddy & Venkataraman, 1999). They are most significant for their absorption properties and their inhibition of cloud formation (Ackerman et al., 2000; Kaufman & Nakajima, 1993). Black carbon has a direct radiative forcing of about -0.20±0.15 Wm^{-2} the semi-direct effect non inclusive while Organic carbon aerosol has a direct radiative forcing of about -0.05 ±0.05 Wm^{-2}.

1.3 Types of Aerosols

Since aerosols are formed by different processes and are subject to both vertical and horizontal circulation in the atmosphere. These aerosols are mixed together at micro scale and large scale diffusion and coagulation. Aerosol types largely depend on sources and nature of production.

1.3.1 Soil derived aerosols

These aerosols are formed by weathering of soil and they are ejected into the atmosphere as ultra-fine particle by the wind especially in the arid regions of the world. They form a significant constituent of aerosols even in locations far away from their sources due to their transportation by convection currents and general circulation systems. They exist in the coarse mode with radius range of $0.1 < r < 100$ μm especially at the source region. As they are transported to distant regions their radius becomes smaller in the range $0.1 < r < 5$ μm. They exist mainly in the troposphere having high variability in the imaginary part of the refractive index which determines their climate forcing. The reported range of direct RF goes from -0.56 to + 0.1Wm^{-2}.

1.3.2 Sea-salt aerosols

Their production is normally associated with bursting of whitecap bubbles. After production they rise by evaporation until they attain equilibrium with the ambient relative humidity (Blanchard & Woodcock, 1980). They remain either as a crystalline matter or as a solution

droplet. Their radius is generally less than 0.1 μm and contributes the highest percentage to the global aerosol population.

1.3.3 Rural Continental aerosols

In rural areas, aerosols are less of anthropogenic sources but more of natural origin. They are characterized by two modes number distribution with diameters of about 0.02 and 0.08 μm while the mass distribution of the coarse mode is centered at about 7 μm (Hobbs et al., 1985; Jaenicke, 1993).

1.3.4 Urban aerosols

Aerosols in the urban areas are multi-modal in nature consisting of nucleation, accumulation and coarse modes. The mechanically generated coarse mode is more of dust and sea-salt whereas the accumulation mode is majorly from combustion sources and the nucleation mode is a gas-to-particle conversion resulting from chemical reactions of nitrates, sulphates and ammonium. The accumulation mode tends to have a higher concentration than the other modes.

1.3.5 Polar aerosols

The number concentration of this type of aerosol is influenced significantly by Arctic haze. Apart from the fact that they are aged, they contain carbonaceous material from sea salt, mineral dust and mid-latitude pollen sources.

1.3.6 Remote Continental aerosols

This type of aerosol can be characterized three modes number distribution and of diameters 0.02, 0.1 and 2μm are made up of pollens, dust and waxes (Jaenicke, 1993; Koutsenogii & Jaenicke, 1994).

1.3.7 Extra-terrestrial aerosols

Aerosols of this type are commonly found in the stratosphere with a size ranging from tenth of a micron to several millimeters in diameter. They are formed from meteor showers and comet debris and responsible for zodiacal light.

1.4 Aerosols sinks

Aerosols once formed do not remain suspended in the air indefinitely, they can be destroyed alter or removed. Their residence time is affected by their size, location and atmospheric condition. Aerosol sinks occur in different ways:

1.4.1 Wet deposition

When aerosol deposition involves water it is termed ‘wet deposition’ and it takes several forms; sweepout, rainout, washout and occult deposition.

1. Sweepout - When there is rain, some aerosol just below the cloud of rain are sometimes incorporated into the rain drop and subsequently deposited along with the rain drop.

2. Rainout – This occurs when cloud condensation nuclei is removed from the atmosphere due the gravitational settling of cloud producing rain.

3. Washout – When aerosol is incorporated into cloud and the cloud grows big enough to fall as a rain droplet, then it is a washout. These three mentioned processes are technically different and there effects are calculated differently.

4. Occult deposition - Here aerosol of larger size impact more on a surface feature than those of smaller size with likelihood called impact efficiency.

1.4.2 Dry deposition

When aerosols fall under gravity, they are said to undergo dry deposition. The fall is determined by the diffusion coefficient and the fall velocity. The fall rate is proportional to the size and inversely proportional to the density of the atmosphere.

The table-1 summarizes the properties of the major aerosol species, their sources and sinks and their lifetime.

Table 1: Key aerosol properties of the main aerosol species in the troposphere. Terrestrial primary biological aerosol particles (PBAPs), brown carbon and marine primary organic aerosols (POA) are particular types of organic aerosols (OA) but are treated here as separate components because of their specific properties. The estimated lifetimes in the troposphere are based on the AeroCom models, except for terrestrial PBAPs which are treated by analogy to other coarse mode aerosol types. (Source: WG1AR5 IPCC, 2013)

Aerosol Species	Size Distribution	Main Sources	Main Sinks	Tropospheric Lifetime	Key Climate Relevant Properties
Sulphate	Primary: Aitken, accumulation and coarse modes Secondary: Nucleation, Aitken, and accumulation modes	Primary: marine and volcanic emissions. Secondary: oxidation of SO2 and other S gases from natural and anthropogenic sources	Wet deposition Dry deposition	~ 1 week	Light scattering. Very hygroscopic. Enhances absorption when deposited as a coating on black carbon. Cloud condensation nuclei (CCN) active.
Nitrate	Accumulation and coarse modes	Oxidation of NOx	Wet deposition Dry deposition	~ 1 week	Light scattering. Hygroscopic. CCN active.
Black carbon	Freshly emitted: <100 nm Aged: accumulation mode	Combustion of fossil fuels, biofuels and biomass	Wet deposition Dry deposition	1 week to 10 days	Large mass absorption efficiency in the shortwave. CCN active when coated. May be ice nuclei (IN) active.
Organic aerosol	POA: Aitken and accumulation modes. SOA: nucleation, Aitken and mostly accumulation modes. Aged OA: accumulation mode	Combustion of fossil fuel, biofuel and biomass. Continental and marine ecosystems. Some anthropogenic and biogenic non-combustion sources	Wet deposition Dry deposition	~ 1 week	Light scattering. Enhances absorption when deposited as a coating on black carbon. CCN active (depending on aging time and size).
... of which brown carbon	Freshly emitted: 100–400 nm Aged: accumulation mode	Combustion of biofuels and biomass. Natural humic-like substances from the biosphere	Wet deposition Dry deposition	~ 1 week	Medium mass absorption efficiency in the UV and visible. Light scattering.
... of which terrestrial PBAP	Mostly coarse mode	Terrestrial ecosystems	Sedimentation Wet deposition Dry deposition	1 day to 1 week depending on size	May be IN active. May form giant CCN
Mineral dust	Coarse and super-coarse modes, with a small accumulation mode	Wind erosion, soil resuspension. Some agricultural practices and industrial activities (cement)	Sedimentation Dry deposition Wet deposition	1 day to 1 week depending on size	IN active. Light scattering and absorption. Greenhouse effect.
Sea spray	Coarse and accumulation modes	Breaking of air bubbles induced e.g., by wave breaking. Wind erosion.	Sedimentation Wet deposition Dry deposition	1 day to 1 week depending on size	Light scattering. Very hygroscopic. CCN active. Can include primary organic compounds in smaller size range
... of which marine POA	Preferentially Aitken and accumulation modes	Emitted with sea spray in biologically active oceanic regions	Sedimentation Wet deposition Dry deposition	~ 1 week	CCN active.

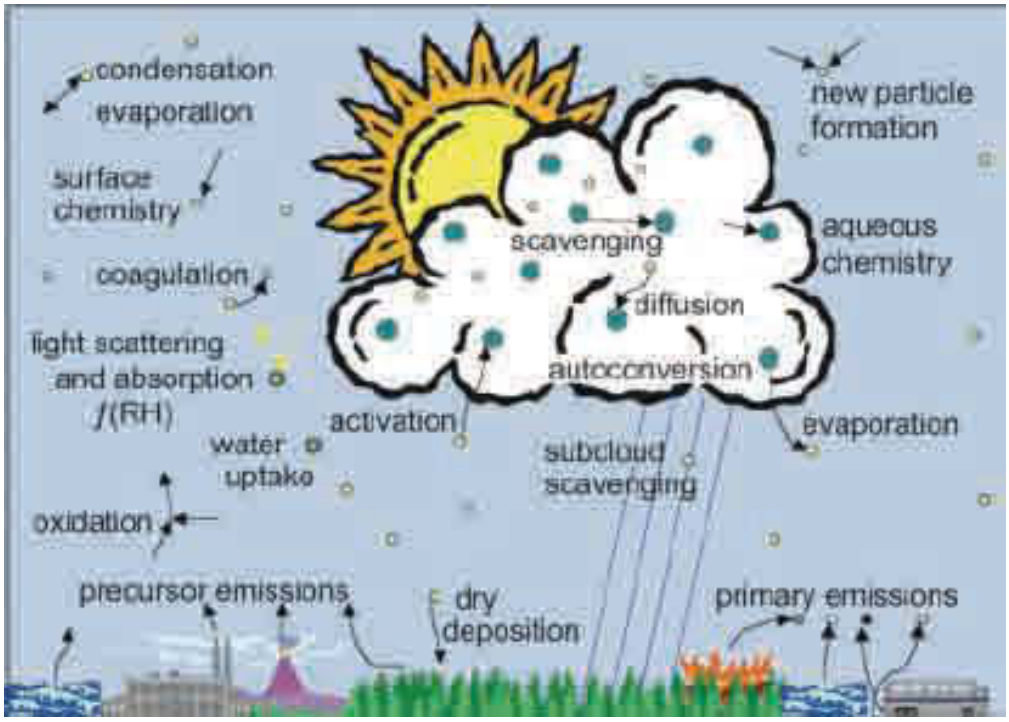

Fig 3**:** Major aerosol processes relevant to their impact on climate Particles are ultimately removed from the atmosphere, scavenged by falling raindrops or settling by dry deposition. [Report from U.S. Climate Change Science Program (2009)]

1.5 Effects of Aerosols

Aerosols have multidimensional effects including visibility reduction, respiratory disease, and interference with photosynthesis and climate effects. The effects are both health and non-health related and can be briefly summarized as follows:

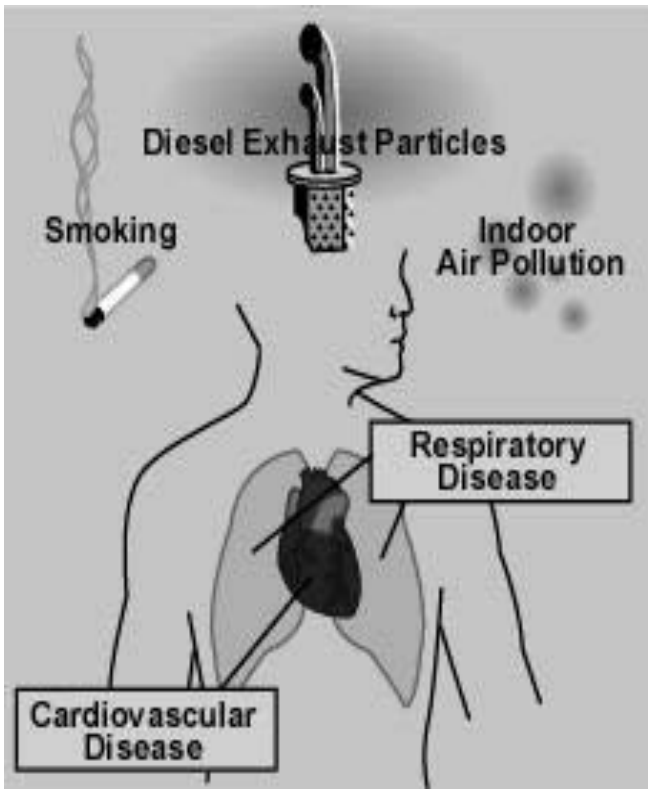

Fig 4: Some sources of indoor pollution and their health effect [Source: SASAS conference, 2013]

1.5.1 Health effects

The effect of aerosol on health are determined by three factors; toxicity concentration, susceptibility of individuals and duration of exposure. Aerosols can cause:

1. Cardio-vascular diseases
2. Carcinogenic effects
3. Respiratory Hazards
4. Morphological changes
5. Increase mortality and morbidity

The effects are more pronounced in people with asthma, cardiovascular problems and general respiratory problems.

1.5.2 Non-health effects

Aerosols impact on regional and global climate, this effect has been attracting attention among all nations. It causes visibility impairment and damage to vegetation. The long-term effects of industrial pollutants such as lead; arsenic and fluorine leads to low fertility reduced production of milk and also block the stomata in plants.

1.6 Aerosol-Cloud Interaction

The formation and life cycle of clouds are altered by anthropogenic aerosol as shown by a wide range of measurements (Kaufman et al., 2005; Kim et al., 2003; Penner et al., 2004; Schwartz & Benkovitz, 2002). To be able to correctly interpret and understand climate change there is a need to understand and quantify the microphysical impact of aerosols on clouds. This can only be effectively done through focusing on their microphysical relationship and their response to large-scale weather systems (Anderson et al., 2003; Knutti et al., 2002; Myhre et al., 2007). The impact of aerosol on cloud can be summarized into:

1. Effect on water cloud droplets

When there is an increase in cloud condensation nuclei as a result of aerosol loading, the number of water cloud droplets is enhanced though with reduced sizes, this will result into an increase in cloud optical thickness and solar insolation reflectivity (Twomey, 1977). When the cloud droplet size is reduced, precipitation can be inhibited. This in turn can increase cloud lifetime so that cloud evolve into greater height thereby resulting in the increase in cloud optical thickness (Khain et al., 2005; Williams et al., 2002).

2. Effect on cloud cover

Aerosol causes evaporation of existing clouds and blocking of surface heating. This have a very strong impact on radiative balance (Johnson et al., 2004; Penner et al., 2003). Studies on ice clouds show that the number of ice nuclei is potentially influenced by anthropogenic aerosols (Lohmann and Feichter, 2005). When precipitation is suppressed, aerosol is capable of changing cloud structure such that open Bernard cells can be closed thus increasing the cloud cover (Rosenfeld et al., 2006).

As efforts are being geared towards reduction in the uncertainty of the contribution of anthropogenic aerosol to climate change, scientists see the need to obtain and analyze data from a coordinated multiple platforms involving in-situ measurements, numerical modeling, remote sensing from ground-based, satellite, aircraft and ship etc. (Anderson et al., 2005;

Diner et al., 2004; Kaufman et al., 2002). This research work is therefore aimed at the following objectives:

- To characterize major aerosol types by their optical, microphysical and radiative properties.
- To validate aerosol measurements from satellite remote sensing instruments using surface based instrument.
- To address a coordinated platform of measurements for characterising aerosol properties and related aerosol cloud interactions.
- To fully exploit the existing information in satellite observations to study long term trend of aerosol optical depth.
- To execute the aerosol-climate model for assessing the aerosol radiative forcing on the earth.
- To identify the impact of long range transport of distant aerosols in the regional scale (especially over Southern Africa region).

1.7 Thesis Outline

This work reports aerosol climatology over Southern Africa with particular interest in South Africa (SA). One of the major types of aerosol that contributes to climate effect of aerosol in South Africa is biomass burning and a larger percentage of this comes from neighboring countries like Zambia and Mozambique. The work begins by considering the major instruments employed in this research work. The work largely was based on ground-based

and satellite-based remote sensing instruments. The ground-based instrument used in the work is the sun-sky sunphotometer of NASA's Aerosol Robotic Network (AERONET). The network has a world-wide coverage and the data is readily available for research purposes, so that it is possible to study aerosol and its properties from short and long term basis as some of the instruments have archive data for number of years. The satellite-based instruments used include Moderate Resolution Imaging Spectroradiometer (MODIS). The monthly and the daily products of both the MODIS (Terra and the Aqua) were employed in this study. The Multi-angle Imaging Spectroradiometer (MISR) was used for intercomparison of satellites as some satellite instrument performs better than others under different geographical and climate conditions. Ozone Monitoring Instrument (OMI) ultra-violet aerosol index was used to determine the absorption property of aerosol at a specific location. The Multi-sensor Aerosol Products Sampling System (MAPSS) helped in the comparative analysis of the different satellite and their validation using the surface-based instrument. Other web-based software models like HYSPLIT and SBDART are also employed. In chapter 3, the optical, microphysical and radiative properties of aerosol over Pretoria was studied based on one year AERONET based sunphotometer measurements installed at Council for Scientific and Industrial Research (CSIR) in Pretoria. In this manuscript, we analyzed an annual cycle of aerosol loading over Pretoria. AOD showed two maxima occurring in February and August. The seasonal average showed highest value coming up in summer and not spring as found by some earlier researchers which could be due to anthropogenic aerosols from the highly industrialized Highveld region of the country. The Angstrom exponent (AE) for Pretoria was generally high throughout the year with a seasonal peak of 1.67 in the summer which

indicates that aerosol sizes were more of fine particles. The volume size distribution shows a bimodal lognormal distribution with fine mode dominating. Aerosol radiative forcing was positive throughout the year implying a heating effect over Pretoria.

This chapter is to be cited as:

Adesina, A. J., Kumar, K. R., Sivakumar, V., Griffith, D. (2014), Direct radiative forcing of urban aerosols over Pretoria (25.75° S, 28.28° E) using AERONET Sunphotometer data: First scientific results and environmental impact. *Journal of Environmental Sciences*, 2459-2474.

In chapter 4, using six months data obtained from AERONET sunphotometer stationed at Gorongosa in Mozambique, investigation was carried out from the data recorded during the period July–December, 2012, and particular attention was paid to how aerosol loading evolves during the biomass burning season (spring) including pre- and post-months. From this study, we could confidently affirm that Mozambique was one of the major sources of biomass burning aerosol advected over South Africa. The aerosol optical depth (AOD_{500}) was found to increase from July to September where it reaches a maximum and subsequently started decreasing to November before it increases. The September maximum coincides with the corresponding biomass burning season. The Angstrom exponent was highest at the same month confirming the abundance of fine particle aerosols. Composite fire images of fresh smoke emitted from burning of forest fires were captured by Terra and Aqua MODIS at local

overpass time over Mozambique for twelve consistent years were also presented in the chapter.

This chapter needs to be cited as:

Adesina, A. J., Kumar, K. R., & Sivakumar,V. (2014): Variability in aerosol optical properties and radiative forcing over Gorongosa (18.97^{o}S, 34.35^{o}E) in Mozambique *Meteorology and Atmospheric Physics*, 1-12. DOI 10.1007/s00703-014-0352-2

Chapter 5 reports the validation and intercomparison of multiple satellite sensors from aerosol long term measurements. This chapter which was focused on two contrasting regions (Skukuza and Richards Bay) in South Africa also reported the long term trend of aerosol optical depth and its absorption properties using coordinated platforms. The study shows that MISR performs better than MODIS product in the study regions. The trend analysis suggests that aerosol loading is increasing over the ten years period. Richards Bay, a coastland area has higher aerosol loading than Skukuza, a hinterland area. The ultra violet absorption index (UVAI) for both locations shows increasing trend for the study period.

The Chapter is to be cited as:

Adesina, A. J., Kumar, K. R., Sivakumar, V. (2015) Assessment of satellite derived aerosol optical depth over two contrasting regions in South Africa: Trend estimation and characteristics of absorption aerosols (To be submitted).

In Chapter 6, selected major locations from six provinces in South Africa were studied using the Terra MODIS satellite monthly product for a period of 5 years. The study focused on the temporal and spatial relationship between AOD and various cloud parameters. The aerosol optical depth at 550 nm over the selected cities was generally not high and has maximum value during the spring season except in one of the locations where the maximum occurred in summer. Apart from one of the locations, the AE was generally high through the greater part of the year. The spatial correlation pattern between AOD and Water Vapor suggests that aerosol hardly undergo hygroscopic growth. Cloud Fraction and Cloud Optical Depth correlates with AOD in a reverse trend. Cloud Top Pressure and Cloud top Temperature exhibit similar correlation pattern with AOD.

The chapter is to be cited as:

Adesina, A. J., Kumar, K. R., Sivakumar, V. (2015) Spatio-temporal heterogeneity in AOD and its impact on cloud properties over major cities in South Africa as retrieved from MODIS (To be submitted).

Chapter 7 summarizes the results presented with some insights into further work.

REFERENCES

Ackerman, A. S., Toon, O., Stevens, D., Heymsfield, A., Ramanathan, V., & Welton, E. (2000). Reduction of tropical cloudiness by soot. *Science, 288*(5468), 1042-1047.

Anderson, T., Charlson, R., Bellouin, N., Boucher, O., Chin, M., Christopher, S., . . . Ogren, J. (2005). An "A-Train" strategy for quantifying direct aerosol forcing of climate. *Bull. Am. Met. Soc, 86*(12), 1795-1809.

Anderson, T. L., Charlson, R. J., Schwartz, S. E., Knutti, R., Boucher, O., Rodhe, H., & Heintzenberg, J. (2003). Climate forcing by aerosols--a hazy picture. *Science(Washington), 300*(5622), 1103.

Andreae, M. (1995). Climatic effects of changing atmospheric aerosol levels World Survey of Climatology, 16. *Future Climates of the World A. Henderson-Sellers*, 341-392.

Benkovitz, C. M., Berkowitz, C. M., Easter, R. C., Nemesure, S., Wagener, R., & Schwartz, S. E. (1994). Sulfate over the North Atlantic and adjacent continental regions: Evaluation for October and November 1986 using a three-dimensonal model driven by observation-derived meteorology. *Journal of Geophysical Research: Atmospheres (1984–2012), 99*(D10), 20725-20756.

Blanchard, D. C., & Woodcock, A. H. (1980). THE PRODUCTION, CONCENTRATION, AND VERTICAL DISTRIBUTION OF THE SEA-SALT AEROSOL*. *Annals of the New York Academy of Sciences, 338*(1), 330-347.

Charlson, R. J., Lovelock, J. E., Andreae, M. O., & Warren, S. G. (1987). Oceanic phytoplankton, atmospheric sulphur, cloud albedo and climate. *Nature, 326*(6114), 655-661.

Charlson, R. J., Schwartz, S., Hales, J., Cess, R. D., COAKLEY, j. J., Hansen, J., & Hofmann, D. (1992). Climate forcing by anthropogenic aerosols. *Science, 255*(5043), 423-430.

Diner, D. J., Ackerman, T. P., Anderson, T. L., Bsenberg, J., Braverman, A. J., Charlson, R. J., . . . Hostetler, C. A. (2004). Progressive Aerosol Retrieval and Assimilation Global Observing Network (PARAGON): An integrated approach for characterizing aerosol climatic and environmental interactions. *Bull. Amer. Meteo. Soc, 85*(10), 1491-1501.

Graf, H. F., Feichter, J., & Langmann, B. (1997). Volcanic sulfur emissions: Estimates of source strength and its contribution to the global sulfate distribution. *Journal of Geophysical Research: Atmospheres (1984–2012), 102*(D9), 10727-10738.

Gundel, L., Guyot-Sionnest, N., & Novakov, T. (1989). A study of the interaction of NO2 with carbon particles. *Aerosol science and technology, 10*(2), 343-351.

Haywood, J., & Boucher, O. (2000). Estimates of the direct and indirect radiative forcing due to tropospheric aerosols: A review. *Reviews of Geophysics, 38*(4), 513-543.

Hidy, G. (1984). *Aerosols: an industrial and environmental science*: Elsevier.

Hobbs, P. V., Bowdle, D. A., & Radke, L. F. (1985). Particles in the lower troposphere over the high plains of the United States. Part I: Size distributions, elemental compositions and morphologies. *Journal of climate and applied meteorology, 24*(12), 1344-1356.

Hoppel, W. (1979). Measurement of the size distribution and CCN supersaturation spectrum of submicron aerosols over the ocean. *Journal of the atmospheric sciences, 36*(10), 2006-2015.

Jaenicke, R. (1993). Tropospheric aerosols. *International Geophysics, 54*, 1-31.

Johnson, B., Shine, K., & Forster, P. (2004). The semi-direct aerosol effect: Impact of absorbing aerosols on marine stratocumulus. *Quarterly Journal of the Royal Meteorological Society, 130*(599), 1407-1422.

Kaskaoutis, D., & Kambezidis, H. (2006). Investigation into the wavelength dependence of the aerosol optical depth in the Athens area. *Quarterly Journal of the Royal Meteorological Society, 132*(620), 2217-2234.

Kaufman, Y. J., Koren, I., Remer, L. A., Rosenfeld, D., & Rudich, Y. (2005). The effect of smoke, dust, and pollution aerosol on shallow cloud development over the Atlantic Ocean. *Proceedings of the National Academy of Sciences of the United States of America, 102*(32), 11207-11212.

Kaufman, Y. J., & Nakajima, T. (1993). Effect of Amazon smoke on cloud microphysics and albedo: Analysis from satellite imagery.

Kaufman, Y. J., Tanré, D., & Boucher, O. (2002). A satellite view of aerosols in the climate system. *Nature, 419*(6903), 215-223.

Khain, A., Rosenfeld, D., & Pokrovsky, A. (2005). Aerosol impact on the dynamics and microphysics of deep convective clouds. *Quarterly Journal of the Royal Meteorological Society, 131*(611), 2639-2663.

Kim, B. G., Schwartz, S. E., Miller, M. A., & Min, Q. (2003). Effective radius of cloud droplets by ground-based remote sensing: Relationship to aerosol. *Journal of Geophysical Research: Atmospheres (1984–2012), 108*(D23).

Knutti, R., Stocker, T. F., Joos, F., & Plattner, G.-K. (2002). Constraints on radiative forcing and future climate change from observations and climate model ensembles. *Nature, 416*(6882), 719-723.

Koutsenogii, P. K., & Jaenicke, R. (1994). Number concentration and size distribution of atmospheric aerosol in Siberia. *Journal of Aerosol Science, 25*(2), 377-383.

Lohmann, U., & Feichter, J. (2005). Global indirect aerosol effects: a review. *Atmospheric Chemistry and Physics, 5*(3), 715-737.

Myhre, G., Stordal, F., Johnsrud, M., Kaufman, Y., Rosenfeld, D., Storelvmo, T., . . . Isaksen, I. (2007). Aerosol-cloud interaction inferred from MODIS satellite data and global aerosol models. *Atmospheric Chemistry and Physics, 7*(12), 3081-3101.

Penner, J. E., Dong, X., & Chen, Y. (2004). Observational evidence of a change in radiative forcing due to the indirect aerosol effect. *Nature, 427*(6971), 231-234.

Penner, J. E., Zhang, S. Y., & Chuang, C. C. (2003). Soot and smoke aerosol may not warm climate. *Journal of Geophysical Research: Atmospheres (1984–2012), 108*(D21).

Prospero, J., Charlson, R., Mohnen, V., Jaenicke, R., Delany, A., Moyers, J., . . . Rahn, K. (1983). The atmospheric aerosol system: An overview. *Reviews of Geophysics, 21*(7), 1607-1629.

Pruppacher, H. R., & Klett, J. D. (1978). Microstructure of atmospheric clouds and precipitation *Microphysics of Clouds and Precipitation* (pp. 9-55): Springer.

Raes, F., Bates, T., McGovern, F., & Van Liedekerke, M. (2000). The 2nd Aerosol Characterization Experiment (ACE-2): general overview and main results. *Tellus B, 52*(2), 111-125.

Reddy, M. S., & Venkataraman, C. (1999). Direct radiative forcing from anthropogenic. *Current Science, 76*(7), l0.

Reid, J. S., & Hobbs, P. V. (1998). Physical and optical properties of young smoke from individual biomass fires in Brazil. *Journal of Geophysical Research: Atmospheres (1984–2012), 103*(D24), 32013-32030.

Rosenfeld, D., Kaufman, Y., & Koren, I. (2006). Switching cloud cover and dynamical regimes from open to closed Benard cells in response to the suppression of precipitation by aerosols. *Atmospheric Chemistry and Physics, 6*(9), 2503-2511.

Satheesh, S., & Krishna Moorthy, K. (2005). Radiative effects of natural aerosols: A review. *Atmospheric Environment, 39*(11), 2089-2110.

Schwartz, S. E., & Benkovitz, C. M. (2002). Influence of anthropogenic aerosol on cloud optical depth and albedo shown by satellite measurements and chemical transport modeling. *Proceedings of the National Academy of Sciences, 99*(4), 1784-1789.

Takemura, T., Okamoto, H., Maruyama, Y., Numaguti, A., Higurashi, A., & Nakajima, T. (2000). Global three-dimensional simulation of aerosol optical thickness distribution of various origins. *Journal of Geophysical Research: Atmospheres (1984–2012), 105*(D14), 17853-17873.

Tegen, I., & Fung, I. (1994). Modeling of mineral dust in the atmosphere: Sources, transport, and optical thickness. *Journal of Geophysical Research: Atmospheres (1984–2012), 99*(D11), 22897-22914.

Twomey, S. (1977). The influence of pollution on the shortwave albedo of clouds. *Journal of the atmospheric sciences, 34*(7), 1149-1152.

Williams, E., Rosenfeld, D., Madden, N., Gerlach, J., Gears, N., Atkinson, L., . . . Biazon, B. (2002). Contrasting convective regimes over the Amazon: Implications for cloud electrification. *Journal of Geophysical Research: Atmospheres (1984–2012), 107*(D20), LBA 50-51-LBA 50-19.

CHAPTER TWO

2. INSTRUMENTATION

Aerosol and its forcing on climate became an important field of studies a few years before the close of the last century (Charlson et al., 1992; Twomey et al., 1984). The major challenge faced since that time has been the difficulty in estimating and predicting the changes that occur in climate due to the uncertainty in the contribution of aerosols. The transient and the heterogeneous nature of aerosols make its contribution difficult to quantify (Christopher et al., 1996; Tegen et al., 1996). This gave rise to remote sensing instruments that are capable of measuring with precision a radiative forcing of the order of 1 Wm^{-2} when the optical depth changes in excess of 0.1. In particular, ground based and satellite based remote sensing became an increasingly useful tool in carrying out such measurements. While the ground based system has the advantage of being simple, reliable and being supportive in the

validation of satellite retrievals, it does not have the long term data acquisition capable of reliable measurement and efficient processing of data thereby leading to disjointed data sets that cannot be used for scientific assessments.

2.1 Remote Sensing Techniques

Remote sensing is the art of taking measurements without any physical contact with the object under observation and it is basically divided into two – active and passive. When an instrument depends on energy reflected or emitted from the object then it is a passive instrument but when it has its own energy source, it is active. In most cases the external source of reflection is from sun radiation. Descriptive nomenclatures of some of the common remote sensors are given below:

2.1.1 Radiometer

By design the instrument makes a quantitative measurement of the intensity of radiation in the microwave, infrared or visible region of the electromagnetic spectrum.

2.1.2 Imaging Radiometer

This is a radiometer that is capable of performing scanning mechanically or electronically to produce image from a two-dimensional array of pixels with the aid of array of detectors.

2.1.3 Spectrometer

This is a device that can analyze and measure detected signal from electromagnetic radiation incident on it. To carry out the spectral discrimination, the device makes use of prisms or gratings.

2.1.4 Spectroradiometer

This is a radiometer that takes a multispectral measurement of radiant intensity. The wavelength bands which is normally of high resolution takes measurement of specific parameters like vegetation, cloud characteristics, sea surface temperature, ocean color, etc.

When an instrument provides its own electromagnetic energy for the illumination of the object it is said to be an active instrument. The instrument then depends on the reflected or backscattered signal from the pulse of energy sent to the object.

2.1.5 Radar (Radio Detection and Ranging)

Through the use of transmitter electromagnetic radiation in the microwave or radio frequency is sent through an antennae and the time of arrival of the backscattered signal is used to calculate the distance of the object.

2.1.6 Scatterometer

The instrument measures the backscattered signal of high frequency radiation and can be employed in deriving surface maps, wind speed and direction.

2.1.7 LIDAR (Light Detection and Ranging)

Through the use of laser, the instrument sends out a pulse and the backscattered signal is collected through the sensitive receiver detector. The distance of the object can be known by calculation. It is useful in determining the atmospheric profile of clouds, aerosols, etc.

2.1.8 Laser Altimeter

Through the use of LIDAR the instrument measures the height above the surface or the instrument platform.

Satellite remote sensing came into existence during the space age when several types of sensors were used for imaging surfaces. During those early days, astronauts orbiting the earth take photos out of the windows of their spacecraft. The first set of satellite sensors were not particularly designed for aerosol studies but were somehow applied to it. The Advanced Very High Resolution Radiometer (AVHRR) for example was designed to measure the temperature of sea surface and vegetation index, and the Total Ozone Mapping Spectrometer (TOMS) was designed for measurement of ozone content. In subsequent years, satellites with appropriate technology for aerosol measurements were launched into the space (King et al., 1999). We shall take a closer look at these satellites particularly those that were used in this research work. First we shall look at the ground-based instrument; sunphotometer and then the satellite sensors.

2.2 Aerosol Robotic NETwork (AERONET)

The Aerosol Robotic NETwork (AERONET) is the most coordinated and widely distributed ground based system providing long term data that have been subjected to standardization and regular calibration. The network uses Cimel Sunphotometer for measurement of aerosol properties.

As an automatic instrument, the CIMEL 318 performs basically two types of measurements; the direct sun and the sky radiance following a programmed sequence. The direct sun measurement occurs at light spectral bands 340, 380, 440, 500, 675, 870, 936, 1020 nm. The triplet observations are made at 30 sec per wavelength at every 15 mins corresponding to Langley calibration for morning and afternoon. The triplet observation is enhanced by the fact that aerosol optical depth temporal variation is much lesser than that of cloud optical depth (Holben et al., 1998; Smirnov et al., 2000).

The cloud screening process is twofold, first, the variation in high frequency is eliminated by retaining the stable triplets at all wavelengths and secondly the threshold derivative of the root mean square is used to eliminate the diurnal variation in the temporal optical depth.

Fig 1: CIMEL Sunphotometer installed at the roof of Physics building at University of KwaZulu-Natal (Westville Campus), Durban, South Africa.

2.2.1 Cloud screening

This is based on combination of processes:

1. Data Quality Checks

A minimum optical depth of $\tau_a < -0.01$ at all wavelengths is set such that if it is less, measurements that is observed in the particular channel is totally eliminated while others that are greater are preserved where the negative value that arises is purely from calibration. Atmospheric pressure, uncertainties in the column ozone and certain temperature correction are associated with 1020 nm wavelength. Another condition is the elimination of optical depth corresponding to air mass M > 5 because when the elevation angle of the Sun is low, probability of cloud contamination is higher.

2. Triplet Stability Criterion

When the CIMEL Sun/Sky radiometer takes a triplet measurement, variation of optical depth within that interval of 30 seconds over a total of 1 minute period is expected to be less than $(\tau_{max} - \tau_{min}) < 0.02$, this is classified as a good result of τ_i and the average of the three measurements are taken as cloud screened, otherwise, measurement is eliminated at all wavelengths (Smirnov et al., 2000).

3. Diurnal Stability Check

The next step is the consideration of the standard deviation of the average aerosol optical depth for an entire day measurement. Based on the estimated accuracy of the instrument of about ±0.01 in τ_a (Holben et al., 1998), if the standard deviation for an entire day is less than 0.015 (after the triplet stability criterion has been satisfied), all data for that day is accepted.

4. Smoothness Criteria

This criterion helps to determine the local oscillations arising from cloud interactions. This is obtained by finding the second derivative of aerosol optical depth with time and taking the limit of the root mean square value. An increment will be obtained if there is a substantial presence of such oscillations. The method is largely based on constrained inversion method used in remote sensing (S. Twomey, 1977). By introducing a constraint of the norm of the second derivative not exceeding certain critical value

$$(D_2)^2 = \int_{t_1}^{t_2} \left(\frac{\partial^2 \tau(t)}{\partial t^2}\right)^2 dt \leq D_{critic}^2 \qquad (1)$$

D_{critic}^2 is the predetermined value expressing the expected maximum variability in aerosol optical depth.

In order to ensure a coherent threshold, *D* in extreme cases is of a clear to a very hazy condition. A logarithmic instead of total derivative $d^2\tau/dt^2$(d^2T/dt^2) is employed.

$$\frac{dln\tau(t)}{dt} = \frac{1}{\tau(t)}\frac{d\tau(t)}{dt} \quad (2)$$

since optical depth measurement takes place at in discrete moment of time, differences and not analytical derivatives are used. An index *D* which is the first derivative difference similar but not the same as D_2 is found

$$D = \sqrt{\frac{1}{(n-2)}\sum\left[\frac{Ln\tau_i - Ln\tau_{i+1}}{t_i - t_{i+1}} - \frac{Ln\tau_{i+1} - Ln\tau_{i+2}}{t_{i+1} - t_{i+2}}\right]^2} \leq 16 \quad (3)$$

Where *D*>16, the term responsible is sorted and optical depth associated is eliminated. Diurnal stability check is again applied, after such repeated checks, if only one or two measurements remain, then, the reading for that day is discarded.

5. Three Standard Deviation Criteria

This criterion is against the backdrop that in a normal distribution, values outside the 3σ range is improbable. The check is performed over the measurements of τ_a (500 nm) and $\alpha_{440\text{-}870}$ for entire day period and values that differ from the mean or greater by 3σ is eliminated.

2.2.2 Instrumental Precision

When an instrument is able to reproduce result using uniform technique under same conditions from numerous results, then it is assumed to have precision. There exists in Goddard space flight center a 2-m-diameter integrating sphere which is used to compare how the digital numbers (DN) from sun photometers and sky radiance channel vary from its spectral response thereby determining its gain and offsets. The values of the dark current

obtained from every sky radiance measurement are then examined. The sun channels are then evaluated based on the Langley observations of Mauna Loa Observatory DNs triplet's variability.

2.2.3 Instrument Calibration

The calibration of all instruments takes place at least twice a year while the reference instrument is done almost monthly. The variability from the mean calculated from long term measurement was found to be less than 1% (Holben et al., 1998). In order to convert the instrument measurement (DN) output to a desirable output, a calibration coefficient is needed. The determination of such coefficient is referred to as calibration. Calibration encompasses instrument precision, calibration procedure and the algorithm used. The procedure for finding the calibration coefficients involved computing the average of five or more Langley plots obtained from Mauna Loa observatory (Holben et al., 1998).

2.3 Moderate Resolution Imaging Spectroradiometer (MODIS)

The first MODIS instrument was launched December 1999 aboard Terra satellite and it began data transmission in February 2000. This instrument was designed to provide an improved monitoring for land, ocean and atmospheric research. Its design for the land component combines the characteristics of the Advanced Very High Resolution Radiometer (AVHRR) as well as the Landsat Thematic Mapper. Though the AVHRR are not calibrated on board, MODIS makes use of vicarious calibration techniques using radiances of known targets. This calibration is done in two steps with the use of high altitude cloud and ocean observations.

High altitude bright cloud of ~20 km is selected with the use of AVHRR to identify cloudy pixels between 220 K and 225 K apparent temperature. Clouds below 220 K are not used as they are very cold and mostly compose of ice. An inter-band coefficient and the aerosol optical thickness are computed with the use of Rayleigh scattering. The data obtained are used to filter noisy and cloudy areas as well as areas where the aerosol optical thickness is too high. This method agrees with other vicarious calibration methods as it has shown good stability with RMSE of 2-3%. MODIS instrument ensures a calibration accuracy of 2% relative to the sun's radiance.

MODIS provides 36 spectral bands in three different spatial resolutions ranging from 0.41 to 15 μm. 2 channels to 250 m resolution, 5 channels for 500 m resolution and 29 channels for 1 km resolution. For each of the 1 km spatial resolution, MODIS produces 8 different information: solar azimuth, satellite azimuth, solar zenith angle, satellite zenith angle, and range to the satellite, height above the earth ellipsoid, geodetic latitude and longitude.

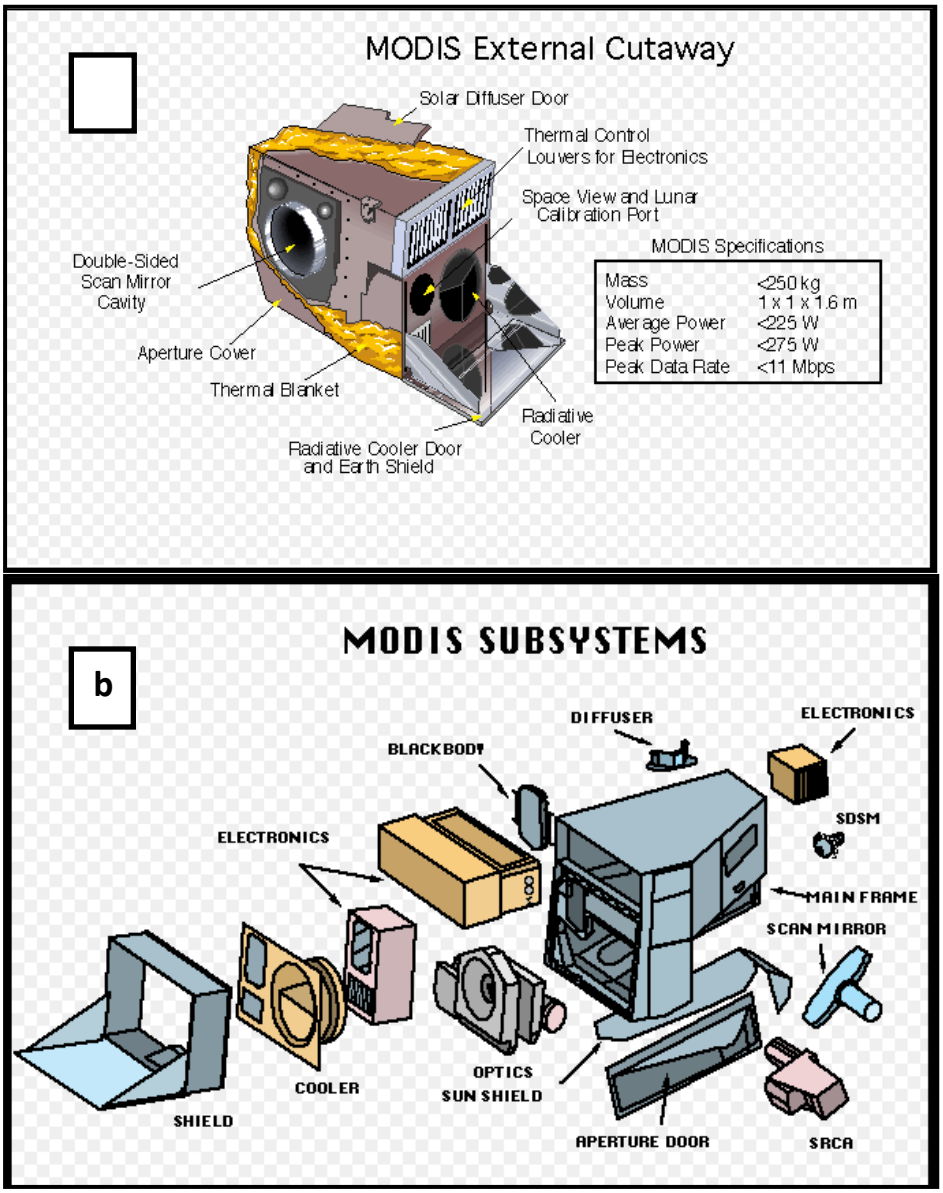

Fig 2: (a & b): Picture describing the components of MODIS
(https://www.google.com/search?q=modis+satellite)

MODIS makes use of the ground control points for the calibration of instrument alignment which improves insight knowledge of the relationship between MODIS instrument and the

reference base of the platform navigation. The ground control points also measures the residual errors automatically. The MODIS instrument algorithm has different levels for various products. Level-1 resamples all MODIS data as well as determines the location of all the bands. Level-2 products are referred to as gridded products and they are from calibrated radiances of previous MODIS products. Level-3 products varies from a single day to an entire year and these products are spatially resampled and averaged to produce a single estimate for each location grid. When MODIS data are incorporated into models to estimate geophysical variables, Level-4 products are generated. These MODIS land products are divided into three groups of Earth Observing System (EOS): Distributed Active Archive Centers (DAAC) which contains Level-2 products, Level 3 snow and ice products are produced at National Snow and Ice Centre (NSIDC) while the remaining Level-3 products and Level-4 products are produced at EOS Data Centre (EDS).

For the determination of aerosol over land and sea, MODIS has two independent algorithms. These algorithms rely on calibrated and geo-located reflectances which are MOD02 and MOD03 for Terra MODIS products and MYD02 and MYD03 for Aqua MODIS products. Since its inception, these algorithms haven't changed although some have evolved. To derive aerosol products over land, there is the need to organize the measured reflectances into three channels corresponding to 20 by 20 or 400 pixels for each box at $\rho_{0.47}$, $\rho_{0.66}$, $\rho_{2.13}$. In order to match the resolutions of the two channels, the 250 m resolution 0.66 μm must be degraded to 500 m. To identify whether the pixel is cloudy, snow/ice or water, the 400 pixels are evaluated pixel by pixel. For ocean retrieval, all 400 pixels must be identified as water while for land retrieval, either one or more pixels identified as ocean is needed, however with

decreased quality. Although the MOD/MYD35 cloud mask supplies information that identifies whether a pixel is land or ocean, additional masking sensitive to small sub-pixel patches has been put in place to identify low clouds as well as a reflectance in the 1.38 channel to identify high clouds. This makes the pixels to be further screened for sub-pixel water by determining the value of the Normalized Difference Vegetation Index (NDVI) for each pixel. If the value identified containing sub-pixel water is less than 0.10, they are excluded with the cloudy and snowy pixels from the remaining algorithm.

To retrieve aerosol optical thickness at 0.47 and 0.66 μm, the estimated surface reflectances (at $\rho_{0.47}$, $\rho_{0.66}$) and the measured mean top of atmosphere reflectances are used as input into the continental model. Satellites give better estimation of aerosol optical thickness compared to aerosol size. However, to retrieve the aerosol size, there is a need for sufficient aerosol loading. When the sizes are fine mode, this corresponds to dust and non-dust sources from local transport but when $\rho_{2.13}$ falls between 0.15 and 0.25, pure dust retrievals are made.

When the sensitivity of the retrieval was tested by introducing a random calibration error of 1% the effects on retrieval size was enhance. When the calibration error is ~1%, there is an uncertainty of ±0.25 for $\eta_{0.55}$ = 1and ±0.50 for $\eta_{0.55}$ = 0 (where η is fine mode fraction). Other consistency checks are put into place before the final results are obtained.

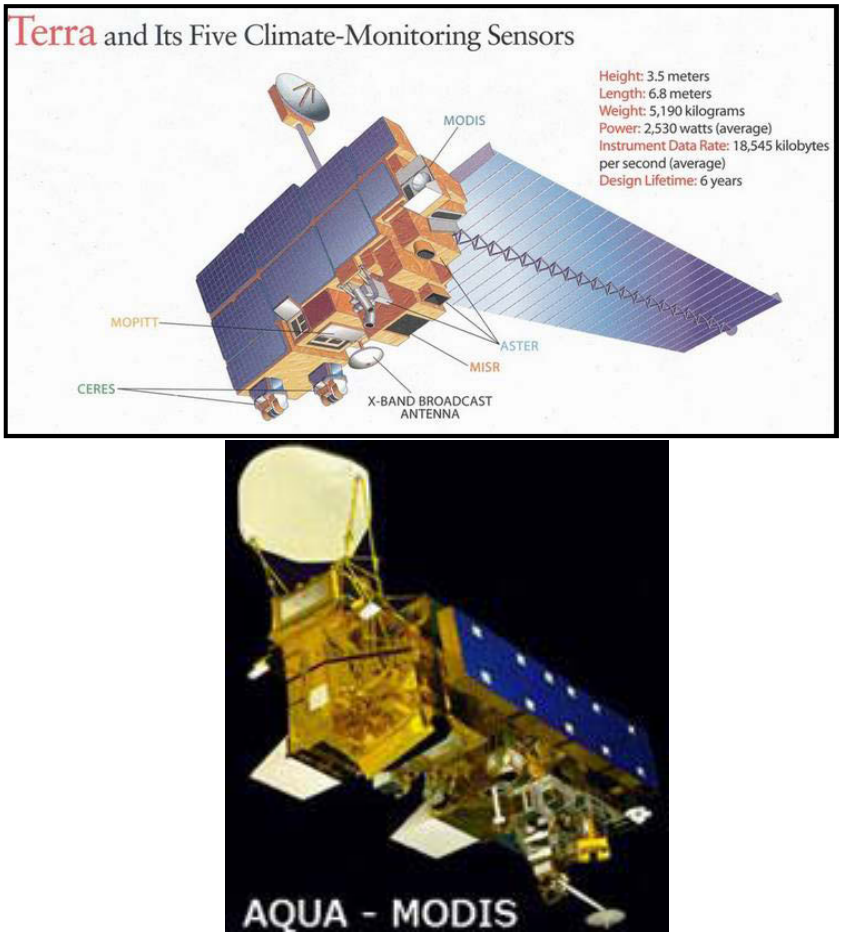

Fig 3: Picture of Terra and Aqua MODIS in space
(https://www.google.com/search?q=modis+satellite)

The condition for output being that the retrieved optical thickness at 0.55μm must be greater than -0.01 and less than 5. The MODIS instrument also indicates if the retrievals are validated, not yet validated, derived, experimental or diagnostic. When errors can be defined and applied to retrieval products by comparing with ground-based data, the products are said to be validated. But when the data have been collected and analysis is underway but the

retrieved parameter is not yet characterized, then the products are not yet characterized. Derived parameters are not directly retrieved while experimental parameters are scientific products. Diagnostic parameters are meant to understand the final products. The MODIS atmospheric correction algorithms over land are over seven bands: 470 nm, 555 nm, 648 nm, 858 nm, 1240 nm, 1640 nm and 2130 nm. The aerosol optical thickness is validated over land with AERONET measurements at the MODIS wavelengths of 0.47 and 0.55 μm. The MODIS over ocean is expected to be more accurate than land algorithm. Likewise, the percentage relative error is smaller over ocean compared to land (Remer et al., 2005).

2.4 Multi-angle Imaging SpectroRadiometer (MISR)

Multi-angle Imaging SpectroRadiometer (MISR) is an instrument that is designed to assist in understanding how our climate is affected by changes in the types, distribution and amounts of airborne particulate, clouds and surface cover (Diner et al., 1998). It was launched, late June, 1998. MISR contains nine different cameras pointing at different discrete angles and four visible/infrared spectral bands. With the aid of the nine discrete angles, it provides an imagery that is global, radiometrically calibrated, geo-rectified and co-registered.

The source of illumination for the imagery of MISR is sunlight. Sunlight shines at different angles, therefore, to handle the angular variation of the reflected sunlight and the characteristics of the scenes that were observed, MISR images the Earth in nine different angles. It traverses in a sun-synchronous near-polar orbit with a 16-day global coverage repeat cycle and crossing the equator at 10:30am.

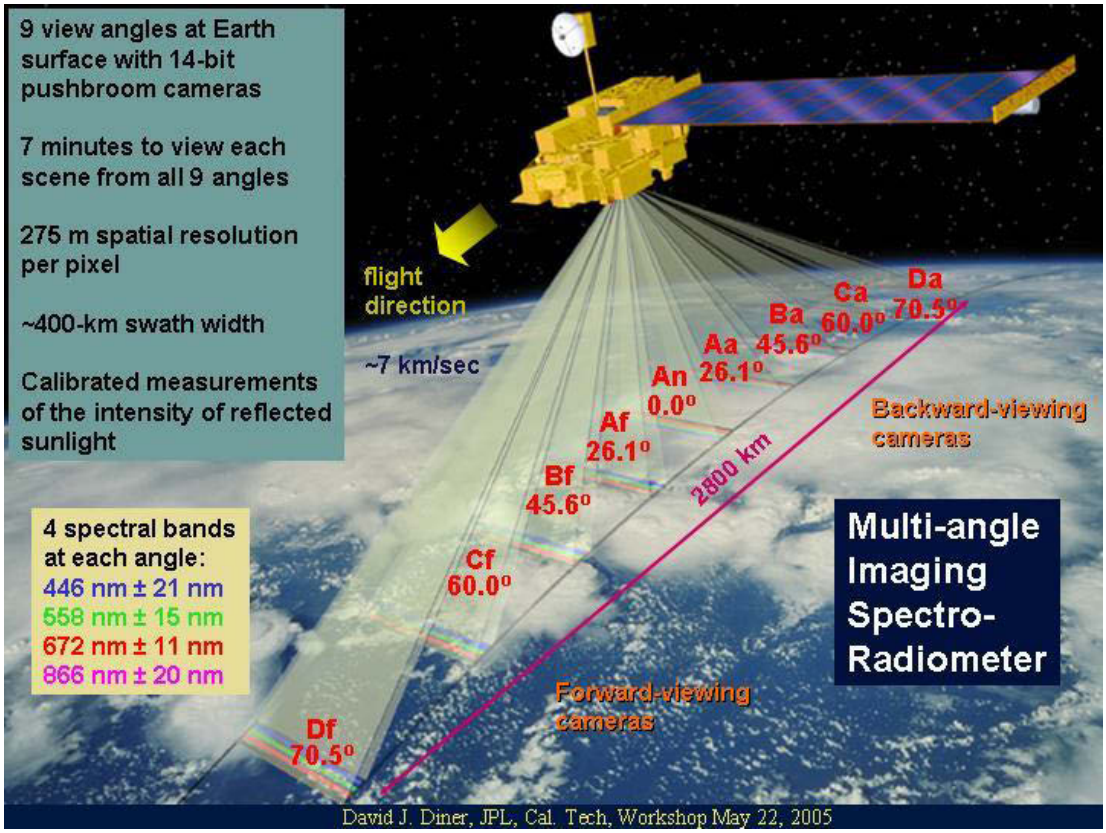

Fig 4: Picture of MISR in space showing all the angles of view
https://www.google.com/search?q=misr+satellite+image

Details of the operation of the instrument can be found at MISR website.

2.5 The Ozone Monitoring Instrument (OMI)

The Ozone Monitoring Instrument (OMI) was launched July 15, 2004 on board the Earth Observing System (EOS) Aura satellite from Vandenberg Air Force base in California. The Aura spacecraft revolves with 98.2^{o} angle of inclination, in a sun synchronous polar orbit at an altitude of 705 km, with equator crossing time of 13.45 in the ascending node and provides 14 orbits daily (Levelt et al., 2006). Along with the Ozone Monitoring Instrument, the Aura

spacecraft also carries the Microwave Limb Sounder (MLS), High Resolution Dynamics Limb Sounder (HRDLS) as well as the Tropospheric Emission Spectrometer (TES).

The Ozone Monitoring Instrument together with the HRDLS, MLS and TES all work together to obtain data and support the Aura objectives which are to detect and explain ozone trends, global impact of pollution and to explain the connections between atmospheric chemistry and climate. OMI is the first among the new generation space borne instruments that combines high resolution with daily measurements (Veefkind et al., 2006). The primary purpose of OMI instrument is to obtain global measurement of trace gases in both the troposphere and stratosphere and high spatial and spectral resolutions. Trace gases such as O_3, NO_2, SO_2, HCHO, BrO and OClO are measured. OMI also provides measurements for aerosol characteristics, UV irradiance at the surface as well as cloud top heights (Dobber et al., 2005). The Ozone Monitoring Instrument has the capacity to distinguish between different aerosol types such as dust, smokes and sulphates. OMI measures reflected solar radiation in two channels in the ultraviolet and visible regions between 270 nm and 500 nm with a spectral resolution of ~ 0.5 nm. The ultraviolet full performance range is between 270 nm and 365 nm while in the visible region, the full performance range is between 365 nm and 500 nm. In the ultraviolet full performance range, there are two sub channels, UV-1 from 270 nm to 310 nm and UV-2 from 310 nm to 365 nm. This makes the spectral and spatial sampling of UV-1 to be reduced by a factor of 2 compared to UV-2.

2.5.1 The Ultraviolet Aerosol Index (UVAI)

OMI has an advantage for aerosol characterization from space, as there are measurements in the near ultraviolet region that can be used to retrieve aerosol properties. This technique is useful for both land and water retrievals due to low UV surface albedo. Two major inversion schemes are used to derive aerosol from OMI, the OMI near UV (OMAERUV) and the multi-wavelength algorithm (OMAERO). The OMAERUV uses two distinct UV wavelengths (354 nm and 388 nm) to derive the UV aerosol index, absorption optical depth as well as aerosol extinction while the OMAERO uses 19 different channels to derive aerosol extinction optical depths at several wavelengths ranging from 330 nm to 500 nm. In the OMAERUV, the reflectance of all terrestrial surfaces not covered with snow is small which makes the retrieval of aerosol products possible over larger land surfaces compared to that in the visible region.

The first step in the OMAERUV algorithm is the calculation of the Lambert Equivalent Reflectivity (LER) at 388 m. This is done by assuming that the atmosphere is bounded by an opaque Lambertian reflector and that the atmospheric scattering is only Rayleigh scattering. When there is scattering from clouds and aerosols, the LER is always more than the true surface reflectivity, however, when the aerosols are highly absorbing, the true surface reflectivity is higher.

The ultraviolet Aerosol Index is obtained through the expression below:

$$UVAI = -100 log_{10}\left[\frac{I_{354}^{obs}}{I_{354}^{calc}(R_{354}^{*})}\right] \qquad (4)$$

Where the $UVAI$ is the estimated error in the satellite radiance at 354 nm obtained from radiance from 388 nm assuming that only the molecular atmosphere is bounded by varying

Lambertian surface. This concept of the Ultraviolet aerosol index was first developed from the Total Ozone Mapping Spectrometer (TOMS) observations. When the atmosphere is free from aerosol or when there is the presence of large non absorbing aerosol particles and clouds with nearly zero Angstrom coefficient, near-zero value of $UVAI$ is obtained. However, when there is the presence of carbonaceous aerosols, desert dusts, volcanic ash, the values of $UVAI$ are positive.

2.6 Multi-sensor Aerosol Products Sampling System (MAPSS)

MAPSS was designed to provide uniform and consistent sampling of aerosol products from various sources. It was also designed to aid the validation of aerosol retrieval algorithm from MODIS aboard Aqua and Terra satellites. It has however been redesigned to facilitate detailed comparative analysis and integrated use of aerosol measurements from multiple satellite sensors. These sensors include: MODIS both on Terra and Aqua, Multi-angle Imaging Spectro-Radiometer (MISR) on Terra, the Ozone Monitoring Instrument (OMI) on Aura, POLarization and Directionality of the Earth's Reflectances (POLDER) on ADEOS and ADEOS-2 satellites, Cloud-Aerosol Lidar with Orthogonal Polarization (CALIOP) on Calipso and the Deep Blue algorithm from Sea-viewing Wide Field-of-view Sensor (SeaWiFS). All these satellites that support MAPSS products are obtained directly from Level-2 retrieval. This level represents the highest spatial resolution for the sensor and algorithm.

AERONET sunphotometers provide three different quality assured categories of aerosol products using ground-based observations in direct solar, principal plane and almucantar. These products are the aerosol optical depth or thickness, spectral deconvolution aerosol

product while the third is the inversion aerosol product. For the validation of these products as well as inter-comparison, AERONET aerosol optical depth are interpolated to obtain MAPSS auxiliary datasets. However, these interpolated values are not quality assured and may possess some inaccuracies from the interpolation process. Aerosol products on MODIS with MAPSS are retrieved at 10 km nominal resolution, nadir viewing. Both MODIS instruments on Terra and Aqua provide precipitable water vapor product based on infrared retrieval at 1 km nominal resolution and near infrared retrieval at 5 km nominal resolution. The MISR retrieves aerosol in 9 independent viewing angles which enables it to measure some aerosol properties which other instruments cannot measure.

Moreover, when climatic conditions are unfavorable, MISR multiple cameras ensure reliable retrievals in the visible wavelength. OMI instrument retrieves aerosol products in the near ultraviolet such as single scattering albedo, aerosol absorption as well as extinction optical depth even under cloudy conditions which pose threat to other instruments. The POLDER makes use of polarization properties of measured radiation to retrieve anthropogenic aerosol optical depth. The CALIOP shows the vertical distribution of aerosol and cloud in the atmosphere as well as the densities and specific properties of each aerosol layers. The SeaWiFS uses the Deep Blue algorithm to retrieve aerosol optical depth and Angstrom exponent over bright desert and vegetated surfaces.

These data are validated with AERONET measurement using an approach developed by Ichoku et al. (2002). This approach entails acquiring the spatial aerosol measurement aboard both Terra and Aqua and sampling them with 50 x 50 km window size taking into consideration that the average aerosol travel speed is 50 km/hr. The 50 x 50 km (5 x 5 pixels)

will then coincide with 1 hour AERONET data. Temporal measurements are then sampled at each satellite overpass time of an hour. It is however important to note that a pixel is only sampled if the distance between the center of the pixel and the ground station is not more than 27.5 km. The number of pixels between the 55 km diameter depends on the pixel shape and size. For MODIS, MISR, OMI, POLDER, CALIOP and SeaWiFS, the maximum number of pixels within the 55 km diameter sample space at nadir are 25, 9, 8, 9, 11 and 16 respectively. It should also be noted that the difference in shape of the sampling space has negligible effect on the derived sample statistics of the data. However, over a ten year period, it was discovered that circle based sampling produced 22% few points compared to square sampling. This difference can be attributed to the fact that when ground stations are located off nadir of the sensor, the number of space in the sample space can be much reduced to one in order to maintain a uniform sampling area. Geometry condition does not however affect square based samplings which results in higher number of sampling points. It was also observed that with the use of Haversine formula for circle based sampling, there was greater accuracy for stations in high latitudes, islands and coastal areas as data points increased compared to the Euclidean distance previously used. Haversine formula has been said to be accurate to ~200 m.

When multiple satellites pass over the same location within an hour time frame, there is the possibility that a single AERONET measurement can be sampled and archived multiple times, it is therefore recommended to account for this duplication when AERONET data in MAPSS archive is performed in order to avoid oversampling. When the sampled data point is sufficient to obtain statistical computation, the slope, azimuth and multiple correlation coefficients are obtained. The minimum number of data points required for aerosol product

for MODIS, MISR, OMI, POLDER, SeaWiFS are 10, 5, 4, 5 and 7 respectively while the minimum number of data points required for AERONET and CALIOP is 2. These statistics can be used to determine the local spatio-temporal distribution as well as the variation of the samples. Azimuth shows the direction of the gradient of an aerosol product as it points towards the lower values of the aerosol product. This direction also indicates the direction of wind flow and plume dispersion from the aerosol source.

There is quality assurance performed on all aerosol products supported in MAPSS. For MODIS, and SeaWiFS, the quality assurance ranges from 0 to 3 (only integer numbers) with 3 indicating the highest quality and 0 representing the lowest quality. Data sampled by MAPSS can be used for comparing space borne observations with corresponding ground-based measurements which makes validation of MODIS aerosol products possible. It can also help to investigate the strengths and weaknesses of different remotes sensing instruments across the globe.

REFERENCES

Charlson, R. J., Schwartz, S., Hales, J., Cess, R. D., COAKLEY, J., Hansen, J., & Hofmann, D. (1992). Climate forcing by anthropogenic aerosols. *Science, 255*(5043), 423-430.

Christopher, S. A., Kliche, D. V., Chou, J., & Welch, R. M. (1996). First estimates of the radiative forcing of aerosols generated from biomass burning using satellite data. *Journal of Geophysical Research: Atmospheres (1984–2012), 101*(D16), 21265-21273.

Diner, D. J., Beckert, J. C., Reilly, T. H., Bruegge, C. J., Conel, J. E., Kahn, R. A., . . . Gerstl, S. A. (1998). Multi-angle Imaging SpectroRadiometer (MISR) instrument description and experiment overview. *Geoscience and Remote Sensing, IEEE Transactions on, 36*(4), 1072-1087.

Dobber, M., Dirksen, R., Voors, R., Mount, G. H., & Levelt, P. (2005). Ground-based zenith sky abundances and in situ gas cross sections for ozone and nitrogen dioxide with the Earth Observing System Aura Ozone Monitoring Instrument. *Applied optics, 44*(14), 2846-2856.

Holben, B., Eck, T., Slutsker, I., Tanre, D., Buis, J., Setzer, A., . . . Nakajima, T. (1998). AERONET—A federated instrument network and data archive for aerosol characterization. *Remote sensing of environment, 66*(1), 1-16.

Ichoku, C., Chu, D. A., Mattoo, S., Kaufman, Y. J., Remer, L. A., Tanré, D., . . . Holben, B. N. (2002). A spatio-temporal approach for global validation and analysis of MODIS aerosol products. *Geophysical Research Letters, 29*(12), MOD1-1-MOD1-4.

King, M. D., Kaufman, Y. J., Tanré, D., & Nakajima, T. (1999). Remote sensing of tropospheric aerosols from space: Past, present, and future.

Levelt, P. F., Hilsenrath, E., Leppelmeier, G. W., van den Oord, G. H., Bhartia, P. K., Tamminen, J., . . . Veefkind, J. P. (2006). Science objectives of the ozone monitoring instrument. *Geoscience and Remote Sensing, IEEE Transactions on, 44*(5), 1199-1208.

Remer, L. A., Kaufman, Y., Tanré, D., Mattoo, S., Chu, D., Martins, J. V., . . . Kleidman, R. (2005). The MODIS aerosol algorithm, products, and validation. *Journal of the atmospheric sciences, 62*(4), 947-973.

Smirnov, A., Holben, B., Eck, T., Dubovik, O., & Slutsker, I. (2000). Cloud-screening and quality control algorithms for the AERONET database. *Remote sensing of environment, 73*(3), 337-349.

Tegen, I., Lacis, A. A., & Fung, I. (1996). The influence on climate forcing of mineral aerosols from disturbed soils. *Nature, 380*(6573), 419-422.

Twomey, S. (1977). Introduction to the mathematics of inversion in remote sensing and indirect measurements, 1977. *Mineola, NY: Dover, 243*.

Twomey, S. A., Piepgrass, M., & Wolfe, T. (1984). An assessment of the impact of pollution on global cloud albedo. *Tellus B, 36*(5), 356-366.

Veefkind, J. P., de Haan, J. F., Brinksma, E. J., Kroon, M., & Levelt, P. F. (2006). Total ozone from the Ozone Monitoring Instrument (OMI) using the DOAS technique. *Geoscience and Remote Sensing, IEEE Transactions on, 44*(5), 1239-1244.

CHAPTER THREE

Direct radiative forcing of urban aerosols over Pretoria (25.75° S, 28.28° E) using AERONET Sunphotometer data: First scientific results and environmental impact

This chapter to be cited as:

Adesina, A. J., Kumar, K. R., Sivakumar, V., Griffith, D. (2014), Direct radiative forcing of urban aerosols over Pretoria (25.75° S, 28.28° E) using AERONET Sunphotometer data: First scientific results and environmental impact. *Journal of Environmental Sciences*, 2459-2474.

JOURNAL OF ENVIRONMENTAL SCIENCES 26 (2014) 2459–2474

Available online at www.sciencedirect.com

ScienceDirect

www.journals.elsevier.com/journal-of-environmental-sciences

Direct radiative forcing of urban aerosols over Pretoria (25.75°S, 28.28°E) using AERONET Sunphotometer data: First scientific results and environmental impact

Ayodele Joseph Adesina[1], *Kanike Raghavendra Kumar*[1,2,*], *Venkataraman Sivakumar*[1], *Derek Griffith*[3]

1. Discipline of Physics, School of Chemistry and Physics, College of Agriculture, Engineering and Science, Westville Campus, University of KwaZulu–Natal, Durban 4000, South Africa
2. Key Laboratory for Aerosol-Cloud-Precipitation of China Meteorological Administration, School of Atmospheric Physics, Nanjing University of Information Science and Technology, Nanjing 210044, China
3. Optronic Sensor Systems, Council for Scientific and Industrial Research (CSIR)–DPSS, Pretoria 0001, South Africa

ARTICLE INFO

Article history:
Received 8 January 2014
Revised 26 March 2014
Accepted 17 April 2014
Available online 22 October 2014

Keywords:
Pretoria
AERONET
Aerosol optical depth
Single scattering albedo
Radiative forcing

ABSTRACT

The present study uses the data collected from Cimel Sunphotometer of Aerosol Robotic Network (AERONET) for the period from January to December, 2012 over an urban site, Pretoria (PTR; 25.75°S, 28.28°E, 1449 m above sea level), South Africa. We found that monthly mean aerosol optical depth (AOD, τ_a) exhibits two maxima that occurred in summer (February) and winter (August) having values of 0.36 ± 0.19 and 0.25 ± 0.14, respectively, high-to-moderate values in spring and thereafter, decreases from autumn with a minima in early winter (June) 0.12 ± 0.07. The Angstrom exponents ($\alpha_{440\text{-}870}$) likewise, have its peak in summer (January) 1.70 ± 0.21 and lowest in early winter (June) 1.38 ± 0.26, while the columnar water vapor (CWV) followed AOD pattern with high values (summer) at the beginning of the year (February, 2.10 ± 0.37 cm) and low values (winter) in the middle of the year (July, 0.66 ± 0.21 cm). The volume size distribution (VSD) in the fine-mode is higher in the summer and spring seasons, whereas in the coarse mode the VSD is higher in the winter and lower in the summer due to the hygroscopic growth of aerosol particles. The single scattering albedo (SSA) ranged from 0.85 to 0.96 at 440 nm over PTR for the entire study period. The averaged aerosol radiative forcing (ARF) computed using SBDART model at the top of the atmosphere (TOA) was −8.78 ± 3.1 W/m^2, while at the surface it was −25.69 ± 8.1 W/m^2 leading to an atmospheric forcing of +16.91 ± 6.8 W/m^2, indicating significant heating of the atmosphere with a mean of 0.47 K/day.

Introduction

Tropospheric aerosols, also known as particulate matter (PM), are produced by both natural and anthropogenic processes. Natural sources include windblown mineral dust, precursor gases from volcanic eruptions, natural wild fires, vegetation and oceans. Anthropogenic sources include emissions from fossil fuel and bio fuel combustions, industrial processes, agricultural practices, human induced biomass burning and photochemically induced smog primarily, due to vehicle emissions (Levy et al., 2007; Tesfaye et al., 2011). Unlike greenhouse gases (GHGs), tropospheric aerosols have short life time (about few weeks or less), and

* Corresponding author. E-mail: krkumar@nuist.edu.cn (Kanike Raghavendra Kumar).

http://dx.doi.org/10.1016/j.jes.2014.04.006
1001-0742/

therefore, their spatial distribution is highly inhomogeneous and strongly correlated with their sources. Also, they vary in size by orders of magnitude and their properties change as they interact within the atmosphere (Rajeev et al., 2000). They are being removed by clouds and dry deposition processes. Despite relatively short average residence times, they travel long distances.

Atmospheric aerosols, derived from natural as well as anthropogenic emission sources, are important and significantly contribute to Earth's radiation budget through a variety of pathways such as direct effects on scattering and absorption of solar radiation, indirect effects on cloud microphysics, and semi-direct effects (Kaufman et al., 2002; Yoon et al., 2005; Ramanathan et al., 2007; Ramanathan and Carmichael, 2008; Kim et al., 2010). These aerosols are known to affect the air quality, human health and radiation budget, and understanding their climatic and environmental effects has been a central theme for the global scientific community. Most of the aerosol particles such as sulfate and sea salt, mainly scatter solar radiation, while black carbon aerosols strongly absorb radiation (Ramanathan and Carmichael, 2008). Regardless of whether the aerosol absorbs or scatters radiation, less solar radiation penetrates to the Earth's surface (Lohmann et al., 2010). Furthermore, such effects are determined by their optical, physical, radiative and chemical characteristics in concert with source, strength and/or advection by local synoptic meteorological processes.

The direct radiative effect (DRE) due to aerosols is defined as the effect of total aerosols (both natural and anthropogenic) on the radiative fluxes primarily due to the direct scattering and absorption of solar radiation by aerosols and is measured in terms of watts per square meter termed as aerosol direct radiative forcing (ADRF or simply ARF) (Chung et al., 2005; Srivastava et al., 2012). The values of radiative forcing (RF) at the bottom (RF_{BOA}) and top (RF_{TOA}) of the atmosphere are key parameters in the quantification of the impact of aerosols on climate. The ARF due to aerosols is one of the largest sources of uncertainties in estimating climate perturbations due to large spatial variability of aerosols and the lack of an adequate database on their radiative properties (IPCC, 2007). Some estimates suggest that anthropogenic aerosols and biomass burning have climate forcing enough to offset warming caused by GHGs such as carbon dioxide (Kiehl and Briegle, 1993).

According to the Intergovernmental Panel on Climate Change (IPCC, 2001) Fourth Assessment Report, the global average radiative forcing by aerosols is −1.2 W/m^2, whereas, it is about 2.6 W/m^2 for GHGs. Much attention has been paid to quantifying the radiative forcing by aerosols (Panditharai et al., 2008). Therefore, measuring and understanding changes in aerosol loading over time are highly essential to predict climate change (Tesfaye et al., 2011). For this purpose, different ground- and satellite-based remote sensing techniques are providing a systematic retrieval of aerosol optical properties on the global and regional scale (Kaufman et al., 2002; Kahn et al., 2010; More et al., 2013; Alam et al., 2014). Satellite data does not provide a complete characterization of the optical properties of aerosols, or information on their other characteristics (Eck et al., 2005). A major advance in this respect has been the introduction of the Aerosol Robotic Network (AERONET) (Holben et al., 1998), which means that satellite remote sensing of aerosols no longer needs to be largely independent but can be tied in to this coordinated and harmonised ground data network. Ground-based remote sensing has become a powerful method for characterizing atmospheric aerosols (Dubovik and King, 2000) as it is able to present a clear picture of the optical properties of each of the aerosol species (Dubovik et al., 2002; Cattrall et al., 2005).

South Africa is a developing country and lies in the extreme bottom of southern part of African continent. It has four distinct seasons; summer (December–February; DJF), autumn (March–May; MAM), winter (June–August; JJA) and spring (September–November; SON). Aerosol radiative forcing (ARF) and optical properties have not been studied in the Pretoria (PTR; 25.75°S, 28.28°E, 1449 m above sea level) (Fig. 1) region where atmospheric brown clouds (ABCs) are frequently observed (Ramanathan and Carmichael, 2008) with large amount of absorbing aerosols emitted due to biomass burning and/or forest fires which includes black carbon (Queface et al., 2011). In this study, the previously reported work by Kumar et al. (2013a) has been expanded to give detailed description of aerosol optical, microphysical and radiative properties for the first time over PTR, an urban site in the northwest part of South Africa.

The data from the AERONET Sunphotometer over PTR for one year period of 2012 has been used in the present work to study the significant changes in the aerosol properties. Here we examined the aerosol optical, microphysical and radiative properties in terms of aerosol optical depth (AOD), Ångström wavelength exponent ($\alpha_{440\text{-}870}$), particle volume size distribution, single scattering albedo (SSA), and asymmetry parameter (ASP), together with the real (Re) and imaginary (Im) parts of the complex refractive index (RI). Airmass trajectories (7-day back-trajectory) have been used to trace the source, path and spatial extent of mineral dust and smoke events using National Oceanic and Atmospheric Administration (NOAA) Hybrid Single-Particle Lagrangian Integrated Trajectory (HYSPLIT) model. Further, the monthly average ARF and forcing efficiencies were calculated using the Santa Barbara DISORT Atmospheric Radiative Transfer (SBDART) model (Ricchiazzi et al., 1998), and compared with the magnitudes derived from AERONET to know the impact on environment and climate change.

1. Experimental site, instrumentation and methods

1.1. Site description

An automatic sun/sky radiometer (Cimel Electronique, Paris, France) was set up at PTR operational since July 2011 under the joint collaboration between NASA and the Pretoria's office of Council for Scientific and Industrial Research (CSIR). PTR is one of the three capital cities of the nation, serving as the administrative capital. It is situated in a transitional belt between the plateau of the Highveld to the south and the lower lying Bushveld to the north approximately 55 km northeast of Johannesburg city in South Africa. The city has a humid subtropical climate with long hot and rainy summers, and short cool and dry winters. The major industries in PTR include the manufacture of motorcycles, chemicals, pharmaceuticals, engineering products, construction materials, steel industries, oil refineries, cement factories, and power plants. In addition to the industrial emissions, other anthropogenic sources that include vehicular emissions from main highways, coal combustion, agricultural and biomasses burning are the major local sources of aerosol in this capital city of South Africa. The aerosols derive mainly from soil or road dust, sea-salt particles from the Indian Ocean and secondary aerosols produced from biomass burning.

1.2. Measurements

Sun/sky radiometer (Model: CE318, Cimel Electronique, Paris, France), which is placed on the roof of a building to make free from tall buildings and trees, takes measurements of the direct beam and sun/sky almucantar radiance measurements provide column-integrated spectral aerosol optical depths (AODs) from 340 to 1020 nm and 440–1020 nm, respectively (Holben et al., 1998). Seven of the eight bands are used to

Fig. 1 – Satellite map showing the region of study (Pretoria) in South Africa denoted with a yellow color needle pointer and other surrounding areas. Source: Google Earth Maps.

acquire AOD data, while the eight band 940 nm is used to estimate total columnar water vapor (CWV) in the atmosphere. A careful assessment of the overall uncertainty in computed AOD due to calibration uncertainty typically for a field instrument is ±0.01 to ±0.02 which is spectral dependent with higher errors in the UV spectral range (Eck et al., 1999; Smirnov et al., 2002). Furthermore, from the almucantar measurements and the spectral deconvolution algorithm (SDA) retrievals, aerosol volume size distribution (VSD), single scattering albedo (SSA), asymmetry parameter (ASP), refractive index (RI), fine- and coarse-mode AODs are also available for large solar zenith angles (>50°) and high aerosol loading conditions (AOD440 > 0.4) (Dubovik et al., 2000). More details about the instrument, uncertainties, error estimation etc., are discussed by several earlier researchers (Holben et al., 1998; Eck et al., 1999; Dubovik et al., 2002). The data of PTR station are obtained from the AERONET website (http://aeronet.gsfc.nasa.gov/) and version 2.0/level 2.0 of the quality assured daily points' format data of direct sun and inversion products are used for the study period of January–December, 2012.

1.3. Methods to obtain AOD and inversion products

The effect of radiative transfer is proportional to the amount of particles present in the column but it also depends on their intrinsic optical properties. The spectral variation of AOD provides useful information on columnar size distribution and can be best represented by Ångström power law relationship, given by Ångström (1964):

$$\tau_a(\lambda) = \beta\lambda^{-\alpha} \quad (1)$$

where, $\tau_a(\lambda)$ is the AOD at wavelength λ (in micrometers), β is the turbidity coefficient, indicating total aerosol loading, which equals to τ_a at $\lambda = 1$ μm, and α is widely known as the Ångström exponent (AE), which is a good indicator of aerosol particle size (Eck et al., 1999). AE largely depends on aerosol size distribution and is a measure of the ratio of coarse- to fine-mode aerosols, with higher values representing increased abundance of fine-mode aerosols and lower values representing increased abundance of coarse-mode aerosols (Kumar et al., 2009; Srivastava et al., 2012).

Besides the information contained directly in the AOD and its spectral dependence, an inversion algorithm developed by Dubovik and King (2000) and subsequently modified by Dubovik et al. (2002) can be used to retrieve the columnar aerosol's characteristics from the direct sun and diffuse sky radiance measurements. In the most recent version (Version 2.0) of the inversion algorithm (Dubovik et al., 2006), the vertically averaged aerosol volume size distribution (dV/dlnr in a range of radii between 0.05 and 15 μm, the real and imaginary parts of the aerosol complex refractive index, the scattering phase function, which in turn allows computation of the asymmetry parameter (g), and the single scattering albedo (SSA) are retrieved in the inversion data products of AERONET data. The above last two quantities are crucial inputs for the radiative transfer codes used for the quantification of the aerosol's impact on radiative transfer. Another important addition in the Version 2.0 inversion products is that a new set of radiative properties is given at any AERONET station. More details and computations of these parameters were described elsewhere by many researchers to name a few, El-Metwally et al. (2011) and Esteve et al. (2014) in their respective works.

1.4. HYSPLIT trajectory model

The HYSPLIT_4 (http://www.arl.noaa.gov; Air Resources Laboratory, National Oceanic and Atmospheric Administration, USA) model is a system with simple graphical user interface for computing trajectories and air concentrations (Draxler and Hess, 1998). Gridded meteorological data at regular time intervals are used in the calculation of airmass trajectories. For back-trajectories, data are obtained from existing archives. A complete description of input data, methodology, equations involved, and sources of error for calculation of airmass trajectory can be found in Draxler and Hess (1998). The model is run directly on the web (http://www.arl.noaa.gov/ready/hysp_info.html) by giving necessary inputs or on local PC after installing the software and input data set. The executables and meteorological data are provided by the NOAA ARL (Air Resources Laboratory) for free for back-trajectory analysis and registration is required for forecast analysis. The model gives output in the form of post-script image and as well as ASCII form that can be imported in other programs for plotting.

2. Results and discussion

2.1. Synoptic meteorological conditions

The monthly mean variations of prevailing background meteorological conditions over the site (PTR) during the study period are shown in Fig. 2a–c. The data was provided by South African Weather Service (SAWS) from the surface at an altitude of 1449 m above sea level during the study period. The total annual rainfall recorded for the study period stands at 573.4 mm (Fig. 2a). The station experienced high wind speed during the spring and summer and low during the autumn and winter. The maximum value was recorded in the September of 1.6 ± 0.6 m/sec and minimum in the month of May, which is 0.5 ± 0.2 m/sec (Fig. 2b). The direction of wind is generally from the south, apart from July-August where it is from the southeast. Ambient air temperature is the lowest in June during the winter and keeps on increasing till November. It goes down a little in December and January and rose to another peak in February and thereafter, it decreases till June. The maximum air temperature at the two maxima was noticed to be 30.3°C in February and November, while the minimum of 5.5°C was recorded in June (not shown in figure). The average monthly temperature was observed high in February with a value of 24.9 ± 1.2°C and low value of 12.8 ± 2.0°C in June (see Fig. 2c). Relative humidity ranges from 36% in August to 63% in December due to an increase in diurnal temperatures (Fig. 2c). It fairly decreases from January to August and begins to rise till December.

2.2. Variabilities in aerosol optical properties

The aerosol optical depth is representative of the airborne aerosol loading in the atmospheric column, and is important

for the identification of aerosol source regions and aerosol evolution. Fig. 3a–c illustrates the monthly averaged AOD_{500}, CWV and $\alpha_{440-870}$ for twelve months (January–December 2012) in PTR with the standard deviation. A total of 333 daily averages contributed to the statistics to represent the figures. It can be easily found that AOD showed a distinct seasonal variation in this urban area with high values that mainly occurred in summer. Two maxima of AOD_{500} were recorded during the year in February (summer) and August (early of spring or late winter) with values of 0.36 ± 0.19 and 0.25 ± 0.14, respectively, while the minimum was observed in April/June (late autumn or winter) which is of 0.12 ± 0.07 (Fig. 3a). The appearance of high values of AOD_{500} in summer was related to high convective activity and contribution of dust and smoke particles emitted from surrounding regions by the long-range transport, which is clearly evident from HYSPLIT model described in the following paragraphs (Fig. 4a–d).

The occurrence of high value in urban region was also related to the anthropogenic pollution and local prevailing meteorological conditions. The high temperatures during January/February play an important role in heating ground and lifting the loose soil particles with association of wind speed (Devara et al., 2005; Yu et al., 2009; Kumar et al., 2009). Sometimes, the very high values of AOD_{500} (>0.5) noticed in the present study may possibly due to the presence of optically thin high altitude clouds over the experimental site. Further, higher AOD values particularly during the late winter months are considered to be due to combination of large-scale circulation processes and elevated temperature inversion-caused haze layer formations (Devara et al., 2005).

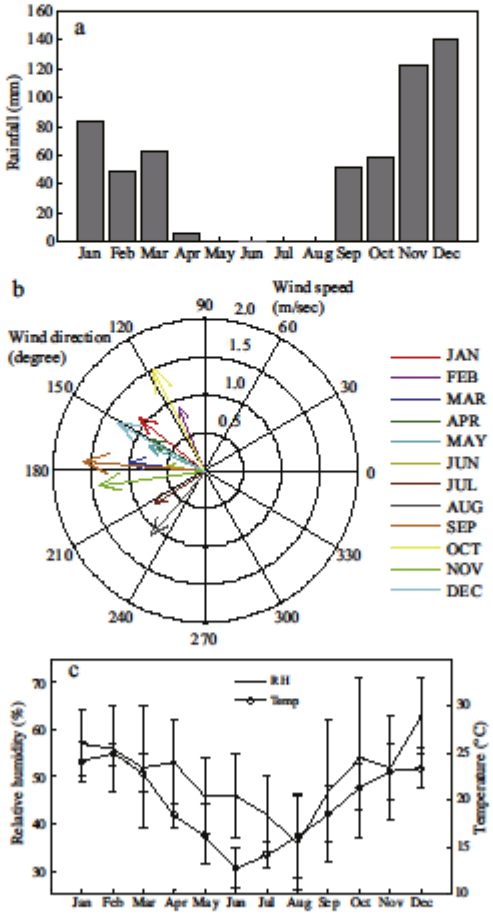

Fig. 2 – Monthly mean variations in (a) total annual rainfall, (b) polar chart representing wind speed and direction, and (c) average values of relative humidity and air temperature during the study period January–December, 2012 prevailing over Pretoria. Source: SAWS.

The decrease in AOD values has been observed during June compared to May because of dispersal of aerosol due to stronger wind speeds (see Fig. 2b), cloud-scavenging and rain-washout processes (Kumar et al., 2009).

In order to understand the origin of airmasses arriving in the studied region, we performed 7-day back-trajectory analyses based on the NOAA HYSPLIT model (Draxler and Rolph, 2003) with the GDAS as the meteorological input for the trajectory model. These trajectories are computed at three different levels 500 m, 1500 m and 3000 m above sea level. Fig. 4 represents 168 hr back-trajectories ending at observation site for typical days on 19th February, 10th April, 7th June and 7th October during four different seasons for the period of study. These trajectories are considered to be representative of the entire time period analyzed. Fig. 4a and d obtained on high AOD days during which the airmass parcels coming from the mainland of South Africa and surrounding arid/semi-arid regions traveling a short distance before reaching the measuring site. Fig. 4b, c indicates low AOD days where the trajectory at different levels has a long history originating from the pristine marine environment. These trajectories transport sea-salt (coarse) particles that get settled down before reaching the site due to their smaller residence times. Fig. 4d is obtained to show evidence of long-range transport of smoke particles emitted from biomass burning and/or forest fires traversing through Mozambique and Madagascar which occur every year during the spring season.

The CWV followed a pattern with high values in January (2.08 ± 0.32 cm) and February (2.10 ± 0.38 cm) followed by a decrease until June (0.68 ± 0.34 cm), July (0.66 ± 0.22 cm) and then an increase until December (2.00 ± 0.24 cm) (see Fig. 3b). The high (low) value of CWV which was noticed in February (July) corresponds to the high (low) aerosol loadings (AOD_{500}) which shows that AOD and CWV follow similar seasonal trend throughout the year. The correlation coefficient between CWV and AOD were found to be 0.41, which clearly suggests that aerosol particles over PTR are more hygroscopic and is consistent with the general synoptic pattern over the region. Ångström exponent (α) was a measure of the wavelength dependence of AOD and a good indicator of aerosol particle-size. It is clearly depicted from Fig. 3c that the monthly mean values of $\alpha_{440\text{-}870}$ were always greater than 1.5 throughout the year with more or less similar values in all months/seasons, except in the winter. These results signify the presence of greater contribution of aerosols in the fine-mode to the extinction for the present study period. The values range from 1.30 ± 0.26 in June to 1.70 ± 0.20 in January. The high values of both $\alpha_{440\text{-}870}$ and AOD_{500} which occurred in summer indicated that there was an increase in the contribution of fine-mode particles during the high temperature period (Lyamani et al., 2006).

In terms of seasonal variations, AOD_{500} has its peak value of 0.24 ± 0.16 in summer, followed by 0.20 ± 0.12 in spring, 0.18 ± 0.10 in winter and a low value of 0.16 ± 0.09 in autumn. This is unlike Skukuza (South Africa) or Mongu (Zambia) where the highest AOD_{500} occurred during the spring (biomass burning) season (Queface et al., 2011; Kumar et al., 2013b). We pointed out in our earlier study that this occurrence in summer in PTR can be attributed to the contribution of pollutant particles emitted from local anthropogenic sources and prevailing meteorological conditions, such as high temperature and the growth of hygroscopic particle with the increase in CWV during this period (Kumar et al., 2013a). The high value of 2.06 ± 0.32 cm for CWV was observed in summer, followed by 1.40 ± 0.50 cm in spring, 1.25 ± 0.42 cm in autumn and 0.69 ± 0.31 cm in winter. The $\alpha_{440\text{-}870}$ likewise, has its peak value of 1.67 ± 0.23 in summer, followed by 1.60 ± 0.23 in autumn, 1.52 ± 0.22 in spring and 1.41 ± 0.25 in winter.

The scatter plot of daily $\alpha_{440\text{-}870}$ versus AOD_{500} was shown in Fig. 5a; this allows one to define physically interpretable cluster regions for different types of aerosols or qualitative indication on aerosol load due to particles of different sizes (Smirnov et al., 2002; Bi et al., 2011; Sumit Kumar et al., 2011; Kumar et al., 2013b). For $AOD_{500} < 0.4$, the $\alpha_{440\text{-}870}$ values ranges between 0.8 and 1.2, a case of a mixture of both fine mode and coarse mode aerosols with dominance of fine mode aerosols. CWV and AOD_{500} shows a poor correlation ($R^2 = 0.41$) (Fig. 5b). For

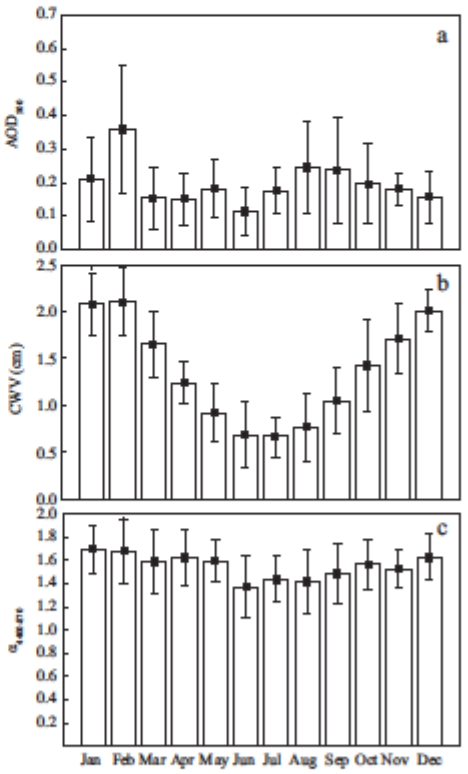

Fig. 3 – Monthly average (a) aerosol optical depth (AOD) at 500 nm, (b) columnar water vapor (CWV), and (c) Ångstrom exponent ($\alpha_{440\text{–}870}$) measured from Cimel Sunphotometer over Pretoria. The solid rectangular dot represents the mean and the vertical bars indicate the standard deviations of the mean.

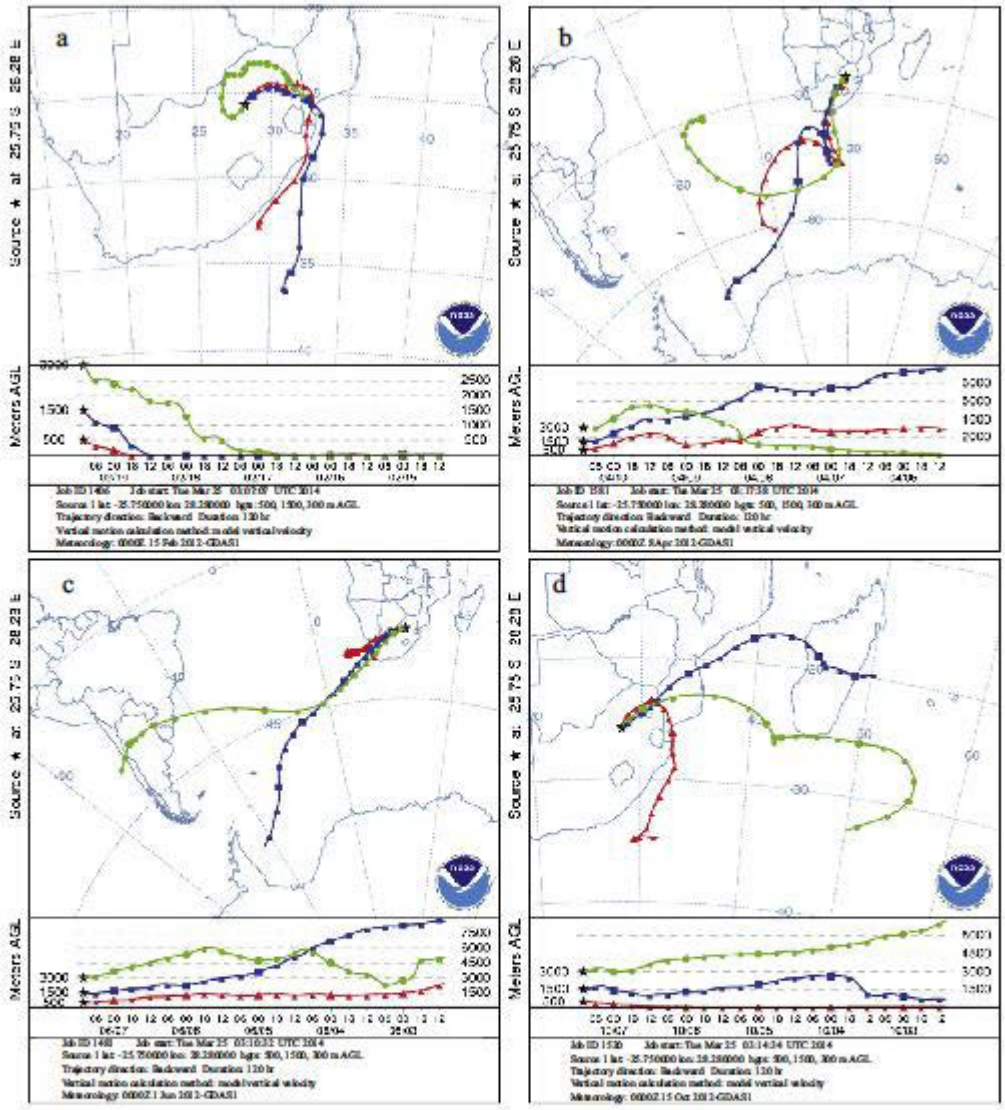

Fig. 4 – NOAA-HYSPLIT model run five-day backward trajectory analysis of airmass pathways at 500, 1500 and 3000 m altitudes on typical representative days during high AOD (a, d) and low AOD (b, c) in four different seasons over Pretoria.

AOD < 0.4, CWV ranges from 0.25 to 2.5. This may be the fact that aerosol and water vapor were being transported at different heights. Scatter plot of CWV and $\alpha_{440\text{-}870}$ which is showed in Fig. 5c has a significant correlation with coefficient of 0.55 as hygroscopic effect tends to make aerosol increase in their size.

Fig. 6 is the AOD_{500}, CWV and $\alpha_{440\text{-}870}$ showing the percentage of occurrences categorized by individual seasons. The autumn has the narrowest probability distribution with a modal value of 0.1 followed by the winter with same modal value. However, summer has the widest distribution with a modal value of 0.1 and spring has the modal value of 0.2. The highest seasonal value recorded is due to the fact that AOD_{500} of 0.2 and 0.3 values is quite appreciable forming over 40%. For $\alpha_{440\text{-}870}$, apart from summer when the modal was 1.8, the

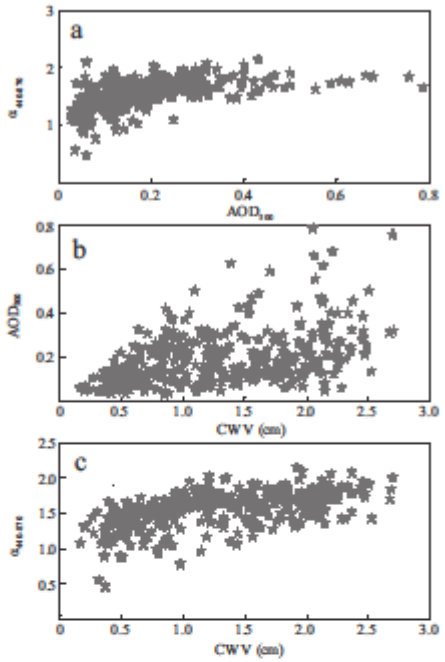

Fig. 5 – Scatter plots between different aerosol optical parameters during the study period over Pretoria.

modal value remained at 1.6 in all the seasons. The columnar water vapor ranges from 1.0–3.0 cm for summer with a modal value of 2.1 cm. The autumn and spring showed a wide distribution from 0.4–2.4 cm with a modal value of 1.2 cm, while in the winter, the range of distribution is from 0.2 to 1.5 cm with a modal of 0.5 cm.

2.3. Aerosol volume size distribution

The iterative inversion algorithm for retrieval of aerosol optical and microphysical properties including VSD, SSA, real (Re) and imaginary (Im) parts of refractive indices and asymmetry parameter (ASP) from sun and sky radiance data is contained in the work of Dubovik and King (2000). The inversion algorithm produces retrievals, which correspond to the effective optical properties for the total atmospheric column. In the retrieval algorithm, the aerosol particles are assumed to be poly-dispersed homogenous spheres (Smirnov et al., 2002). Dubovik et al. (2000) showed that the size distribution, in the case of nonspherical dust aerosols, can be retrieved reasonably well when the angular range of sky radiances is limited to angles smaller than 30°–40°. However, in order to retrieve the SSA the sky radiances acquired in the whole almucantar are needed along with the direct sun measurements. Thus for nonspherical dust aerosols, we should use the early morning or late afternoon (scattering angle range is large) sky radiance measurements to retrieve a single scattering albedo and sky radiances acquired around midday (scattering angle is small) to extract aerosol size distributions (Smirnov et al., 2002).

The aerosol VSD is an important parameter, which has an intense effect on climate. The worldwide aerosol size distribution exhibits two distinct modes: fine particles with particle size < 0.6 μm and coarse with particle size > 0.6 μm (Dubovik et al., 2002). In the present study, the AERONET VSDs (dV(r)/dlnr) are retrieved from spectral and sun radiance data using the Dubovik and King (2000) approach, with the following initial guess: $dV(r)/d\ln r = 0.0001$, $n(\lambda_i) = 1.50$, $k(\lambda_i) = 0.005$, where dV/dlnr denotes aerosol volume size distribution, and $n(\lambda_i)$ and $k(\lambda_i)$ denote real and imaginary parts of the complex refractive index at a wavelength λ_i. The AERONET aerosol size distributions are retrieved from the Sunphotometer using 22 radius size bins in the size range of 0.05–15 μm. The volume size distributions exhibit a bimodal structure, which can be characterized by the sum of two log-normal distributions as follows:

$$\frac{dV(r)}{d\ln r} = \sum_{i=1}^{2} \frac{C_{Vi}}{\sqrt{2\pi}\sigma_i} \exp\left[-\frac{(\ln r - \ln r_{Vi})^2}{2\sigma_i^2}\right] \quad (2)$$

where, σ_i is the standard deviation, r_{Vi} is the volume median radius and C_{Vi} is the volume concentration for fine and coarse modes. More information about the calculation of different quantities involved in the above Eq. (2) was described by Alam et al. (2011).

Table 1 shows the parameters of the bimodal lognormal volume size distribution which reflects the monthly mean of each parameter. The volume geometric mean radius for fine aerosol was stable at 0.15 μm throughout the autumn. This size ranges between 0.14 and 0.15 μm in the winter and spring but goes higher in the summer ranging from 0.16 μm in December and January to 0.18 μm in February. The geometric mean radius for coarse mode aerosol was the lowest in December (3.02 μm) and the highest in June (3.27 μm) corresponding to the lowest value of $\alpha_{440\text{-}870}$. The volume concentration for fine aerosol doubled between January and February; whereas in the coarse, the volume concentration in August and September is nearly double than in January. The variations in VSD over PTR were mainly attributed due to the changes in the concentration of aerosol fine mode fraction with coefficient of variation (COV), defined as standard deviation to the mean, equal to 74%. The annual average fine and coarse mode particles geometric mean radii were 0.15 ± 0.02 and 3.17 ± 0.26, respectively. The COV yielded 14% for the fine mode R_f and 10% for σ_f, while 8% and 6% for the coarse mode and σ_c, respectively.

The seasonal average VSD (dV(r)/dlnr) as shown in Fig. 7 represents a bimodal lognormal distribution with fine mode dominating at a radius of about 0.15 μm, whereas the coarse-mode is dominant with a radius of about 4 μm. The VSDs in the fine-mode are higher in the spring season than in the summer season and lower in the autumn season. The higher values in spring are due to the frequent biomass burning activities and forest fire events, whereas in the summer season it is due to the transport of mineral dust over this region and also due to meteorological conditions,

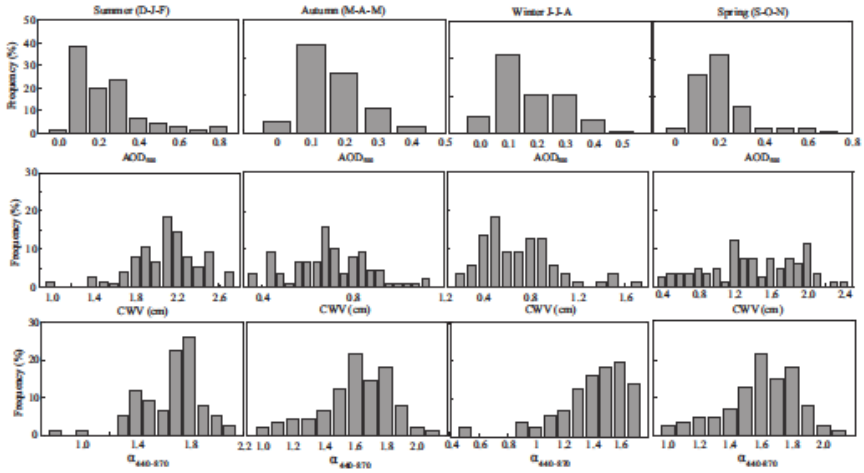

Fig. 6 – Seasonal frequency (%) distribution of AOD_{500}, CWV and $\alpha_{440-870}$.

Table 1 – Mean monthly of derived parameters from aerosol volume size distribution over Pretoria for 2012.

Month	Fine-mode				Coarse-mode			
	V_f	$R_{eff\ (f)}$	R_f	σ_f	V_c	$R_{eff\ (c)}$	R_c	σ_c
Jan-12	0.032	0.15	0.16	0.43	0.024	2.41	3.06	0.68
Feb-12	0.063	0.16	0.18	0.45	0.089	2.58	3.18	0.64
Mar-12	0.029	0.13	0.15	0.42	0.031	2.54	3.23	0.66
Apr-12	0.028	0.14	0.15	0.42	0.027	2.52	3.18	0.66
May-12	0.031	0.14	0.15	0.41	0.038	2.50	3.17	0.66
Jun-12	0.015	0.13	0.14	0.44	0.033	2.57	3.27	0.65
Jul-12	0.026	0.13	0.14	0.41	0.046	2.52	3.22	0.66
Aug-12	0.036	0.14	0.15	0.41	0.046	2.47	3.17	0.67
Sep-12	0.031	0.14	0.15	0.43	0.042	2.43	3.13	0.68
Oct-12	0.040	0.13	0.14	0.41	0.031	2.43	3.16	0.69
Nov-12	0.039	0.13	0.14	0.41	0.039	2.44	3.14	0.68
Dec-12	0.025	0.15	0.16	0.46	0.021	2.38	3.02	0.67
Mean	0.032	0.14	0.15	0.43	0.036	2.49	3.17	0.67
SD	0.024	0.02	0.02	0.04	0.015	0.24	0.26	0.04
VC	0.740	0.12	0.14	0.10	0.433	0.10	0.08	0.06

V_f, V_c ($\mu m^3/\mu m^2$) are the volume concentrations; R_{eff} (f), R_{eff} (c) (μm) are the effective radii; R_f, R_c (μm) are the volume mean radii and; σ_f and σ_c are the geometric standard deviations; all parameters for fine- and coarse-mode particles, respectively.

such as temperature and relative humidity. The VSDs in the coarse-mode are higher in winter and lower in the summer season, which is attributed to hygroscopic growth of ambient particles (Singh et al., 2004; Tripathi et al., 2005; Pandithurai et al., 2008; Alam et al., 2012). There observed a noticeable transition from the coarse-mode dominance to the fine-mode at the end of the winter season to the beginning of the spring. This may be due to the onset of the biomass burning in preparation for farming as most of the fine mode particles are anthropogenic in origin (Eck et al., 2005; Tesfaye et al., 2013). The fine-mode aerosol size distribution indicated that the fine peak radius increased from that of the spring (0.15 μm) to the summer (0.2 μm) which denoted an increase in anthropogenic aerosol concentration. Tripathi et al. (2005) reported an increase in volume concentration in the coarse-mode by 50% during summer season. Pandithurai et al. (2008) found an increase in volume size distribution in summer over Delhi, India. Wang et al. (2011) observed an increase trend in the fine-mode peak radius from summer to winter season for Kanpur AERONET site in India. Alam et al. (2011) also found an increase in volume concentration in the coarse-mode by 40%–70% during the summer season compared to the other seasons over Karachi in Pakistan.

2.4. Single scattering albedo, asymmetry parameter, refractive index

The single scattering albedo (SSA) provides important information regarding scattering and absorption properties of aerosols and is used as a key parameter for estimating ARF. The sign at the top-of-atmosphere (TOA) forcing can change depending on the aerosol SSA (Takemura et al., 2002). It has thus a vital role in understanding the climatic effects of the aerosols. SSA is defined as the ratio between the particle scattering coefficient and total extinction coefficient. The values of SSA strongly depend on the aerosol composition and size distribution (Dubovik et al., 2002). It is zero for pure absorption (*e.g.*, soot) and one for pure scattering (*e.g.*, sulfate). SSA for urban-industrial aerosol as retrieved from worldwide AERONET stations ranging from 0.90 to 0.98 and for biomass burning between 0.88 and 0.94 at lower wavelength (Dubovik et al., 2002; Eck et al., 2003a). SSA was found to be wavelength dependent due to the influence of dust and anthropogenic activities during both the summer and winter seasons. Spectral variations in the SSA differ between dust and urban anthropogenic pollution, with the SSA tending to increase rapidly with increasing wavelength during dust events but to decrease during periods of increased urban pollution (Dubovik et al., 2002).

The seasonal mean spectral variation of SSA over the period of January–December 2012 is shown in Fig. 8a and the vertical bars represent the standard deviation to the mean. It is clear from the figure that the SSA values are lower in winter and higher in summer. The maximum SSAs are found in summer and are 0.976, 0.962, 0.953, and 0.950 at 440, 675, 870 and 1020 nm, respectively. When dust is not the major contributor to the atmospheric optical state, SSA has a selective spectral dependence i.e., SSA decreases with increase in wavelength, which is clearly seen from Fig. 8a and is attributed to the presence of a mixture of aerosols from multiple sources. The SSA being greater than 0.9 for all the wavelengths during the summer suggests the abundance of anthropogenic aerosols of urban-industrial pollution which are absorbing in nature rather than scattering, while the spring time value of SSA between 0.8 and 0.9 suggests dominance of aerosols from biomass burning or forest fires. The SSA during the onset of the spring (November) was a little bit higher than 0.9 at lower wavelength which suggests that the urban aerosol tends to have more input in the aerosol loading when compared to the biomass aerosol. The winter SSA wavelength dependence is similar to that of the spring, while that of autumn is closer to the summer. It can be inferred that the fine mode aerosols prevalent over PTR originates from both urban-industrial and biomass burning sources.

The asymmetry parameter (ASP, *g*) is a simple, single-valued representation of the angular scattering and is a key property controlling the aerosol contribution to forcing. It is defined as the first moment of the particle scattering phase function for clear atmosphere. It is also defined as the intensity-weighted average cosine of the scattering angle and is expressed mathematically as follows:

$$g = \frac{1}{2}\int_0^{\pi} \cos\theta P(\theta)\sin\theta d\theta \quad (3)$$

where, θ is the angle between the transmitted and the scattered radiation and $P(\theta)$ is the phase function (angular distribution of scattered light). The value of g ranges between −1 for entirely backscattered light to +1 for entirely forward scattered light. Like the SSA, the ASP is also a spectral dependent parameter. Fig. 8b shows the spectral variation of ASP for different seasons. There is a consistent decrease in ASP values with increasing wavelengths showing the spectral dependence following a similar trend as AOD. Values of ASP decrease in the visible spectral region and slightly increase in

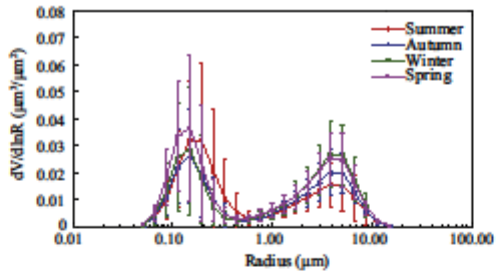

Fig. 7 – Seasonal variations with standard deviations of aerosol volume size distributions derived from sky radiance as a function of particle radiance.

the near infrared region. The average ASP value ranges from 0.71–0.67 to 0.61–0.59 at 440 and 1020 nm, respectively. The greater decrease in ASP was thus observed for the spring (September–November). The results suggest that during this period of the year, the anthropogenic (absorbing) pollutants were relatively in abundance. Similar results were reported by Pandithurai et al. (2008) and Alam et al. (2011, 2012, 2014) over urban areas in India and Pakistan, respectively.

The retrieved real (Re) and imaginary (Im) parts of complex refractive index (RI) for aerosol convey the ability of the scattering and absorption to incoming radiation. The higher real part values correspond to the scattering types and the higher imaginary values correspond to the absorbing type aerosol (Sinyuk et al., 2003). It was reported that the real and imaginary part of urban aerosol has a range of values of 1.40–1.47 and 0.009–0.14, respectively and for biomass burning, the real and imaginary parts have 1.47–1.52 and 0.009–0.02, respectively from four known regions of the world (Dubovik et al., 2002) except, for Moldova where, the imaginary refractive index is 0.0005 for all the wavelengths (Eck et al., 2003b). Fig. 9a and b shows the seasonal mean of the retrieved real and imaginary parts of the refractive indices at 440, 675, 870 and 1020 nm. For the real part, it ranges from 1.38 to 1.45 and imaginary part ranges between 0.004 and 0.024 at 440 nm with weak wavelength dependence. In the case of summer season, no significant wavelength dependence (almost flat) is observed due to the increased anthropogenic pollution over the region. In our investigation, the real (imaginary) part of refractive indices ranges between 1.44 and 1.46 (0.017–0.016) in the spring, from 1.40 to 1.39 (0.004–0.0043) in the summer, from 1.45 to 1.50 (0.023–0.015) in the winter and in the autumn it varies between 1.38 and 1.40 (0.007-0.005). The real values over PTR were highest in the winter season and lowest in the summer. The high values in winter were due to a mixture of aerosols from different sources in the study region. Our results are consistent with those obtained by Alam et al. (2012) over Karachi, Pakistan.

2.5. *Aerosol radiative forcing and efficiency:* Model vs. observations

The aerosol radiative forcing (ARF or RF) at the top-of-atmosphere (TOA) and at the bottom-of-atmosphere/surface (BOA) is defined as the net change in radiative flux (down minus up) in W/m^2 with (F_{si}) and without (F°_{si}) aerosol brought about by instantaneous change of aerosol content in the

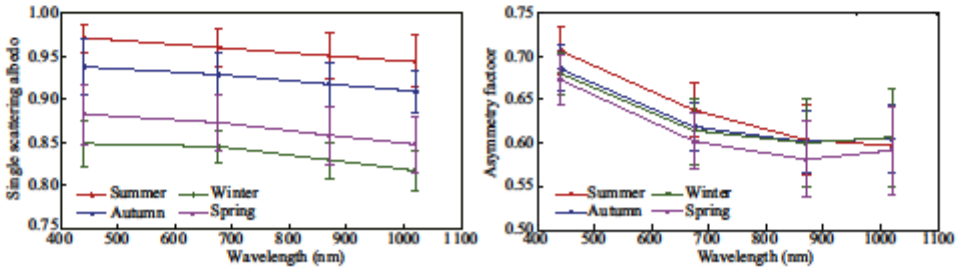

Fig. 8 – Spectral variation of single scattering albedo (SSA) (a) and asymmetry parameter (b) for four seasons.

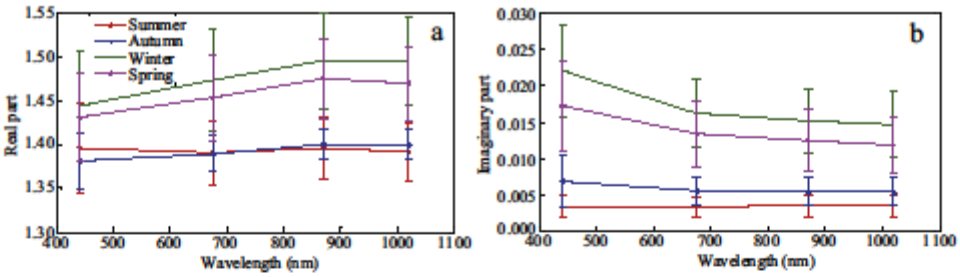

Fig. 9 – Spectral variation of the complex refractive index (a) and real part (b) imaginary part at 440 nm, 675 nm, 870 nm and 1020 nm for four seasons.

atmosphere. The radiative forcing at BOA is given by:

$$RF_{BOA} = F_{N,BOA} - F^{a}_{N,BOA}. \quad (4)$$

The radiative forcing for the atmosphere (RF_{ATM}) can be derived from the radiative forcings at TOA and BOA:

$$RF_{ATM} = RF_{TOA} - RF_{BOA}. \quad (5)$$

Basically, RF_{BOA} represents the combined effects of scattering and absorption of solar radiation by air suspended particles on the net flux at the surface, RF_{TOA} accounts for the reflection of solar radiation to space by aerosols, and RF_{ATM} for the absorption of solar radiation within the atmosphere due to absorbing particles (*e.g.*, Mallet et al., 2006). With the sign criteria adopted here, negative values of RF correspond to an aerosol cooling effect and positive values to warming. In our present study, we made use of TOA and BOA forcing values obtained directly from AERONET inversion product and also computed using Santa Barbara DISORT Atmospheric Radiative Transfer (SBDART) model (Ricchiazzi et al., 1998) to estimate atmospheric radiative forcing.

AERONET Inversion product comes with TOA and BOA representing the upward and downward fluxes measured by the Sunphotometer. These fluxes are integrated over the 0.3–4.0 μm range including their values in the absence of aerosols. All the broadband fluxes are simulated using an interpolation and extrapolation of the real and imaginary parts of the complex refractive index retrieved at AERONET wavelengths. The spectral dependence of surface reflectance is interpolated/extrapolated from surface albedo values assumed in the retrieval of the wavelengths of sun/sky radiometer. The aerosol radiative forcing efficiency (FE) which provides the actual or total radiative effects of atmospheric aerosol is defined as the rate at which the atmosphere is forced per unit of aerosol optical depth taken at a reference wavelength (500 nm, in this work) which can be calculated at both BOA (and TOA) with:

$$FE_{BOA} = RF_{BOA}/AOD_{500}. \quad (6)$$

Table 2 – Comparison of monthly mean AERONET derived and SBDART calculated aerosol radiative forcing (ARF) and forcing efficiencies at the surface (BOA) and top of the atmosphere (TOA) along with the heating rate (HR).

Month	AERONET derived ARF				SBDART calculated ARF				
	Radiative forcing (W/m^2)		Forcing efficiency (W/m^2)		Radiative forcing (W/m^2)		Forcing efficiency (W/m^2)		Heating rate (K/day)
	TOA	BOA	TOA	BOA	TOA	BOA	TOA	BOA	
Jan-12	−12.92	−22.74	−91.17	−172.58	−7.48	−17.1	−44.35	−101.41	0.27
Feb-12	−23.04	−40.76	−82.68	−159.51	−18.31	−35.44	−53.85	−104.27	0.48
Mar-12	−11.05	−22.87	−91.05	−189.59	−7.35	−18.14	−48.91	−120.74	0.30
Apr-12	−10.65	−23.07	−84.12	−196.40	−8.43	−19.35	−56.72	−130.23	0.31
May-12	−12.28	−31.24	−78.62	−210.39	−10.68	−24.20	−57.90	−131.22	0.37
Jun-12	−6.60	−22.77	−65.63	−262.34	−3.49	−20.32	−32.78	−190.56	0.47
Jul-12	−10.07	−35.78	−66.31	−247.99	−8.65	−27.28	−49.99	−157.62	0.52
Aug-12	−11.39	−49.04	−53.41	−244.97	−9.70	−37.17	−39.12	−149.93	0.77
Sep-12	−11.91	−41.99	−62.51	−231.73	−9.63	−38.60	−42.23	−169.31	0.81
Oct-12	−12.01	−36.14	−70.10	−232.60	−7.41	−30.75	−36.28	−150.59	0.65
Nov-12	−12.70	−31.05	−82.09	−207.16	−7.14	−24.35	−38.64	−131.78	0.48
Dec-12	−11.24	−21.19	−90.49	−173.56	−7.13	−15.65	−46.42	−101.89	0.23

The two factors, radiative forcing and radiative forcing efficiency are not independent of Solar Zenith Angle (SZA) and the forcing efficiency for different types of aerosol is calculated using similar ranges of SZA values (El-Metwally et al., 2011).

Recently, many earlier researchers have discussed the working principles of this model (Prasad et al., 2007; Alam et al., 2011, 2012; Srivastava et al., 2011, 2012 and references therein). A brief explanation therefore is provided in this paper. In modeling of aerosol effects on atmospheric radiation, the following aerosol optical properties like AOD, SSA, ASP were obtained from PTR AERONET site. Besides these, other input parameters include model atmospheric profile and surface albedo values were obtained from Moderate resolution Imaging Spectroradiometer (MODIS) satellite data over PTR. Another such parameter is the SZA, which is calculated by using a small code in the SBDART model specifying a particular date, time, latitude, and longitude (Alam et al., 2012).

A very good correlation was observed between AERONET derived forcing values and SBDART computed forcing magnitude (figure not shown). The correlation coefficient for the above two is 0.84 in the case of TOA, and the surface forcing is about 0.94 while the ARF stands at 0.88. The monthly variations are listed in Table 2 which shows that both AERONET and SBDART have negative TOA values for all the months which are an indication of net cooling. The TOA value ranges from −6.6 W/m^2 in June to −23 W/m^2 in February, with an annual mean value of −12.2 W/m^2 for AERONET whereas, the SBDART model computed value ranges between −3.5 W/m^2 in June to −18.3 W/m^2 in February and an annual mean of −8.8 W/m^2. The surface forcing for AERONET ranges from −21.2 W/m^2 in December to −49 W/m^2 in August with an annual mean of −31.6 W/m^2. While for SBDART, it is in the range from −15.6 W/m^2 in December to −37.2 W/m^2 in August and annual mean of −25.7 W/m^2. The resultant atmospheric forcing (ARF) values derived from AERONET range from 9.8 W/m^2 in January to 37.6 W/m^2 in August having all values positive throughout the year indicating a warming effect with an annual mean of +19.4 W/m^2 and for SBDART, it ranges from 8.5 W/m^2 in December to 29 W/m^2 in September and annual mean of +16.9 W/m^2. Although the AOD was highest in February, the results show that there is significant heating of the atmosphere between August and September/October (see Table 2) which corresponds to increase in temperatures and production of carbon from biomass burning during the spring months.

The forcing efficiency at the TOA (BOA) from AERONET ranges from −53.4 W/m^2 (−159.5 W/m^2) in August (February) to −91 W/m^2 (−262 W/m^2) in January (June) with an annual mean of −76.5 W/m^2 (−210.7 W/m^2). In the case of SBDART, the TOA (BOA) values range from −32.8 (−101.4) W/m^2 in June (January) to −57.9 W/m^2 (−190.5 W/m^2) in May (June) with an annual mean of −45.6 W/m^2 (−136.6 W/m^2) (see Table 2). An important feature of these results is that the surface level relative forcing was not governed primarily by the AOD values as reflected from the results obtained from AERONET and that calculated using SBDART unlike the work reported by Srivastava et al. (2011), where the surface forcing at Kanpur and Gandhi College (two AERONET sites in India) was primarily governed by the magnitude of AOD values. A similar comparison of RF values at BOA, TOA and ATM for different stations of urban environment over the globe is presented in Table 3.

The net atmospheric forcing given by Eq. (5) represents the amount of radiative flux absorbed by the atmosphere due to the presence of aerosols. This energy is converted into heat inside the layers containing the absorbing particles, which results in an increase of their temperature and alters regional climate (e.g., Ramanathan et al., 2007; Pilewskie, 2007). Using the basic laws of thermodynamics, the derivation of the temporal rate of this increase (atmospheric heating rate) is straightforward (Liou, 2002):

$$\frac{\partial T}{\partial t} = \frac{g}{C_p}\frac{\Delta F}{\Delta P}. \quad (7)$$

In this equation, the left hand term represents the atmospheric heating rate (HR) in K/sec where T is the temperature in Kelvin (K), t is the time in seconds (sec), g is the gravitational acceleration (9.8 m/sec^2), C_p is the specific heat capacity of dry air at constant pressure (1006 J/kg/K) and ΔP is the height of the column containing the aerosol particles expressed as the difference of atmospheric pressure between its bottom and its top. The radiative heating was therefore

Table 3 – Comparison of aerosol radiative forcing (ARF) at the surface (BOA) and top of the atmosphere (TOA) along with the heating rate (HR) derived in the present study with that of the previous studies reported over some urban stations.

Site	Study period	BOA (W/m^2)	TOA (W/m^2)	ARF (W/m^2)	HR (K/day)	Reference
Pretoria	Jan–Dec, 2012	−15 to −39	−7 to −18	+8 to +29	0.2 to 0.8	Present study
Delhi	2007	−69 to −78	–	+78 to +98	–	Srivastava et al. (2012)
Kanpur	2001–2010	−42 to −57	−12 to −18	+25 to +44	0.8 to 1.2	Kaskaoutis et al. (2013)
Hyderabad	2008–2009	−65 to −80	−17 to −23	+50 to +70	1.6 to 2.0	Sinha et al. (2013)
Bangalore	Nov 2004–May 2005	−20 to −40	+2 to +5	+20 to +45	–	Satheesh et al. (2010)
Ahmedabad	2006–2008	−31 to −41	−4 to −12	+23 to +36	0.4 to 0.6	Ramachandran and Kedia (2012)
Pune	Oct 2004–May 2005	−33 to −47	−0.5 to +0.6	+33 to +48	–	Panicker et al. (2010)
Gosan	2001–2008	−27.5	−15.8	+10 to +16	1.5 to 3.0	Kim et al. (2010)
Cairo	Oct 2004–Mar 2006	−46 to −81	−15 to −25	+29 to +45	1.3 to 2.3	El-Metwally et al. (2011)
Lahore	Mar 2009–Nov 2010	−93 to −98	−19 to −28	+70 to +74	–	Alam et al. (2014)
Spain	2003–2011	−6 to −29	−1.5 to −3.9	–	–	Esteve et al. (2014)
Nanjing	2011–2012	–	−6.9 to +4.5	–	–	Zhuang et al. (2014)

generally higher from August to October than the other months with values 0.77, 0.81 and 0.65 K/day (Table 2). The annual mean heating rate being 0.47 K/day observed for the entire study period over PTR. In terms of seasonal effect, aerosol contributes 0.33 K/day both in summer and autumn, 0.58 K/day in winter and 0.65 K/day in spring which is almost twice that of summer and autumn.

3. Summary and conclusions

Analysis of spectral aerosol optical properties and inversion retrievals of column integrated aerosol microphysical properties over the entire annual cycle was performed over an urban city (PTR) in South Africa. One year data (January–December, 2012) has been used in the present study which is obtained from the AERONET website measured using Cimel Sunphotometer to analyze the aerosol loading in association with local meteorology and estimated the atmospheric radiative forcing from SBDART model. Continuous monitoring of aerosol properties is necessary in order to assess more accurately and in characterizing the annual cycle, since only one year of data has been used in the present study. The aerosol optical depth (AOD) showed two maxima occurring in February and August with magnitude of 0.36 and 0.25, respectively, while the minimum was noticed in April/June (0.12). The seasonal average showed the highest in the summer of 0.24 and the lowest of 0.16 during the autumn. In most of the Southern African countries, the spring season is known to have the highest AOD due to seasonal changes in anthropogenic emission, meteorological conditions or specific topography of the study region.

The monthly mean Angstrom exponent $\alpha_{440\text{-}870}$ has a peak value of 1.70 in the month of January and the lowest in June of 1.38, whereas in terms of seasonal variation, the summer has its highest at 1.67 and the lowest in winter with a magnitude of 1.41. For $AOD_{500} < 0.4$, a wide range of α exist between 0.8 and 2.0 and the correlation coefficient between AOD_{500} and $\alpha_{440\text{-}870}$ is 0.52. CWV ranges between 0.3 and 2.5 with a correlation coefficient of 0.41 with AOD_{500}, while α showed a positive correlation of 0.55 with CWV.

Optical inversions of sky radiance indicate that the variation in aerosol volume size distribution (VSD) showed a bimodal lognormal distribution with dominance in aerosol fine-mode. The SSA was generally greater than 0.9 for all wavelengths during the summer, while in the spring time, SSA values fall between 0.8 and 0.9. The asymmetry parameter (ASP) ranges between 0.59 and 0.70 during most of the year suggesting that the atmosphere was not generally clean. The average atmospheric forcing computed from SBDART model during the study period was 16.91 ± 6.8 W/m^2, indicating significant heating of the atmosphere with an annual mean heating rate of 0.47 K/day over Pretoria.

Acknowledgments

The authors sincerely thank UKZN, South Africa and NUIST, China for providing enabling environment to carry out the present work. The present work is also supported through Africa Laser Centre (Pretoria) collaborative project and funded NRF bi-lateral project (Grand UID: 78682). One of the authors (AJA) acknowledges the coordinator mastering the Master's program, Fortune Shonhiwa for organizing a writing retreat as the manuscript was prepared. The author KRK thanks Prof. Yin Yan, Dr. Yiwei Diao, Dr. Na Kang and Dr. Xingna Yu for their kind and meticulous help to get settle down at NUIST, China. Authors are grateful to the PIs of AERONET site at Pretoria_CSIR_DPSS and his assistants for the upkeep of the instrument and availability of the online data. We also acknowledge the South Africa Weather Service (SAWS) for utilizing the meteorological data used in this publication. Thanks are also due to Prof. Hongxiao Tang, Editor-in-Chief of the journal and the two anonymous reviewers for their critical comments and insightful suggestions which helped to improve the clarity and scientific content of the original paper.

REFERENCES

Alam, K., Trautmann, T., Blaschke, T., 2011. Aerosol optical properties and radiative forcing over mega-city Karachi. Atmos. Res. 101 (3), 773–782.

Alam, K., Trautmann, T., Blaschke, T., Majid, H., 2012. Aerosol optical and radiative properties during summer and winter season over Lahore and Karachi. Atmos. Environ. 50, 234–245.

Alam, K., Sahar, N., Iqbal, Y., 2014. Aerosol characteristics and radiative forcing during pre-monsoon and post-monsoon seasons in an urban environment. Aerosol Air Qual. Res. 14 (1), 99–107.

Ångström, A., 1964. The parameters of atmospheric turbidity. Tellus 16 (1), 64–75.

Bi, J.R., Huang, J.P., Fu, Q., Wang, X., Shi, J.S., Zhang, W., et al., 2011. Toward characterization of the aerosol optical properties over Loess Plateau of Northwestern China. J. Quant. Spectrosc. Radiat. Transf. 112 (2), 346–360.

Cattrall, C., Reagan, J.A., Thome, K., Dubovik, O., 2005. Variability of aerosol and spectral lidar and backscatter and extinction ratios of key aerosol types derived from selected Aerosol Robotic Network locations. J. Geophys. Res. 110 (D10). http://dx.doi.org/10.1029/2004JD005124.

Chung, C.E., Ramanathan, V., Kim, D., Podgorny, I.A., 2005. Global anthropogenic aerosol direct forcing derived from satellite and ground-based observations. J. Geophys. Res. 110, D24207. http://dx.doi.org/10.1029/2005JD006356.

Devara, P.C.S., Saha, S.K., Raj, P.E., Sonbawne, S.M., Dani, K.K., Tiwari, Y.K., et al., 2005. A four-year climatology of total column tropical urban aerosols, ozone and water vapor distributions over Pune, India. Aerosol Air Qual. Res. 5 (1), 103–114.

Draxler, R.R., Hess, G.D., 1998. An overview of the HYSPLIT_4 modelling system for trajectories, dispersion and deposition. Aust. Meteorol. Mag. 47 (4), 295–308.

Draxler, R.R., Rolph, G.D., 2003. HYSPLIT Model Access via NOAA ARL READY Website (http://www.arl.noaa.gov/ready/hysplit4.html). NOAA Air Resources Laboratory, Silver Spring, MD.

Dubovik, O., King, M.D., 2000. A flexible inversion algorithm for retrieval of aerosol optical properties from Sun and sky radiance measurements. J. Geophys. Res. 105 (D16), 20673–20696.

Dubovik, O., Smirnov, A., Holben, B.N., King, M.D., Kaufman, Y.J., Eck, T.F., et al., 2000. Accuracy assessments of aerosol optical properties retrieved from Aerosol Robotic Network (AERONET)

Sun and Sky radiance measurements. J. Geophys. Res. 105 (D8), 9791–9806.
Dubovik, O., Holben, B.N., Eck, T.F., Smirnov, A., Kaufman, Y.J., King, M.D., et al., 2002. Variability of absorption and optical properties of key aerosol types observed in worldwide location. J. Atmos. Sci. 59 (3), 590–608.
Dubovik, O., Sinyuk, A., Lapyonok, T., Holben, B.N., Mishchenko, M., Yang, P., et al., 2006. Application of light scattering by spheroids accounting for particle non-sphericity in remote sensing of desert dust. J. Geophys. Res. 111, D11208. http://dx.doi.org/10.1029/2005JD006619.
Eck, T.F., Holben, B.N., Reid, J.S., Dubovik, O., Smirnov, A., O'Neill, N.T., et al., 1999. Wavelength dependence of the optical depth of biomass burning, urban and desert dust aerosols. J. Geophys. Res. 104 (D24), 31333–31349.
Eck, T.F., Holben, B.N., Reid, J.S., O'Neil, N.T., Schafer, J.S., Dubovik, O., et al., 2003a. High aerosol optical depth biomass burning events: a comparison of optical properties for different source regions. Geophys. Res. Lett. 30 (20), 2035. http://dx.doi.org/10.1029/2003GL017861.
Eck, T.F., Holben, B.N., Ward, D.E., Mukelabai, M.M., Dubovik, O., Smirnov, A., et al., 2003b. Variability of biomass burning aerosol optical characteristics in southern Africa during the SAFARI 2000 dry season campaign and a comparison of single scattering albedo estimates from radiometric measurements. J. Geophys. Res. 108 (D13), 8477. http://dx.doi.org/10.1029/2002JD002321.
Eck, T.F., Holben, B.N., Dubovik, O., Smirnov, A., Goloub, P., Chen, H.B., et al., 2005. Columnar aerosol optical properties at AERONET sites in central Eastern Asia and aerosol transport to the tropical mid-pacific. J. Geophys. Res. 110 (D6), D06202. http://dx.doi.org/10.1029/2004JD005274.
El-Metwally, M., Alfaro, S.C., Wahab, M.M.A., Favez, O., Mohamed, Z., Chatenet, B., 2011. Aerosol properties and associated radiative effects over Cairo (Egypt). Atmos. Res. 99 (2), 263–276.
Esteve, A.R., Estelles, V., Utrilla, M.P., Lozano, J.A.M., 2014. Analysis of the aerosol radiative forcing over a Mediterranean urban coastal site. Atmos. Res. 137, 195–204.
Holben, B.N., Eck, T.F., Slutsker, I., Tanre, D., Buis, J.P., Setzer, A., et al., 1998. AERONET — a federated instrument network and data archive for aerosol characterization. Remote Sens. Environ. 66 (1), 1–16.
Intergovernmental Panel on Climate Change (IPCC), 2001. Climate Change 2001: The Scientific Basis. In: Houghton, J.T., Ding, Y., Griggs, D.J., Noguer, M., van der Linden, P.J., Dai, X., et al. (Eds.), Contribution of Working Group I to the Third Assessment Report of the Intergovernmental Panel on Climate Change. Cambridge University Press, New York.
Intergovernmental Panel on Climate Change (IPCC), 2007. Climate change 2007: the physical science basis. Contribution of Working Group I to the Fourth Assessment Report of the Intergovernmental Panel on Climate Change: Chapter 2, p. 129.
Kahn, R.A., Gaitley, B.J., Garay, M.J., Diner, D.J., Eck, T.F., Smirnov, A., et al., 2010. Multiangle Imaging Spectroradiometer global aerosol product assessment by comparison with the Aerosol Robotic Network. J. Geophys. Res. 115 (D231), D23209. http://dx.doi.org/10.1029/2010JD014601.
Kaskaoutis, D.G., Sinha, P.R., Vinoj, V., Kosmopoulos, P.G., Tripathi, S.N., Misra, A., et al., 2013. Aerosol properties and radiative forcing over Kanpur during severe aerosol loading conditions. Atmos. Environ. 79, 7–19.
Kaufman, Y.J., Tanre, D., Boucher, O., 2002. A satellite view of aerosols in climate system. Nature 419 (6903), 215–223.
Kiehl, J.T., Briegle, B.P., 1993. The relative roles of sulfate aerosols and greenhouse gases in climate forcing. Science 260 (5106), 311–314.
Kim, S.W., Choi, I.J., Yoon, S.C., 2010. A multi-year analysis of clear-sky aerosol optical properties and direct radiative forcing at Gosan, Korea (2001–2008). Atmos. Res. 95 (2–3), 279–287.
Kumar, K.R., Narasimhulu, K., Reddy, R.R., Gopal, K.R., Reddy, L.S.S., Balakrishnaiah, G., et al., 2009. Temporal and spectral characteristics of aerosol optical depths in a semi-arid region of Southern India. Sci. Total Environ. 407 (8), 2673–2688.
Kumar, K.R., Sivakumar, V., Reddy, R.R., Gopal, K.R., Adesina, A.J., 2013a. Inferring wavelength dependence of AOD and Ångström exponent over a sub-tropical station in South Africa using AERONET data: Influence of meteorology, long-range transport and curvature effect. Sci. Total Environ. 461–462, 397–408.
Kumar, K.R., Adesina, A.J., Sivakumar, V., 2013b. Aerosol radiative forcing from spectral solar attenuation measurements due to aerosol loading using AERONET over Pretoria in South Africa. Proceedings of 2013 IEEE Annual International Conference on Emerging Research Areas: International Conference on Microelectronics, Communications and Renewable Energy., IEEE, Kanjirappally, Kerala, India., 1–4, June 4–6.
Levy, R.C., Remer, L.A., Dubovik, O., 2007. Global aerosol optical properties and application to moderate resolution imaging spectroradiometer: aerosol retrieval over land. J. Geophys. Res. 112, D13210. http://dx.doi.org/10.1029/2006JD007815.
Liou, K.N., 2002. An Introduction to Atmospheric Radiation. Elsevier, New York, p. 583.
Lohmann, U., Rotstayn, L., Storelvmo, T., Jones, A., Menon, S., Quaas, J., et al., 2010. Total aerosol effect: radiative forcing or radiative flux perturbation? Atmos. Chem. Phys. 10, 3235–3246.
Lyamani, H., Olmo, F.J., Alcantara, A., Alados-Arboledas, L., 2006. Atmospheric aerosols during the 2003 heat wave in south-eastern Spain I: spectral optical depth. Atmos. Environ. 40 (33), 6453–6464.
Mallet, M., Pont, V., Liousse, C., Roger, J.C., Dubuisson, P., 2006. Simulation of aerosol radiative properties with the ORISAM-RAD model during a pollution event (ESCOMPTE 2001). Atmos. Environ. 40 (40), 7696–7705.
More, S., Kumar, P.P., Gupta, P., Devara, P.C.S., Aher, G.R., 2013. Comparison of aerosol products retrieved from AERONET, MICROTOPS, and MODIS over a tropical urban city, Pune, India. Aerosol Air Qual. Res. 13 (1), 107–121.
Pandithurai, G., Dipu, S., Dani, K.K., Tiwari, S., Bisht, D.S., Devara, P.C.S., et al., 2008. Aerosol radiative forcing during dust events over New Delhi, India. J. Geophys. Res. 113, D13209. http://dx.doi.org/10.1029/2008JD009804.
Panicker, A.S., Pandithurai, G., Safai, P.D., Dipu, S., Lee, D.I., 2010. On the contribution of black carbon to the composite aerosol radiative forcing over an urban environment. Atmos. Environ. 44 (25), 3066–3070.
Pilewskie, P., 2007. Climate change: aerosols heat up. Nature 448 (7153), 541–542.
Prasad, A.K., Singh, S., Chauhan, S., Srivastava, M.K., Singh, R.P., Singh, R., 2007. Aerosol radiative forcing over the Indo-Gangetic plains during major dust storms. Atmos. Environ. 41 (29), 6289–6301.
Queface, A.J., Piketh, S.J., Eck, T.F., Tsay, S.C., Mavume, A.F., 2011. Climatology of aerosol optical properties in Southern Africa. Atmos. Environ. 45 (17), 2910–2921.
Rajeev, K., Ramanathan, V., Meywerk, J., 2000. Regional aerosol distribution and its long-range transport over the Indian Ocean. J. Geophys. Res. 105 (D2), 2029–2043. http://dx.doi.org/10.1029/1999JD900414.
Ramachandran, S., Kedia, S., 2012. Radiative effects of aerosols over Indo-Gangetic plain: environmental (urban vs. rural) and seasonal variations. Environ. Sci. Pollut. Res. 19 (6), 2159–2171.
Ramanathan, V., Carmichael, G., 2008. Global and regional climate changes due to black carbon. Nat. Geosci. 1 (4), 221–227.
Ramanathan, V., Ramana, M.V., Roberts, G., Kim, D., Corrigan, C.E., Chung, C.E., Winker, D., et al., 2007. Warming trends in Asia

amplified by brown cloud solar absorption. Nature 448 (7253), 575–578.
Ricchiazzi, P., Yang, S., Gautier, C., Sowle, D., 1998. SBDART: a research and teaching software tool for plane-parallel radiative transfer in the Earth's atmosphere. Bull. Am. Meteorol. Soc. 79 (10), 2101–2114.
Satheesh, S.K., Vinoj, V., Moorthy, K.K., 2010. Radiative effects of aerosols at an urban location in southern India: observations versus model. Atmos. Environ. 44 (39), 5295–5304.
Singh, R.P., Dey, S., Tripathi, S.N., Tare, V., Holben, B.N., 2004. Variability of aerosol parameters over Kanpur city, northern India. J. Geophys. Res. 109 (D23). http://dx.doi.org/10.1029/2004JD004966.
Sinha, P.R., Dumka, U.C., Manchanda, R.K., Kaskaoutis, D.G., Sreenivasan, S., Moorthy, K.K., et al., 2013. Contrasting aerosol characteristics and radiative forcing over Hyderabad, India due to seasonal mesoscale and synoptic-scale processes. Q. J. R. Meteorol. Soc. 139 (671), 434–450.
Sinyuk, A., Torres, O., Dubovik, O., 2003. Combined use of satellite and surface observations to infer imaginary part of the refractive index of Saharan dust. Geophys. Res. Lett. 30 (2), L1081. http://dx.doi.org/10.1029/2002GL016189.
Smirnov, A., Holben, B.N., Dubovik, O., O'Neill, N.T., Eck, T.F., Westphal, D.L., et al., 2002. Atmospheric aerosol optical properties in the Persian Gulf. J. Atmos. Sci. 59 (3), 620–634.
Srivastava, A.K., Tiwari, S., Devara, P.C.S., Bisht, D.S., Srivastava, M.K., Tripathi, S.N., et al., 2011. Pre-monsoon aerosol characteristics over the Indo-Gangetic Basin: implications to climatic impact. Ann. Geophys. 29 (4), 789–804.
Srivastava, A.K., Singh, S., Tiwari, S., Bisht, D.S., 2012. Contribution of anthropogenic aerosols in direct radiative forcing and atmospheric heating rate over Delhi in the Indo-Gangetic Basin. Environ. Sci. Pollut. Res. 19 (4), 1144–1158.
Sumit Kumar, S., Devara, P.C.S., Dani, K.K., Sonbawane, S.M., Saha, S.K., 2011. Sun-sky radiometer-derived column-integrated aerosol optical and microphysical properties over a tropical urban station during 2004–2009. J. Geophys. Res. 116, D10201. http://dx.doi.org/10.1029/2010JD014944.
Takemura, T., Nakajima, T., Dubovik, O., Holben, B.N., Kinne, S., 2002. Single-scattering albedo and radiative forcing of various aerosol species with a global three-dimension model. J. Clim. 15 (4), 333–352.
Tesfaye, M., Sivakumar, V., Botai, J., Tsidu, G.M., 2011. Aerosol climatology over South Africa based on 10 years of Multangle Imaging Spectroradiometer (MISR) data. J. Geophys. Res. 116, D20216. http://dx.doi.org/10.1029/2011JD016023.
Tesfaye, M., Botai, J., Sivakumar, V., Tsidu, G.M., 2013. Evaluation of regional climatic model simulated aerosol optical properties over South Africa using ground-based and satellite observations. ISRN Atmos. Sci. 1–17 http://dx.doi.org/10.1155/2013/237483 (Article ID: 237483).
Tirpathi, S.N., Dey, S., Chandel, A., Srivastava, S., Singh, R.P., Holben, B.N., 2005. Comparison of MODIS and AERONET derived aerosol optical depth over the Ganga Basin, India. Ann. Geophys. 23 (4), 1093–1101.
Wang, S.P., Fang, L., Gu, X.F., Yu, T., Geo, J., 2011. Comparison of aerosol optical properties from Beijing and Kanpur. Atmos. Environ. 45 (39), 7406–7414.
Yoon, S.C., Won, J.G., Omar, A.H., Kim, S.W., Sohn, B.J., 2005. Estimation of the radiative forcing by key aerosol types in worldwide locations using a column model and the AERONET data. Atmos. Environ. 39 (35), 6620–6630.
Yu, X., Zhu, B., Fan, S., Yin, Y., Bu, X., 2009. Ground-based observation of aerosol optical properties in Lanzhou, China. J. Environ. Sci. 21 (11), 1519–1524.
Zhuang, B.L., Wang, T.J., Li, S., Liu, J., Talbot, R., Mao, H.T., et al., 2014. Optical properties and radiative forcing of urban aerosols in Nanjing, China. Atmos. Environ. 83, 43–52.

CHAPTER FOUR

Variability in aerosol optical properties and radiative forcing over Gorongosa (18.97^{o}S, 34.35^{o}E) in Mozambique

This chapter to be cited as:

Adesina, A. J., Kumar, K. R., Sivakumar, V. (2014), Variability in aerosol optical properties and radiative forcing over Gorongosa (18.97^{o}S, 34.35^{o}E) in Mozambique. *Meteorology and Atmospheric Physics*, 1-12.

Meteorol Atmos Phys
DOI 10.1007/s00703-014-0352-2

ORIGINAL PAPER

Variability in aerosol optical properties and radiative forcing over Gorongosa (18.97°S, 34.35°E) in Mozambique

A. Joseph Adesina · K. Raghavendra Kumar · V. Sivakumar

Received: 6 April 2014 / Accepted: 15 October 2014

Abstract This paper reports the observational results of aerosol optical, microphysical and radiative characteristics for the time measured over Gorongosa (18.97°S, 34.35°E, 30 m asl) in Mozambique using a ground-based AERONET sun-sky radiometer. In the present study, the data recorded during the period July–December, 2012 have been used and particular attention was paid to show how aerosol loading evolves during the biomass burning season (spring) including pre- and post-months. The results reveal that the monthly mean aerosol optical depth (AOD) at 500 nm was high (low) with 0.64 ± 0.34 (0.20 ± 0.06) in September (November), while the Ångström Exponent (AE) ($\alpha_{440-870}$) decreased, except September (1.56 ± 0.26) due to increase in the fine-mode aerosol concentration produced from biomass burning. The volume size distribution (VSD) has bimodal lognormal structure and has fine-mode (coarse) maximum at a radius of 0.15 μm (3.0 μm) in September (December). The single scattering albedo (SSA) decreases with wavelength from July to October and almost stable in November and December. The imaginary (Im) refractive index (RI) showed a strong evidence of black carbon aerosol origin during the biomass burning months. Aerosol radiative forcing (ARF) computed from SBDART model shows large negative values at the surface (−89.22 W m^{-2}) and at the top (−22.36 W m^{-2}), with a higher value of atmospheric forcing (+66.87 W m^{-2}) resulting in average tropospheric heating rate of 1.88 K day^{-1} for the study period. Further, the comparison shows good agreement between the ARFs at the top and bottom of the atmosphere derived from AERONET to SBDART.

Responsible Editor: S. T. Castelli.

A. J. Adesina · V. Sivakumar
Discipline of Physics, School of Chemistry and Physics, College of Agriculture, Engineering and Science, Westville Campus, University of KwaZulu-Natal, Durban 4000, South Africa

K. R. Kumar (✉)
Key Laboratory for Aerosol-Cloud-Precipitation of China Meteorological Administration, School of Atmospheric Physics, Nanjing University of Information Science and Technology, Nanjing 210044, Jiangsu, China
e-mail: kanike.kumar@gmail.com; krkumar@nuist.edu.cn

1 Introduction

Atmospheric aerosols play an important role in the Earth's radiation budget by exerting direct and indirect radiative forcing of climate (Charlson et al. 1992; Satheesh and Moorthy 2005; Jayaraman et al. 2006; Alam et al. 2012; Sinha et al. 2013), contributing to significant heating in the troposphere (Babu et al. 2011; Alam et al. 2011) as well as affecting the hydrological cycle and precipitation rates (Rosenfeld et al. 2001; Ramanathan et al. 2001). Aerosols, which are fine particles suspended in the air, comprise of mixture of mainly sulphates, nitrates, sea salt, mineral dust and carbonaceous (organic and black carbon) particles. Black carbon (BC) is a bi-product from incomplete combustion of coal, diesel engines, biofuels and outdoor biomass burning. Biomass burning is produced from increase use of firewood for domestic fuel and clearing of forest lands for agriculture by slash and burning to meet the demands of expanding population. It produces large amounts of trace gases and aerosol particles (BC), which play a pivotal role in tropospheric chemistry and climate (Arola et al. 2007).

BC particles produced from biomass burning are of special interest as they absorb sunlight, heat the air and contribute to global warming, unlike most aerosols which reflect sunlight to space and have cooling effect (Arola et al. 2011;

Published online: 25 October 2014

Bond et al. 2013 and references therein). The main source areas of emissions of BC particles are the tropical and subtropical regions (25°S–25°N) where forest fires are associated with local and regional farming activities. More than 80 % of this burning is in the tropical regions and these submicron smoke particles may have a significant impact on climate by altering the global radiation balance (Badarinath et al. 2009; Kumar et al. 2010; Gadhavi and Jayaraman 2010). The direct radiative effect of smoke from biomass burning and the indirect effect through clouds may be of equal significance to climate (Penner et al. 1992). A high optical depth of aerosol due to biomass burning has epidemiological (as in respiratory diseases), physical (as in visibility) and climatic effects (Eck et al. 2003a; Roberts et al. 2011).

In Southern Africa, the farming activities go on mainly in the dry season with few fires in the wet season (Archibald et al. 2012). Studies show that Southern Africa savannah smoke is the most absorbing of all other major biomass burning regions (Dubovik et al. 2002). To date, there have been several studies on aerosols in southern part of Africa [Eck et al. 2003a, b, 2013; Ogunjobi et al. 2008; Sivakumar et al. 2010; Queface et al. 2011; Tesfaye et al. 2011; Kumar et al. 2013; Adesina et al. 2014 (In Press)]. To the best of our knowledge, no study yet has been conducted to characterise aerosol optical properties and estimation of aerosol radiative forcing (ARF) over Gorongosa. The present study will enable a better understanding of both the regional and local behaviour of aerosol over Mozambique region.

In this study, we used Aerosol Robotic Network (AERONET) data (Holben et al. 1998) of version 2.0 level 1.5 and the results are reported for the first time over Gorongosa in Mozambique by analysing the aerosol optical properties with the aim to investigate the monthly variations in aerosol optical depth (AOD), Ångström exponent (AE) and columnar water vapour (CWV). We also analyse the seasonal variability of volume size distribution (VSD) of aerosols, and investigate the variability of single scattering albedo (SSA), asymmetry parameter (g) as well as real (Re) and imaginary (Im) parts of the refractive index (RI). The aerosol radiative forcing (ARF) computations have been carried out using the Santa Barbara DISORT Atmospheric Radiative Transfer (SBDART) model (Ricchiazzi et al. 1998). Finally, the ARFs of AERONET and SBDART have been compared at the top and bottom of atmosphere.

2 AERONET site and instrumentation

2.1 Site description

Mozambique, lying between latitudes 10°S and 27°S and longitudes 30°E and 41°E, is a country located on the Southeast coast of Africa (see Fig. 1). It is located in the Inter-Tropical Convergence Zone (ITCZ), having a tropical climate, which makes the exact onset of seasons depend on the particular location in the country. It has two major seasons, wet season from November to March with high relative humidity and frequent rains and the dry season from April to October. The study region has been affected with strong and severe seasonal biomass burning and/or forest fires every year during dry period (September and October).

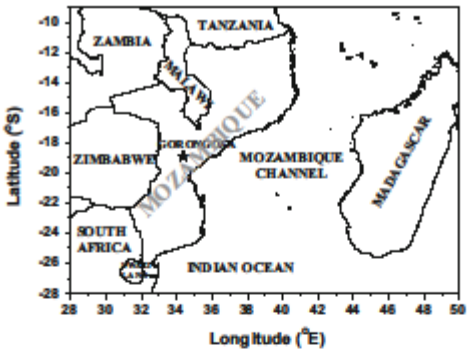

Fig. 1 Location map of the AERONET site in Mozambique along with the surrounding waters and bordering countries. The *star* denotes the geographical position of the study region (Gorongosa)

Gorongosa (18.97°S, 34.35°E, 30 m asl) is located at the southern end of the Great African Rift Valley in the heart of central Mozambique (see Fig. 1) with a National Park nestled in a 4,000 km^2 section of it and a river originates from Mount Gorongosa. It is humid with an average level of rainfall ranging between 900 mm and 1,000 mm. The average temperature in the month of June is about 28 °C and decreases to about 26 °C in July and August with a little chance of rain (figure not shown). Rain is being expected at the end of September as temperature goes to about 30 °C and by October showers are already approaching. November and December are summer months which have both rain and sun and the temperature may go up to about 32 °C on the average.

2.2 AERONET sun-sky radiometer

The observations are carried out with an AERONET sun-sky radiometer of CIMEL (CE–318) make installed on the roof top of workshop area, approximately 6 m high which is located at Chitengo camp, Gorongosa National Park surrounded with few trees in immediate vicinity. Frequent grass fires in the park from August to November and burning of waste periodically approximately 300 m away

surrounds the measurement site. AERONET is a global network of sun-sky radiometers (Holben et al. 1998). The calibrated and quality-checked data are available online at http://aeronet.gsfc.nasa.gov/. The AERONET sun-sky radiometer is being used to take measurements of both direct sun and diffuse sky radiances. The sun measurements are taken at nine wavelengths, in which eight specific wavelengths (340, 380, 440, 500, 675, 870, 940 and 1,020 nm) are used to estimate aerosol optical properties, with 940 nm bandwidth designed to retrieve CWV (Kumar et al. 2013). The sky radiance measurements are obtained at four wavelengths (440, 675, 870, and 1,020 nm) through a large range of scattering angles from the Sun (Dubovik et al. 2000, 2002). A number of studies have already described the sun-sky radiometer, data acquisition, and retrieval algorithms, calibration procedures, which confirm to the standards of the AERONET, as well as the uncertainty in final products and applied cloud-screening procedures (Holben et al. 1998, 2006; Eck et al. 1999; Dubovik and King 2000; Dubovik et al. 2002; Sumit Kumar et al. 2011; Alam et al. 2012; Kumar et al. 2013 and references within); however, a brief description is presented here.

The uncertainty in retrieval under cloud-free conditions for AOD is less than ±0.01 for the wavelengths greater than 0.44 μm and generally less than ±0.02 for shorter wavelengths, while that of sky radiance measurements are less than ±0.05 (Eck et al. 1999; Dubovik et al. 2000). The version 2.0 used in the AERONET data retrieval utilises a bidirectional reflectance distribution function (BRDF) that allows for dynamic reflectance as a function of zenith angle of the sun over land and water. AOD is obtained from the direct sun measurements while SSA, refractive indices (real and imaginary) and VSD are obtained from the inversion products. Level 1.5 AERONET data (cloud screened but not quality checked, Smirnov et al. 2002 from July to December, 2012 have been used in this study, as level 2.0 data are not available or released in the AERONET website over this site from both direct sun and inversion products. We used AOD at five wavelengths (440, 500, 675, 870 and 1,020 nm) along with AE (440–870), SSA, g and complex RI at four wavelengths (440, 675, 870 and 1,020 nm). We have also used true colour composite fire images derived from the MODIS Aqua satellite obtained for the month of September during the last one decade (2002–2013) to show evidence of increased biomass burning and forest fires over Mozambique and in Southern Africa during dry months.

2.3 NCEP/NCAR reanalysis winds

The surface wind flow patterns obtained from NCEP/NCAR (National Center for Environmental Prediction/National Center for Atmospheric Research) reanalysis with a spatial resolution of 2.5° × 2.5° at a pressure level of 850 hPa are also used to ascertain the synoptic meteorological conditions and source variability during the study period (Kalnay et al. 1996). The data have been downloaded from the website www.cdc.noaa.gov.

Table 1 Monthly mean of AOD, CWV and $\alpha_{440\text{-}870}$ along with the standard deviations from the mean

Month	AOD_{500}	CWV (cm)	$\alpha_{440\text{-}870}$
July	0.24 ± 0.12	1.88 ± 0.28	1.54 ± 0.24
August	0.40 ± 0.26	2.18 ± 0.44	1.52 ± 0.26
September	0.64 ± 0.34	2.68 ± 0.34	1.56 ± 0.26
October	0.38 ± 0.16	2.71 ± 0.59	1.48 ± 0.44
November	0.20 ± 0.06	3.06 ± 0.57	1.22 ± 0.16
December	0.24 ± 0.24	4.02 ± 0.77	0.76 ± 0.34

2.4 HYSPLIT trajectories

The Hybrid Single Particle Lagrangian Integrated Trajectory (HYSPLIT) model is the latest version of an integrated system for computing air parcel trajectories, dispersion and deposition simulations (Draxler and Rolph 2003). The 7-day time period (168 h) is applied to derive the air mass back trajectories (http://http://ready.arl.noaa.gov/HYSPLIT.php), since the typical residence time for aerosols in the lower troposphere is 5–7 days.

3 Results and discussion

3.1 Variability in aerosol optical properties and columnar water vapour

Aerosol optical properties are characterised by AOD and Angstrom exponent (AE, α), derived from a multispectral log–log linear fit to τ_a–$\lambda^{-\alpha}$ based on four wavelength range (440–870 nm) (Ångström 1961; Shaw 1983; Gupta et al. 2003; Bi et al. 2011). Table 1 shows the monthly variation of AOD at 500 nm, AE ($\alpha_{440\text{–}870}$) and CWV for the study period and the value next to ± sign represents the standard deviation of the mean. AOD which is strongly dependent on wavelength can be used to identify both the evolution and source region of aerosol as it represent the airborne particles loading in the atmospheric column (Kumar et al. 2013 and references therein). This implies that for shorter wavelengths AOD values are higher than at longer wavelengths (Kumar et al. 2013; Alam et al. 2011). Furthermore, the spectral dependence of AOD is a function of aerosol particle-size distribution (Suman et al. 2013).

It is clearly evident from Table 1 that the monthly mean values of AOD_{500} vary considerably with the highest of 0.64 ± 0.34 observed in September and the lowest of 0.20 ± 0.06 in November. The result is comparable to that of the regions Mongu and Skukuza (Queface et al. 2011; Kumar et al. 2013; Eck et al. 2013) in South Africa with identical regional climate. The AOD recorded a sharp increase from July to a maximum in September, and then decreases in October attaining a minimum value in November with a small increase in AOD again during December. The local and regional pollutants along with atmospheric convection might play a major role in the increase in AOD during December. The factors responsible for seasonal variation are the frequent biomass burning and forest fire activities during the dry period.

Fire detection and monitoring by satellite remote sensing use information of thermal sensor radiance data. To show evidence for the high aerosol loading during spring (September and October months), the fire images showing the red hot spots are obtained from NASA's EOS MODIS rapid response which delivers global hotspots or fire locations through Terra/Aqua satellites at local overpass time (https://earthdata.nasa.gov/data/near-real-time-data/rapid-response). Figure 2 shows the true colour composite maps (band 1-4-3) of active fire locations as detected by Aqua-MODIS over Mozambique at 2 km resolution at local overpass time. The first panel in the top row denotes the fire hot spot locations over Mozambique and surrounding regions in the southern part of Africa as identified by MODIS Aqua satellite for the entire month of September in 2012. Similarly, the fire locations monitored by MODIS Aqua satellite for a typical day in the month of September during 2002–2013 are also shown in Fig. 2 (a–k), except for the year 2005, as no image has been derived from MODIS Aqua sensor. It is clearly depicted from all the figures that there are large number of fire hot spots during September every year resulting from forest fires and/or biomass burning activities over Mozambique and other parts of Africa resulted an increase in the aerosol loading. In addition to this, fresh smoke particles emitted from the fires observed over Madagascar (see Fig. 2) are also transported towards the measurement site during the biomass burning period under favourable winds. Thus, the observations showing high AOD in the September month which is fairly significant with the MODIS fire maps derived from the Aqua satellite.

To understand the role of surface winds stated in the above section, synoptic wind patterns have been obtained from NCEP/NCAR reanalysis data to represent the magnitude and direction of winds for each month during the study period. The contour and length of the arrow represents the magnitude of wind speed in m s^{-1} and the direction of the arrow indicates the wind direction over the region. It is depicted from the figure that high winds in the month of September (Fig. 3c) and October (Fig. 3d) directed from easterlies transport fresh smoke particles generated at Madagascar towards the measurement site. Thus, meteorology also favours for the observed high AOD during the dry period over the study region. Furthermore, the HYSPLIT air mass back trajectories downloaded from NOAA ARL website also support for the measured high and low AODs during the study period. The back trajectories computed at three different heights 500 m, 1,500 m and 3,000 m asl for a typical day in each month from July to December, 2012 also show the possible transport of air parcels from the source region to the study location (Fig. 4a–f). During the dry months (September and October), the air mass trajectories at all levels are originated from Madagascar and the mainland of Africa taking fresh smoke particles generated from forest fires and/or biomass burning activities towards the experimental region, which results in high AOD; whereas in November and December, the air mass pathways are coming from the oceanic environment (Indian Ocean) having long trajectory history bringing coarse-mode sea-salt particles. These particles having smaller residence times settle down before reaching the measurement site resulting in low AOD.

Ångström exponent (AE, $\alpha_{440\text{-}870}$) is a function of aerosol particle size (Gadhavi and Jayaraman 2010). High values of AE indicate the dominance of fine particles, whereas low values indicate the dominance of coarse particles and relatively lower concentration of fine particles. AE was found to be high (>1.4) from July to October (Table 1) which shows the presence of fine particles and from November (1.22) it started to decrease with a low value in December (0.78) which indicates a shift to the coarse mode as the fine particles might have been removed by deposition (Suman et al. 2013). The CWV associated with the seasonality in precipitation constantly increased from July to December with the lowest value of 1.88 ± 0.28 cm in July and the highest of 4.02 ± 0.77 cm in December (see Table 1). This difference in CWV was also reported by Jayaraman et al. (1998) over polar and subtropical/tropical regions. One would expect aerosol particle to become larger due to hygroscopic growth in the presence of higher amount of water vapour (Ranjan et al. 2007), but persistence of fine particles until December implies that water vapour and aerosol may be located at different heights and are not well mixed. Also, non-hygroscopic particle will not grow in the presence of water vapour which is the case with most of BC particles.

3.2 Volume size distribution (VSD)

The size distribution of aerosols is an important parameter in understanding their effect on the climate. Figure 5 shows

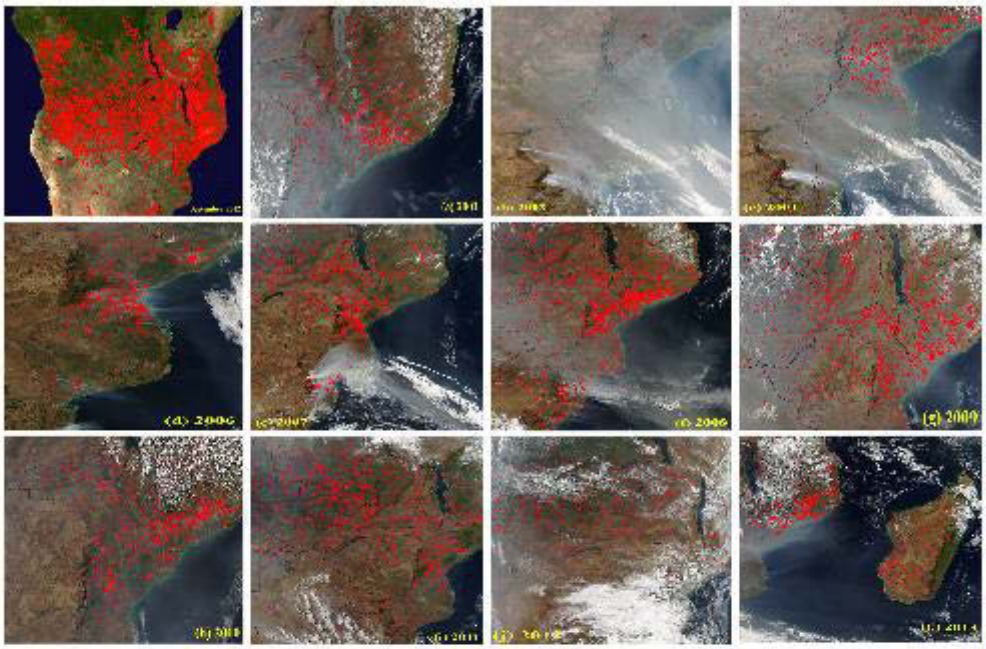

Fig. 2 True colour composite images of fire hotspots derived from Aqua-MODIS over Mozambique and its surrounding regions for the entire month of September, 2012 (First panel on the *top row*). Fresh smoke and fire hot spots detected from MODIS onboard Aqua satellite at local overpass time with 2 km resolution over Mozambique and surroundings for a typical day in the month of September during 2002–2013 (a-k)

the monthly average volume size distribution (dV/dlnR) of aerosols with vertical bars representing the standard deviation of the mean. The variations in these distributions are largely associated with changes in the amplitude and spectral dependence of the AOD. The fine mode ($r < 0.6$ μm) changes significantly, while the coarse mode ($r > 0.6$ μm) shows relative stability. The fine mode with a radius of about 0.15 μm (0.1 μm) has its highest (lowest) values in September (December), while the coarse mode with a radius of about 3.5 μm (4 μm) has its highest (lowest) values in December (July). The bimodal structure of the VSD shows that the aerosol has a mixture of coarse particles which are of sea salt or mineral dust in all the months. Similar observations have been reported by Dubovik et al. (2002) over worldwide locations.

3.3 Single scattering albedo and asymmetry parameter

The aerosol single scattering albedo (SSA), defined as the ratio between the particle scattering coefficient and total extinction coefficient, is usually used to characterise the aerosol absorption properties and is a key variable in assessing the ARF. When dust is not a major contributor to the atmospheric aerosol, the SSA decreases with wavelength (D'Almeida et al. 1991; Hess et al. 1998). In Fig. 6a, two major features of SSA spectral dependence can be observed. The SSA decreases with wavelength from July to September with intermittent values in the October month, while for November and December the spectral dependence is almost neutral except for a slight increase for the wavelengths beyond 875 nm. The above results are comparable to the work carried out by Eck et al. (2003b) at Inhaca Island, Mozambique.

The asymmetry parameter (g) is defined as the intensity-weighted average cosine of the scattering angle:

$$g = \frac{1}{2}\int_0^{\pi} \cos\theta P(\theta)\sin\theta d\theta \quad (1)$$

where θ is the angle between the incident light and scattering direction and $P(\theta)$ is the angular distribution of scattered light (the phase function). The value of g ranges

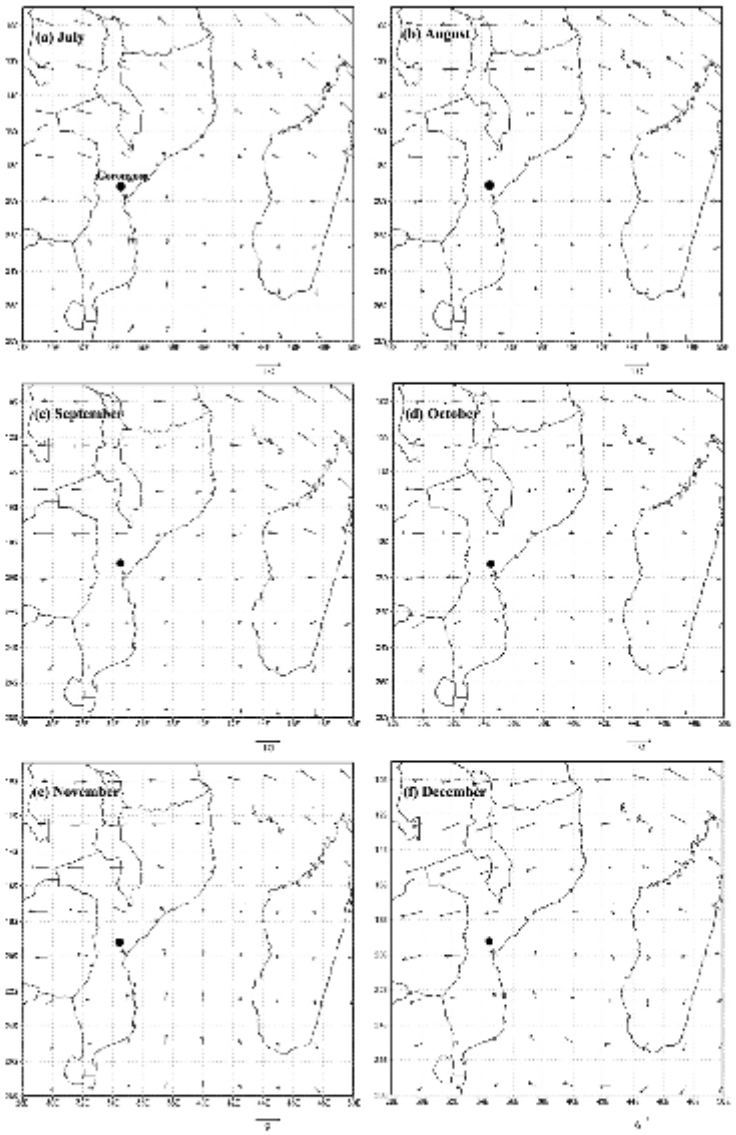

Fig. 3 NCEP/NCAR synoptic wind patterns for different months during July–December, 2012. The *black solid circles* in all the panels represent the geographical location of the study region

between −1 for entirely backscattered light to +1 for entirely forward scattered light. At 500-nm wavelength, it ranges between 0.64 and 0.83 at low relative humidity and between 0.64 and 0.82 at high relative humidity. It is a key parameter in radiative forcing and depends on both the size distribution and composition of aerosols (Andrews et al. 2006; Ramachandran and Rajesh 2008).

The asymmetry parameter (g) is spectral dependent (decrease with increasing wavelengths) as shown in Fig. 6b. The negative gradient is more pronounced in

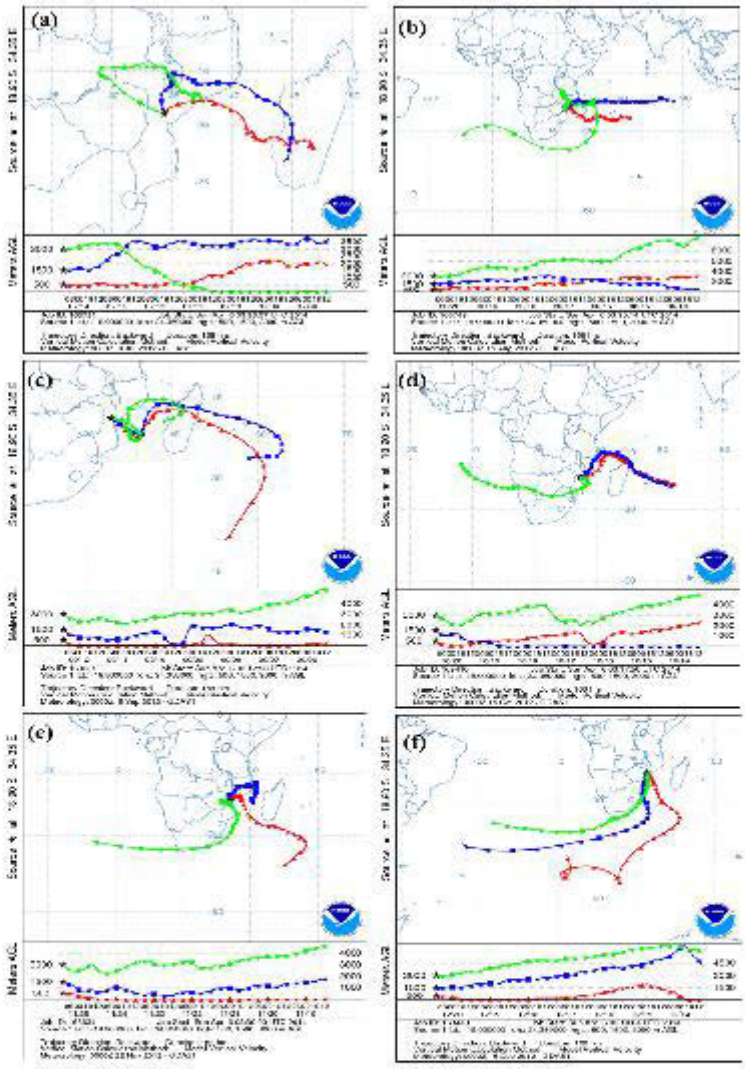

Fig. 4 HYSPLIT back trajectories representing the air mass pathways at three different heights over Gorongosa on a typical day in each month during the study period July–December, 2012 (a–f in sequence)

September where the value decreased from 0.68 ± 0.02 at 440 nm to 0.56 ± 0.06 at 1,020 nm, while in December it increased from 0.72 ± 0.03 at 440 nm to 0.73 ± 0.03 at 1,020 nm. This decrease can be seen in July and August, while it is not so pronounced in October. The decrement suggests that during July and August months anthropogenic absorbing aerosol are relative in abundance, while the increase in the near-IR region in November and December suggests the relative abundance of coarse-size particle (Alam et al. 2012; Srivastava et al. 2011).

3.4 Refractive indices

The real (Re) and imaginary (Im) parts of complex refractive indices reflect the ability of scattering and absorption to incoming radiation, respectively. The

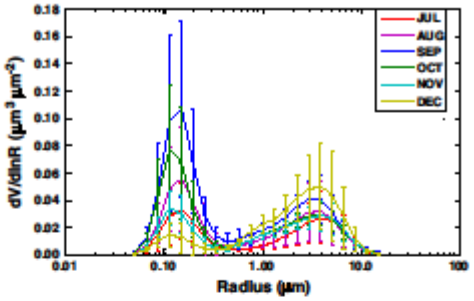

Fig. 5 Monthly variations in aerosol volume size distribution. The *vertical bars* indicate $\pm 1\sigma$ standard deviation from the mean

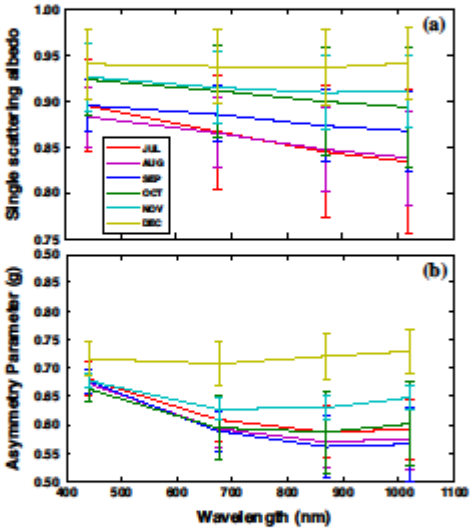

Fig. 6 Spectral variations of single scattering albedo (a) and asymmetry parameter (b) at four wavelengths during the study period

monthly average values of the real part vary within 1.43–1.48 at shorter wavelengths (440 nm) and 1.43–1.49 at longer wavelengths (1,020 nm) which is clearly shown in Fig. 7a. The average values of the imaginary part are relatively large from July to September ranging from 0.015 to 0.019 at 440 nm (Fig. 7b). This suggests that the aerosols present are absorbing type and the values range between 0.003 and 0.008 for October to December indicating coarse dust particle of reflecting type (Bi et al. 2011; Suman et al. 2013). The results support that aerosol type is of BC originated from biomass burning during September

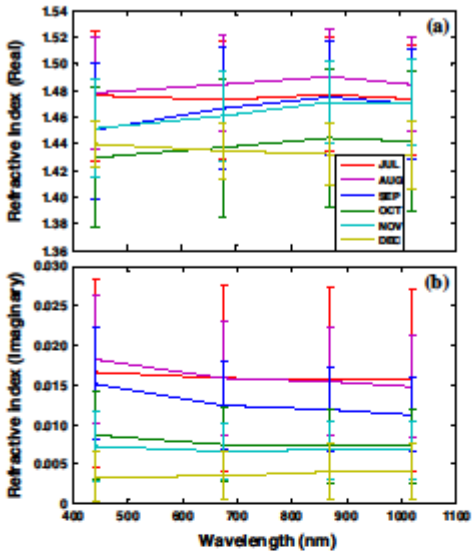

Fig. 7 Monthly mean variations of the real (a) and imaginary (b) parts of refractive indices as a function of wavelength

and October. The obtained values are comparable to the earlier published results reported by Dubovik et al. (2002) and Eck et al. (2003a) over Southern Africa.

3.5 Aerosol radiative forcing

The aerosol radiative forcing (ARF) at the top of the atmosphere (TOA) or at the surface/bottom (BOA) is defined as the difference in the net solar fluxes with and without aerosols. The difference between the BOA and TOA (BOA–TOA, in W m^{-2}) gives the radiative forcing in the complete atmosphere (ATM). In the present case, the net flux was computed in the wavelength ranging from 0.3 to 4.0 μm with and without aerosols at the TOA and at the BOA separately using the SBDART model (Ricchiazzi et al. 1998). The model SBDART is developed by Ricchiazzi et al. (1998) and is widely used by the atmospheric science community for the radiative transfer calculations (Alam et al. 2011, 2012; Sinha et al. 2013 and references therein). This model is dependent on DISORT module which is developed by Stamnes et al. (1988). In the present study, we run the model at 1-h interval for a 24-h period, and the integrated average forcing is estimated during clear sky days for every month during the period from July 2012 to December 2012 for Gorongosa. The parameters crucial for ARF estimations are AOD, SSA, ASY and surface albedo (Gadhavi and Jayaraman 2004). Other input

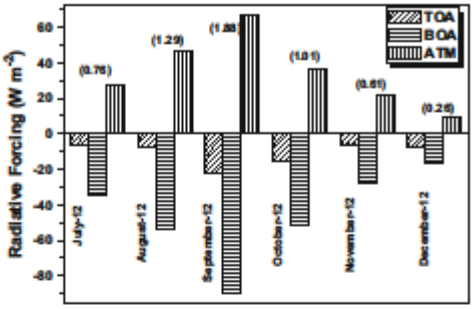

Fig. 8 Monthly averaged variations of simulated aerosol radiative forcing (W m^{-2}) at the TOA, BOA and within the atmosphere (ATM) at Gorongosa during the study period. Heating rates (K day^{-1}) are also shown in the figure within the parenthesis on the top of histograms for each month

parameters in the model include solar zenith angle, which is calculated using one small code in the SBDART (Ricchiazzi et al. 1998) by specifying a particular date, time, latitude and longitude, and atmospheric profiles (humidity, temperature, ozone and other gases). Based on the prevailing weather conditions and measured parameters, we used the mid-latitude summer atmospheric model. The AOD, SSA and ASY have been taken from the Gorongosa AERONET site and are used for the ARF calculations. The surface albedo values are obtained from the Aura OMI version 3 reflectivity data through the Giovanni online data system, developed and maintained by the NASA GES DISC (http://disc.gsfc.nasa.gov/giovanni).

The monthly average ARF variations computed from SBDART at TOA, BOA and ATM during the period of study are shown in Fig. 8. The monthly mean ARF at TOA, BOA and ATM is found to be in the range of −6 to −22 W m^{-2}, −16 to −89 W m^{-2} and +10 to +68 W m^{-2}, respectively. The averaged forcing for the entire period of observations at TOA is −11.01 W m^{-2}, while at the surface it is −45.46 W m^{-2}, leading to an atmospheric forcing of +34.45 W m^{-2}. In September 2012, the average forcing at the TOA and BOA, respectively, is −22 W m^{-2} and −89 W m^{-2}, giving rise to atmospheric forcing with an average value of +67 W m^{-2}. Likewise, the average ARF in August 2012 at BOA, TOA, and ATM is −54 W m^{-2}, −8 W m^{-2} and +46 W m^{-2}, respectively. In contrast to this, the average ARF is the minimum in the month of December 2012. The forcing at the BOA is −17 W m^{-2}, whereas, −7 W m^{-2} at the TOA and it is +9 W m^{-2} in the atmosphere.

The large differences in ARF between TOA and BOA demonstrate that solar radiation is absorbed within the atmosphere, consequently heating the atmosphere, reducing eddy heat convergence, and inducing a reduction in surface temperature (Ge et al. 2010). Furthermore, heating due to absorption of solar radiation by aerosols reaches its maximum close to its uppermost level where the heating is stabilised, which in turn may suppress convective activity and prevent cloud formation (Ackerman et al. 2000; Koren et al. 2004). The ARF values are the highest for the month of September 2012 due to the frequent biomass burning activities and local anthropogenic activities. It can be concluded that the presence of BC aerosols over Mozambique can considerably decrease at the BOA and TOA forcing and enhance the atmospheric forcing. Alam et al. (2011) reported over Karachi that the ARF at the TOA, BOA and ATM is in the range of −7 to −35 W m^{-2}, −56 to −96 W m^{-2} and +38 to +61 W m^{-2}, respectively. Ge et al. (2010) found the surface forcing ranging from −7.9 to −35.8 W m^{-2} over Northwestern China. Kim et al. (2005) also estimated the ARF which lies between −13 and −43 W m^{-2} for three ground sites in Eastern Asia, which is lower than the results obtained in the present study.

The atmospheric heating rate can be estimated by following Liou (2002) as

$$\frac{\partial T}{\partial t} = \frac{g}{C_P}\frac{\Delta F_{ATM}}{\Delta P} \quad (2)$$

where $\partial T/\partial t$ is the heating rate (°K day^{-1}), g is the acceleration due to gravity, ΔF_{ATM} is the atmospheric heating, C_p is the specific heat capacity of air at constant pressure and ΔP is the atmospheric pressure. The average heating rate (°K day^{-1}) over Gorongosa during the winter and spring, respectively, is 1.03 and 1.17 (see Fig. 8). The maximum heating rate noticed in the month of September (1.88 K day^{-1}) was attributed to high atmospheric absorption due to increase in the concentration of BC aerosols generated from biomass burning activity.

Table 2 shows comparisons of ARFs obtained at the BOA and TOA from AERONET to SBDART calculations. The forcing at the TOA is higher in magnitude for AERONET as compared to SBDART during the study period and comparable for the month of December. Likewise, the forcing at the BOA is higher (more negative) in September for SBDART than the AERONET, whereas for other months the forcing at BOA for AERONET and SBDART is almost nearly comparable. The correlation coefficient (R^2) for the whole period of observation for AERONET vs. SBDART at the BOA and TOA is 0.95 and 0.97, respectively. Overall, the comparison shows a convincing agreement for the radiative forcing at the BOA and TOA obtained from AERONET to SBDART. A significant difference has been revealed between the two values as this is due to assumption of inputs in the SBDART model.

Table 2 Comparison of ARFs of AERONET and SBDART at the BOA and TOA over Gorongosa during the study period

Month	SBDART calculated ARF		AERONET derived ARF	
	TOA ($W\ m^{-2}$)	BOA ($W\ m^{-2}$)	TOA ($W\ m^{-2}$)	BOA ($W\ m^{-2}$)
July	−6.99	−34.05	−11.02	−41.36
August	−7.67	−53.73	−14.83	−58.98
September	−22.36	−89.22	−20.33	−80.11
October	−15.46	−51.37	−22.16	−66.03
November	−6.01	−27.66	−13.16	−33.59
December	−7.53	−16.71	−9.36	−21.43

4 Conclusions

The monthly variability in the aerosol optical and microphysical properties over Gorongosa is very significant to understand the impact of fine aerosols produced from biomass burning on regional atmosphere and climatic forcing, although the data size (6 months) is not sufficient to establish definite aerosol climatology of the region. The major findings in the present study can be summarised as follows:

The monthly mean AOD_{500} ranges between 0.20 ± 0.06 and 0.64 ± 0.34, attaining peak in September and the CWV ranges between 1.88 ± 0.28 and 4.02 ± 0.77 increasing constantly during the study period. The Ångström exponent increased from July with its maximum of 1.56 ± 0.26 in the month of September implying the dominance of fine-mode aerosol and started to decrease from October (1.48 ± 0.44) onwards through December (0.76 ± 0.34) showing an increasing dominance of coarse-mode aerosol (relatively smaller amount of fine aerosol). The AODs obtained from AERONET are compared with MODIS-retrieved AODs computed for the same wavelength and the correlation coefficient R^2 was found to be 0.80 and 0.89 for Terra and Aqua-MODIS, respectively, during the study period.

The volume size distribution (VSD) of aerosols showed a bimodal lognormal structure with fine aerosol having the radius between 0.1 and 0.2 μm and the coarse mode from 2.0 to 6.0 μm. The fine mode remains higher from August to October, while the coarse mode is higher in December. The SSA ranges between 0.87 and 0.94 in the wavelength region (440–670 nm) and decreased in wavelength from July to October because of the relative abundance of fine aerosol (absorbing in nature) generated from biomass burning events. The asymmetry parameter decreases with wavelength in the visible region from July to October and increases in near-IR during November and December indicating a shift in dominance from fine-mode to coarse-mode aerosols. The real and imaginary refractive indices indicated the presence of mixed type of aerosols over the study region. The optical state of the atmosphere over the measurement region dominated with absorbing aerosol for the study period especially in the months from July to September, as the imaginary refractive index lies above 0.01.

The present investigation also carried out to study the effect of aerosols on shortwave radiative forcing over Gorongosa using SBDART model. The average forcing for the entire study period was found to be $-11.01\ W\ m^{-2}$ at TOA, $-45.46\ W\ m^{-2}$ at BOA and ARF of $+34.45\ W\ m^{-2}$ with an average heating rate of $0.97\ K\ day^{-1}$ for period July–December, 2012. Finally, the comparison shows good agreement between the ARFs at the BOA and TOA obtained from AERONET to SBDART.

Acknowledgments The authors sincerely thank UKZN, South Africa and NUIST, China for providing enabling environment and infrastructure support to carry out the present work. This work was partly supported by the National Research Foundation (NRF–South Africa) bi-lateral research grant (UID: 78682). Authors are indebted to the AERONET team of NASA, USA for their efforts in making the data available online. We gratefully acknowledge Prof. Brent N. Holben, PI and Dr. Marc Stalmans, site manager of Gorongosa site and their staff effort in establishing and maintaining AERONET site related to this investigation. One of the authors KRK expresses profound gratitude to Yan Yin, Diao Yiwei, Na Kang, Xingna Yu and Liang Xuewei for their support and cooperation. The authors would like to thank the editor and the two anonymous reviewers for their insightful comments and constructive suggestions which in turn helped to improve the clarity and scientific content of the original paper.

References

Ackerman AS, Toon OB, Stevens DE, Heymsfield AJ, Ramanathan V, Welton EJ (2000) Reduction of tropical cloudiness by soot. Science 288:1042–1047

Adesina AJ, Kumar KR, Sivakumar V, Griffith D (2014, In Press) Direct radiative forcing of urban aerosols over Pretoria (25.75°S, 28.28°E) using AERONET Sunphotometer data: first scientific results and environmental impact. J Environ Sci (in press)

Alam K, Trautmann T, Blaschke T (2011) Aerosol optical properties and radiative forcing over mega-city Karachi. Atmos Res 101: 773–782

Alam K, Trautmann T, Blaschke T, Majid H (2012) Aerosol optical and radiative properties during summer and winter season over Lahore and Karachi. Atmos Environ 50:234–245

Andrews R, Sheridan P, Fiebig M, McComiskey A, Ogren J, Arnott P et al (2006) Comparison of methods for deriving aerosol asymmetry parameter. J Geophys Res 111(D5). doi:10.1029/2004JD005734

Ångström A (1961) Techniques of determining the turbidity of the atmosphere. Tellus 13:214–223

Archibald S, Staver AC, Levin SA (2012) Evolution of human driven fire regimes in Africa. Proc Natl Acn Sci 109(3):847–852

Arola A, Lindfors A, Natunen A, Lehtinen KEJ (2007) A case study on biomass burning aerosols: effects on aerosol optical and surface radiation levels. Atmos Chem Phys 7:4257–4266

Arola A, Schuster G, Myhre G, Kazadzis S, Dey S, Tripathi S (2011) Inferring absorbing organic carbon content from AERONET data. Atmos Chem Phys 11(1):215–225

Babu SS, Moorthy KK, Manchanda RK, Sinha PR, Satheesh SK, Prasad VD, Srinivasan S, Arunkumar VH (2011) Free tropospheric black carbon aerosol measurements using high altitude balloon: Do BC layers build 'their own homes' up in the atmosphere? Geophys Res Lett 38(L08803). doi:10.1029/2011GL046654

Badarinath KVS, Latha KM, Chand TRK, Gupta PK (2009) Impact of biomass burning on aerosol properties over tropical wet evergreen forests of Arunachal Pradesh, India. Atmos Res 91:87–93

Bi J, Huang J, Fu Q, Wang X, Shi J, Zhang W et al (2011) Toward characterization of the aerosol optical properties over Loess Plateau of Northwestern China. J Quant Spec Rad Trans 112(2):346–360

Bond TC, Doherty SJ, Fahey DW, Forster PM, Berntsen T, De Angelo BJ, Flanner MG, Ghan S, et al. (2013) Bounding the role of black carbon in the climate system: a scientific assessment. J Geophys Res 118. doi:10.1002/jgrd.50171

Charlson RJ, Schwartz SE, Hales JH, Cess RD, Coakley JA Jr, Hansen JE, Hofmann DJ (1992) Climate forcing by anthropogenic aerosols. Science 255:423–430

D'Almeida GA, Koepke P, Shettle EP (1991) Atmospheric aerosols: Global climatology and radiative characteristics (studies in geophysical optics and remote sensing). A Deepak Publishing, Hampton

Draxler RR, Rolph GD (2003) HYSPLIT (HYbrid Single-Particle Lagrangian Integrated Trajectory) Model access via NOAA ARL READY Website (http://www.arl.noaa.gov/ready/hysplit4.html) NOAA Air Resources Laboratory, Silver Spring, MD, USA

Dubovik O, King MD (2000) A flexible inversion algorithm for retrieval of aerosol optical properties from sun and sky radiance measurements. J Geophys Res 105:20673–20696

Dubovik O, Smirnov A, Holben BN, King MD, Kaufman YJ, Eck TF, Slutsker I (2000) Accuracy assessments of aerosol optical properties retrieved from aerosol robotic network (AERONET) sun and sky radiance measurements. J Geophys Res 105:9791–9806

Dubovik O, Holben BN, Eck TF, Smirnov A, Kaufman YJ, King MD et al (2002) Variability of absorption and optical properties of key aerosol types observed in worldwide locations. J Atmos Sci 59(3):590–608

Eck TF, Holben BN, Reid JS, Dubovik O, Smirnov A, O'Neill NT et al (1999) Wavelength dependence of the optical depth of biomass burning urban and desert dust aerosols. J Geophys Res 104:31333–31350. doi:10.1029/1999JD900923

Eck TF, Holben BN, Ward D, Mukelabai M, Dubovik O, Smirnov A et al (2003a) Variability of biomass burning aerosol optical characteristics in southern Africa during the SAFARI 2000 dry season campaign and a comparison of single scattering albedo estimates from radiometric measurements. J Geophys Res 108(D13). doi:10.1029/2002JD002321

Eck TF, Holben BN, Reid J, O'Neill N, Schafer J, Dubovik O et al (2003b) High aerosol optical depth biomass burning events: a comparison of optical properties for different source regions. Geophys Res Lett 30(20). doi:10.1029/2003GL017861

Eck TF, Holben BN, Reid JS, Mukelabai MM, Piketh SJ, Torres O, Jethva HT et al (2013) A seasonal trend of single scattering albedo in southern African biomass-burning particles: implications for satellite products and estimates of emissions for the World's largest biomass-burning source. J Geophys Res 118:6414–6432. doi:10.1002/jgrd.50500

Gadhavi H, Jayaraman A (2004) Aerosol characteristics and aerosol radiative forcing over Maitri, Antarctica. Curr Sci 86:296–304

Gadhavi H, Jayaraman A (2010) Absorbing aerosols: contribution of biomass burning and implications for radiative forcing. Anna Geophys 28:103–111

Ge JM, Su J, Ackerman TP, Fu Q, Huang JP, Shi JS (2010) Dust aerosol optical properties retrieval and radiative forcing over northwestern China during the 2008 China-US joint field experiment. J Geophys Res 115(D00k12). doi:10.1029/2009JD013263

Gupta P, Gadhavi H, Jayaraman A (2003) Aerosol optical depth variation observed using sun-photometer over Indore. Ind J Rad Spac Phys 32:229–237

Hess M, Koepke P, Schult I (1998) Optical properties of aerosols and clouds: the software package OPAC. Bull Amer Meteo Soc 79:831–844

Holben BN, Eck TF, Slutsker I, Tanre D, Buis J et al (1998) AERONET: a federated instrument network and data archive for aerosol characterization. Rem Sens Environ 66(1):1–16

Holben BN, Eck TF, Slutsker I, Smirnov A, Sinyuk A, Schafer JS, et al. (2006) Aeronet's Version 2.0 quality assurance criteria. Proc SPIE 6408(64080Q). doi:10.1117/12.706652

Jayaraman A, Lubin D, Ramachandran S, Ramanathan V, Woodbridge E, Collins WD, Zalpuri KS (1998) Direct observations of aerosol radiative forcing over the tropical Indian Ocean during the January–February 1996 pre-INDOEX cruise. J Geophys Res 103:13827–13836

Jayaraman A, Gadhavi H, Ganguly D, Misra A, Ramachandran S, Rajesh TA (2006) Spatial variations in aerosol characteristics and regional radiative forcing over India: measurements and modelling of 2004 road campaign experiment. Atmos Environ 40:6504–6515

Kalnay E, Kanamitsu M, Kistler R, Collins W et al (1996) The NCEP/NCAR reanalysis 40-year project. Bull Amer Meteo Soc 77:437–471

Kim DOH, Sohn BJ, Nakajima T, Takamura T (2005) Aerosol radiative forcing over east Asia determined from ground-based solar radiation measurements. J Geophys Res 110(D10S22). doi:10.1029/2004JD004678

Koren I, Kaufman YJ, Remer LA, Martins JV (2004) Measurement of the effect of Amazon smoke on inhibition of cloud formation. Science 303:1342–1345

Kumar KR, Narasimhulu K, Balakrishnaiah G, Reddy LSS, Gopal KR, Reddy RR, Satheesh SK, Moorthy KK, Babu SS (2010) A study on the variations of optical and physical properties of aerosols over a tropical semi-arid station during grassland fire. Atmos Res 95:77–87

Kumar KR, Sivakumar V, Reddy RR, Gopal KR, Adesina AJ (2013) Inferring wavelength dependence of AOD and Ångström exponent over a sub-tropical station in South Africa using AERONET data: influence of meteorology, long-range transport and curvature effect. Sci Tot Environ 461–462:397–408

Liou KN (2002) An Introduction to atmospheric radiation. Elsevier, New York, p 583

Ogunjobi K, He Z, Simmer C (2008) Spectral aerosol optical properties from AERONET Sunphotometric measurements over West Africa. Atmos Res 88(2):89–107

Penner JE, Dickinson RE, O'Neill CA (1992) Effects of aerosol from biomass burning on the global radiation budget. Science 256:1432–1434

Queface AJ, Piketh SJ, Eck TF, Tsay SC, Mavume AF (2011) Climatology of aerosol optical properties in Southern Africa. Atmos Environ 45:2910–2921

Ramachandran S, Rajesh TA (2008) Asymmetry parameters in the lower troposphere derived from aircraft measurements of aerosol scattering coefficients over tropical India. J Geophys Res 113(D16). doi:10.1029/2008JD009795

Ramanathan V, Crutzen PJ, Kiehl JT, Rosenfeld D (2001) Aerosol, climate, and the hydrological cycle. Science 294:2119–2124

Ranjan RR, Joshi HP, Iyer KN (2007) Spectral variation of total column aerosol optical depth over Rajkot: a tropical semi-arid Indian station. Aero Air Qual Res 7:33–45

Ricchiazzi P, Yang S, Gautier C, Sowle D (1998) SBDART: a research and teaching software tool for plane-parallel radiative transfer in the earth's atmosphere. Bull Amer Met Soc 79:2101–2114

Roberts JM, Veres PR, Cochran AK, Warneke C, Burling IR, Yokelson RJ et al (2011) Isocyanic acid in the atmosphere and its possible link to smoke related health effects. Proc Natl Aca Sci 108(22):8966–8971

Rosenfeld D, Rudich Y, Lahav R (2001) Desert dust suppressing precipitation: a possible desertification feedback loop. Proc Natl Acad Sci USA 98:5975–5980

Satheesh SK, Moorthy KK (2005) Radiative effects of natural aerosols: a review. Atmos Environ 39:2089–2110

Shaw GE (1983) Sun photometry. Bull Amer Meteo Soc 64:4–10

Simmov A, Holben BN, Dubovik O, O'Neill NT, Eck TF, Westphal DL et al (2002) Atmospheric aerosol optical properties in the Persian Gulf. J Atmos Sci 59(3):620–634

Sinha PR, Dumka UC, Manchanda RK, Kaskaoutis DG, Sreenivasan S, Moorthy KK, Babu SS (2013) Contrasting aerosol characteristics and radiative forcing over Hyderabad, India due to seasonal mesoscale and synoptic-scale processes. Quar J Roy Meteo Soc 139:434–450

Sivakumar V, Tesfaye M, Alemu W, Sharma A, Bollig C, Mengistu G (2010) Aerosol measurements over South Africa using satellite, sun-photometer and LIDAR. Adv Geosci 16:253–262

Srivastava A, Tiwari S, Devara PCS, Bisht D, Srivatsava MK, Tripathi S et al (2011) Pre-monsoon aerosol characteristics over the Indo-Gangetic Basin: implications to climatic impact. Ann Geophys 29:789–804

Stamnes K, Tsay S, Wiscombe W, Jayaweera K (1988) Numerically stable algorithm for discrete-ordinate-method radiative transfer in multiple scattering and emitting layered media. Appl Opt 27:2502–2509

Suman MNS, Gadhavi H, Kiran VR, Jayaraman A, Rao SVB (2013) Role of coarse and fine mode aerosols in MODIS AOD retrieval: a case study. Atmos Meas Tech Diss 6:9109–9132

Sumit Kumar, Devara PCS, Sonbawne S, Saha S (2011) Sun-sky radiometer derived column integrated aerosol optical and physical properties over a tropical urban station during 2004–2009. J Geophys Res 116(D10201). doi:10.1029/2010JD014944

Tesfaye M, Sivakumar V, Botai J, Tsidu GM (2011) Aerosol climatology over South Africa based on 10 years of Multiangle Imaging Spectroradiometer (MISR) data. J Geophys Res 116(D20216). doi:10.1029/2011JD16023

CHAPTER FIVE

Assessment of satellite derived aerosol optical depth over two contrasting regions in South Africa: Trend estimation and characteristics of absorption aerosols

This chapter to be cited as

Adesina, A. J., Kumar, K. R., Sivakumar, V. (2015), Assessment of satellite derived aerosol optical depth over two contrasting regions in South Africa: Trend estimation and characteristics of absorption aerosols (To be submitted for review– Journal of Atmospheric Research).

Assessment of satellite derived aerosol optical depth over two contrasting regions in South Africa: Trend estimation and characteristics of absorption aerosols

A. Joseph Adesina[1], K. Raghavendra Kumar[2] and V. Sivakumar[1]

[1]*Disicipline of Physics, School of Chemistry and Physics, University of KwaZulu-Natal, Durban 4000, South Africa*

[2]*Key Laboratory of Aerosol-Cloud-Precipitation of China Meteorological Administration, School of Atmospheric Physics, Nanjing University of Information Science and Technology, Nanjing 210044, China*

ABSTRACT

To build a long term database and improve on the accuracy of the satellite products used for aerosol studies, there is a need to periodically carry out intercomparison and validation of these instruments with ground-based instruments. Using the ground-based instrument of Aerosol Robotic Network (AERONET) at Skukuza, we have carried out the validation of Multiangle Imaging Spectroradiometer (MISR) and Moderate Resolution Imaging Spectroradiometer (Terra and Aqua) level 3 Aerosol optical depth (AOD) products using the data for the year 2010. We also calculated and carried out regression analysis on these satellite products using a 10 years dataset (2004–2013) to evaluate their performance at a hinterland and coastland. The validation showed that MISR was better correlated with AERONET having a coefficient of determination (R^2) of 0.94, and MODIS-Terra and Aqua with R^2=0.68 and 0.77, respectively. The long term regression analysis at the two selected locations showed MODIS products underestimating MISR. At the hinterland, MISR showed an increasing trend while MODIS Terra and Aqua products showed a decreasing trend over the study period. While at the coastland, MISR showed negative and positive trends with Terra and Aqua MODIS, respectively. When the two MODIS products were compared, they were better correlated at the coastland (R^2=0.66) than hinterland (R^2=0.59). When they compared based on seasonal variations, they were better correlated in the winter season in both locations than any other seasons. Further, the Ozone Monitoring Instrument (OMI) Ultra-Violet Aerosol Index (UVAI) which was used to monitor the absorption property of aerosols over the two locations showed an increasing trend with 0.0089/yr at hinterland and 0.0022/yr at coastland.

Key Words: MISR; MODIS; OMI; Aerosol optical depth; Aerosol index.

1. INTRODUCTION

As efforts are being made to unravel the actual role aerosol plays in influencing our climate, there is the need to study aerosol properties using a coordinated platform of instruments. When this is done contributions from various instruments like satellite, surface (ground) measurements and models employed will enhance the study of aerosols (Kahn et al., 2010; Kaufman et al., 2005). Though the surface-based instruments can measure aerosol properties to a very good accuracy, there is the disadvantage of limitation in spatial coverage and long term measurements which are readily provided for by satellite-based instruments (Hansen et al., 1997; Kaufman et al., 2002; Prasad & Singh, 2007; Rotstayn et al., 2000). The ground-based instruments are then being employed in the validation of the satellite measurements (Diner et al., 2001; Ichoku et al., 2002; Kahn et al., 2005). Also due to their ability to take long term measurements, satellite products are useful in building a long term base for climatological studies. However places with high surface reflectance can pose some challenges to satellite measurements as errors may be introduced to the derived aerosol products.

Aerosol optical depth (AOD) is the most far reaching quantity from which we can infer the

aerosol loading and yet this quantity somewhat differs from one satellite instrument to the other even when their measurement is over same location. The difference is due to the various algorithms upon which these instruments are based (Kahn et al., 2007; Kokhanovsky et al., 2007; Mishchenko et al., 2009). Therefore employing the use of specific satellite product which satisfies some specific accuracy is important for the identification and characterization of a defined aerosol property over specific surface types.

A number of intensive field campaigns had been carried out in Southern Africa in the past. These includes the Southern Tropical Atlantic Region Experiment (STARE) in 1992, Transport and Atmospheric Chemistry near the Equator-Atlantic (TRACE-A) and Southern African Fire-Atmosphere Research Initiative (SAFARI). While TRACE focused on the impact of emissions from Brazil, SAFARI concentrated on fire emission from Southern Africa (Andreae et al., 1996; Ichoku et al., 2003). In SAFARI 2000 MODIS and MISR satellite were used for observation, although TOMS (Total Ozone Mapping Spectrometer) satellite was used in SAFARI-92 for the purpose of monitoring the ozone concentration (Diner et al., 2001; Ichoku et al., 2003). Recently, there was a study over nineteen locations in South Africa (SA) to determine the air quality using multiple platforms (Hersey et al., 2014).

The present study was undertaken using Moderate Resolution Imaging Spectroradiometer (Terra and Aqua), Multiangle Imaging Spectroradiometer (MISR) and Ozone Monitoring Instrument (OMI) Ultra-Violet Aerosol Index (UVAI) to compare aerosol loading over a hinterland and a coastland areas in SA for a period of 10 years during 2004–2013. First, validation was carried out on MISR and MODIS (Terra and Aqua) satellite observations with ground Aerosol Robotic Network (AERONET) measurements and then we estimated and compared the long term trend for the data obtained from these two sensors. Later, we then proceeded to see the performance of MODIS Terra and Aqua in these two terrains. Finally using UVAI data obtained from OMI, we explore the aerosol absorption index in the two locations based on interannual and seasonal variabilities for a period of 9 years between 2005 and 2013 since OMI product is available from late 2004.

2. STUDY AREA, DATASETS

2.1 Study area

Richards BAY (RBAY; 24° 48′S, 32° 06′) is a coastal town with a total land area of 142.78 Km^2 and is located in the KwaZulu-Natal province of SA with a population of 57, 387 (2011 census) at about 180 km from Durban. It has the largest Coal Terminal and the export facility in the world with a planned capacity of 91 million tons per year by the first half of 2009. It is characterized by a subtropical climate with warm wet summers and mild moist to dry winter. The town has an annual rainfall of 1228 mm with an annual mean temperature of 21.5°C. SKZ (SKZ; 25° 00′S 31^0 35′) is in the Mpumalanga province of SA with an area of 4.98 km and a population of 1,599 as per 2011 census. It receives about an annual of 353 mm with most rainfall occurring during the summer. The temperature ranges from 24.5°C in July to 31.7°C in January. For more details about the meteorology over several locations of SA, the readers are requested to look up Kumar et al. (2014) and Hersey et al. (2014). The above meteorology measurements (temperature and rainfall) were recorded as per the data provided by South African Weather Service (SAWS).

Fig 1: Google Earth Map showing the locations of Skukuza (A) and Richards Bay (B)

2.2 MODIS satellite

The Moderate resolution Imaging Spectrometer (MODIS) which has been flying aboard Terra since December 1999 and Aqua since May 2002 provides a lot of aerosol products from land and ocean as well as cloud. It has 36 spectral channels ranging from 0.4 µm to 14.4 µm. The aerosol products available over land include AOD at three

wavelengths, a measure of the fraction of AOD attributed to fine-mode particles and several parameters including reflected spectral solar flux at the top of the atmosphere (Remer et al., 2005). Both the land and ocean aerosol algorithm rely on calibrated, geolocated reflectance from the first seven MODIS bands (0.47–2.1 μm) provided by MODIS characterization support team. These reflectance data are first corrected for trace gas and water vapor columns and final aerosol parameters are retrieved for 10 km x 10 km boxes using results by geolocation and cloud screened data. Individual pixels inside the 10 km x10 km boxes are classified as ocean and land. If the entire pixels in a box are determined as ocean, then ocean algorithm is performed. If the pixels are land, then land retrieval is applied. After the land or ocean is concluded, the algorithm merges some parameters into combined land and ocean products for convenience (Ichoku et al., 2005; Levy et al., 2010).

The data are categorized into three levels. Level 1 consists of reflectance values but no derived parameters, Level 2 (retrieved geophysical products) calculated on 10 km x 10 km resolution. Level 3 datasets consist of global gridded data of aerosol parameters at a resolution of 1^ox1^o (~110 km). Level 3 after gridding at 1^ox1^o is used for the present study. The daily/monthly MODIS (Terra/Aqua) level 3 products MOD08_D3.051/ MYD08_D3.051and D08_M3.05/MYD08_M3.051 were obtained from the website (http://disc.sci.gsfc.nasa.gov/giovanni) and data were downloaded in the ASC format. The estimated uncertainty in MODIS AOD product was reported to be 0.03±0.05 (AOD) over the ocean and 0.5±0.15 AOD over land (Alam et al., 2011).

2.3 MISR satellite

Multi Imaging SpectroRadiometer (MISR) was launched in December 1999 into a sun-synchronous polar orbit to take measurement of the properties of tropospheric aerosols over a scene by making repeated coverage of that scene between two and nine days depending on the latitude of the scene. As it moves aboard the terra satellite of NASA Earth Observing System, it crosses the equator at about 10:30 local time (Cheng et al., 2012;Diner et al., 1998; Kaufman et al., 1998). It observes the scattering and reflection of solar radiation at 446, 558, 672 and 866 nm wavelengths from nine viewing angles on the flight path at nadir, 26.1^o, 45.6^o, 60.0^o and 70.5^o. It is enabled to retrieve aerosol optical depth over areas like desert which have surfaces with high reflectance. Through spatial contrast it retrieves aerosols over land by separating atmospheric and surface leaving path radiances. The surface-leaving radiation field is then used to determine the best fitting aerosol compositional models each consisting of a mixture of prescribed basic aerosol components. Using chi squared statistics to set that the residuals between the observed and the synthesized radiation field does not go below the threshold values, identification is made of the associated aerosol optical depth with usable aerosol mixtures (Martonchik et al., 1998). In this study Level 3 MISR (MIL3MAE.004) monthly aerosol data was used.

OMI DATASET

The Ultra-Violet Aerosol Index (UVAI) is provided by the Ozone Monitoring Instrument (OMI) downloaded from the website at http://gdata1.sci.gsfc.nasa.gov/daac-bin/G3/gui.cgi?instance_id=omi. The previous versions that existed before OMI were versions (version #8 Nimbus 7 TOMS available from 1978 to 1993; Meteor-3 (1991-1994) and Earth Probe (1996-2005). The successor OMI provides data since August 2004 and continuing to the present. Its algorithm is applied to measurements performed at 354 and 388 nm. The UVAI is mathematically defined as:

$$UVAI = -100\left[\frac{I_{354}^{obs}}{I_{354}^{calc}(R_{354}^{*})}\right] \qquad (1)$$

First the Lambert Equivalent Reflectivity (LER) R_{388}^{*} at 388 nm is calculated with the assumption that the atmosphere undergoes Rayleigh scattering and bounded by a reflectance of R_{388}^{*} called opaque Lambertian reflector. Except aerosols are highly absorbing, the true surface reflectivity would normally be smaller thanR_{388}^{*}. Estimation then is made for LER at 354 nm by correcting R_{388}^{*} through appropriate pre-computed climatology to obtainR_{354}^{*}. When there are no aerosols or there are purely non-absorbing aerosol UVAI will be near-zero value but in the presence of absorbing aerosols like desert dust, volcanic ash or carbonaceous aerosols the UVAI will be positive(Torres et al., 1998 and 2007). OMAERUV data product for the period from 2005 to 2013 was obtained in the readable ascii format and then processed.

2.4 MAPSS

Multi-sensor Aerosol Products Sampling System (MAPSS) as a framework was designed to assist in uniformly and consistently sampling of aerosol

products from different sensors. In its original design, it was for validation of MODIS retrieval algorithm but was later redesigned to facilitate an integrated and extensive comparative analysis of aerosol products from different satellite sensors. Chu et al. (2002) and (Ichoku et al., 2002) pointed out the challenges associated with validation of satellite product with ground-based instrument. First was the pixel size of 10 km x 10 km of MODIS when AERONET is just occupying a small location, MODIS make global coverage once or twice a day while AERONET sunphotometer takes reading at 15 minutes interval on the average. There is also the possibility of cloud cover of sunphotometer while only few pixels of MODIS may be affected also the time of MODIS overpass may not coincide with the time of sunphotometer measurement. MAPSS has now taken care of these challenges. Detailed description of how MAPSS work can be found in the works of Petrenko and Ichoku, 2013 and Petrenko et al., 2012. The validation carried out in this work was based on the data downloaded for year 2010 from AERONET at SKZ. Data can be downloaded at http://giovanni.gsfc.nasa.gov/mapss/ .

3. RESULTS AND DISCUSSION

3.1 Validation of MISR and MODIS satellites

In order to validate satellite or model aerosol product, comparison must be made with the ground or in situ realities (Cheng et al., 2012). The spatio-temporal data analysis carried out between satellite and ground-based instruments help both in identifying the uncertainties of these retrievals and their local spatial behavior (Ichoku et al., 2002). In earlier validation works, MODIS and MISR were found to perform well over SA although the work was limited to a short period of July to September (Chu et al., 2002; D. Diner et al., 2001). Ichoku et al. (2005) showed that MODIS in SA slightly tend towards underestimation. The validation of MISR and MODIS satellites derived AOD were performed using AERONET Sunphotometer obtained for SKZ site is shown in Fig. 2. The station has continuous long-term data and had existed since June 1, 1993. The slope of the least-square fitted line implies that MISR AODs are on the average 10% higher than AERONET while Aqua and Terra MODIS AODs are 24% and 41% lower than AERONET respectively (Kiran Kumar et al., 2013). Moreover the non-unitary of the slope shows the irregularity between microphysical-optical properties and the surface reflectance used in the satellite retrieval algorithm as well as the ground truth revealed by the AERONET. While the intercepts from which can deduce the biasing of the algorithm indicated a good match since it tends to zero (Alam et al., 2014; More et al., 2013; Tripathi et al., 2005; Zhao et al., 2002). The correlation coefficient was noticed to be highest for MISR (0.94) followed by Aqua MODIS (0.77) and was lowest for Terra MODIS (0.68). The high correlation coefficients suggest that seasonal variability is well captured by the satellites in spite of differences in their absolute values. In this location, results suggest that the MISR provides a better agreement with AERONET than with MODIS sensors.

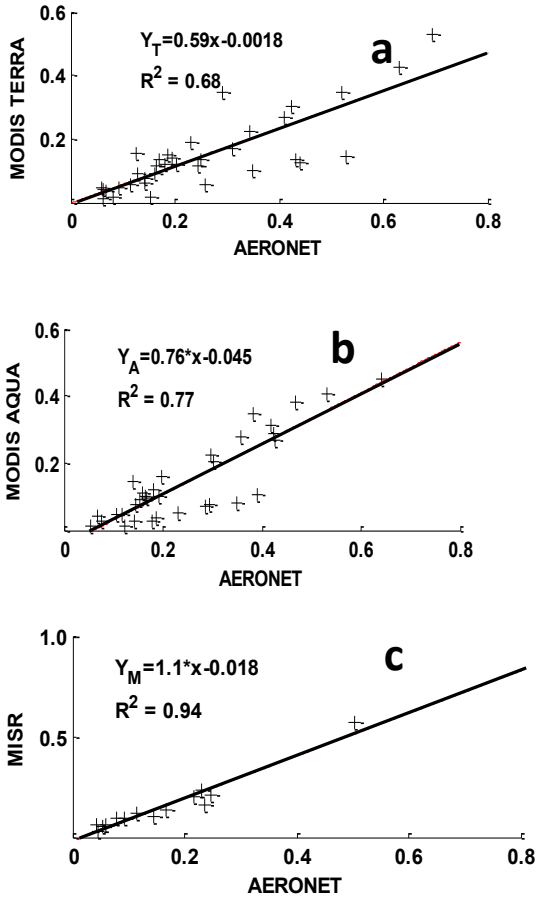

Fig 2: Comparison of AOD at 550 nm from MODIS (a) Terra (b) Aqua and AOD at 555 nm from (c) MISR with AERONET sunphotometer measurements at Skukuza for the year 2010 (showing the current performance of the sensors). The solid line represents linear fit to the data and also shown is the regression equation and squared correlation coefficient.

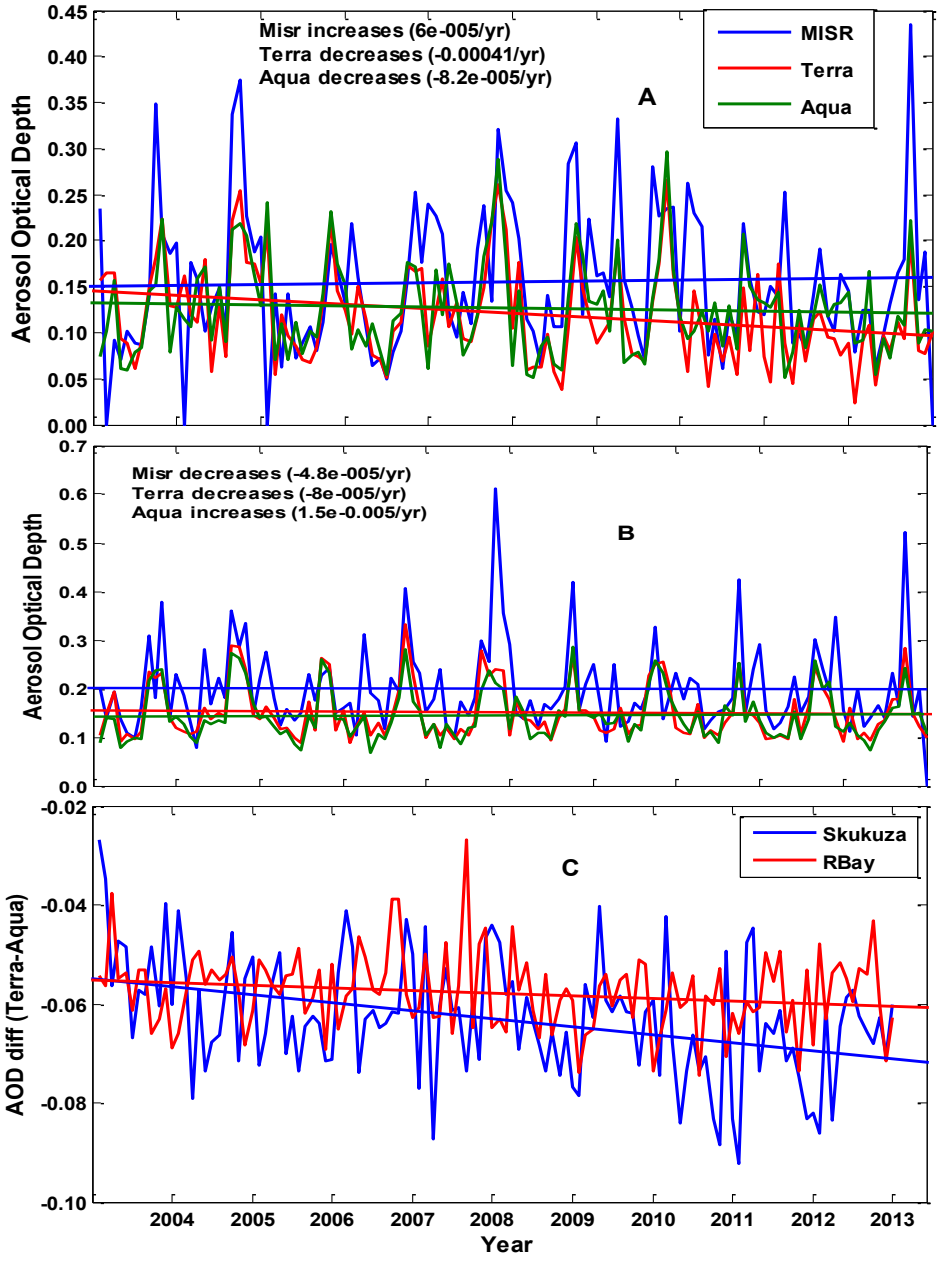

Fig 3: Time series of averaged 550 nm AOD derived from Terra and Aqua MODIS and 555 nm AOD from MISR satellites for 2004 – 2013 over (a) Skukuza (b) Richards Bay with linear fit showing the trend of each satellite sensor. (c) Time series of AOD differences at 550 nm derived from Terra and Aqua MODIS for 2004 – 2013 over Skukuza and Richards Bay with Terra underestimating Aqua at both locations.

Finally, there are factors that must be borne in mind when employing multiple sensor sources which includes instrument calibration, sampling differences, revisit times, consistency and data availability (Liu et al., 2007; Kahn et al., 2007; Xiao et al., 2009).
MISR for instance characterizes surface properties in the red and near-infrared bands using the clear sky whereas, MODIS uses extended target approach (Remer et al., 2005; Vermote et al., 2007).

3.2 Aerosol climatology over two regions

To establish a long-term database for climatological studies, there is a need to inter-compare AOD values derived from different satellite sensors. This also have the advantage of improving the accuracy and the coverage not achievable by single sensor (Alam et al., 2014; Prasad & Singh, 2007). Fig. 2(a–c) shows the temporal variation of monthly AOD values retrieved over two stations (SKZ and RBAY) during the study period (2004–2013) for MODIS (Terra/Aqua) and MISR. The figure reveals a significant month to month variability in AOD values. It is evident from Fig.2 that in both locations MODIS products underestimate the MISR. The AOD_{550} Terra varies from 0.02 to 0.27 and Aqua varies from 0.09 to 0.33 while AOD_{555} MISR varies from 0.00 to 0.43 for SKZ. In RBAY, Terra MODIS varies from 0.05 to 0.30 and Aqua MODIS varies from 0.07 to 0.29 while MISR varies from 0.00 to 0.61 (see Fig.2b). In SKZ, MISR shows an increasing trend in AOD over the study period while the MODIS products showed a decreasing trend but in RBAY, MISR and Terra MODIS showed a decreasing trend while Aqua MODIS showed an increasing trend. Since RBAY is a coastal town and it is expected that Aqua MODIS perform better here. Generally MISR is found to perform better in most sites as it is capable of retrieving optical properties of aerosol over a variety of terrains and takes into consideration dust-like aerosols that are non-spherical while MODIS does not (Cheng et al., 2012; Mishchenko et al., 2003). The performance of MODIS tends to be regional since aerosol types is one of the factors it depends on. In both locations, Terra underestimates Aqua by various degrees. When the differences between Terra and Aqua (Terra-Aqua) AOD was plotted, it varies between -0.03 to -0.09 at SKZ having a negative trend over the entire period while at RBAY it varies from -0.03 to -0.07 also having a negative trend over the entire period. Cheng et al. (2012) found similar result of Terra underestimating Aqua over China after the year 2005.
Figure 4 and 5 shows the contour maps of monthly mean aerosol loading over the study locations for the ten year period (2004-2013). In SKZ, the three sensors indicated high AOD from August to October as a yearly phenomenon. MISR and Terra MODIS showed that December to March also experiences high loading.

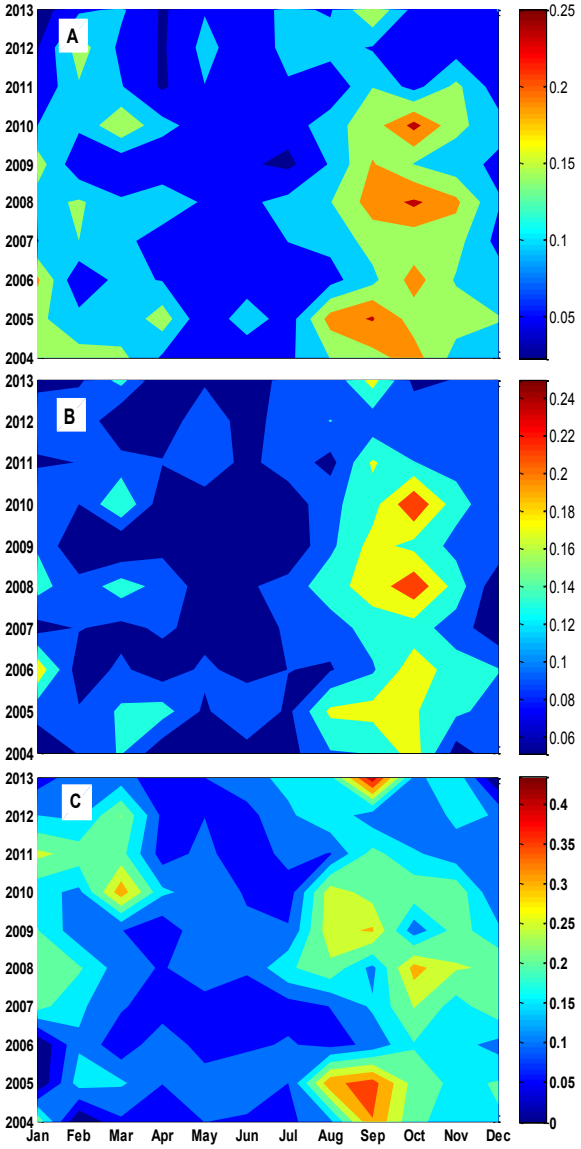

Fig 4: Averaged inter-annual AOD variation over Skukuza from (a) MODIS-Terra (b) MODIS-Aqua and (c) MISR for the ten year period from 2004 to 2013.

Also in SKZ, all sensors indicated that 2005, 2008 and 2010 have very high aerosol loading during September and October months. MODIS showed that the peak in AOD is during October whereas; MISR indicated high aerosol concentration in the September.

At RBAY, all sensors agreed to show high aerosol loading from August to October except Aqua MODIS showed the peak of the loading in September only.

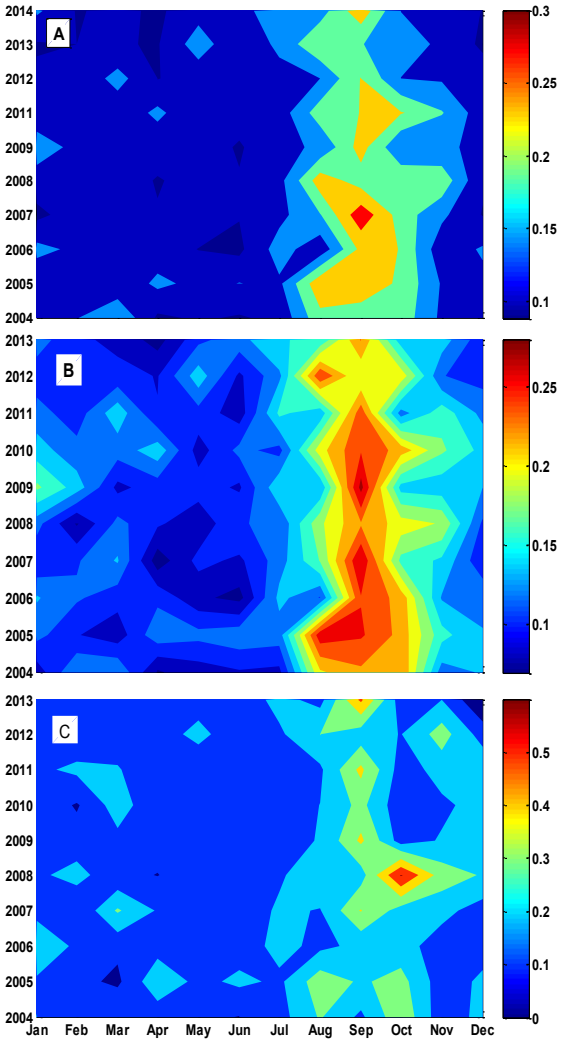

Fig.5: Same as Fig.3 but for Richards Bay.

Many authors found the months of August-September-October as a high aerosol loading in SA (Kumar et al., 2014; Queface et al., 2011; Tesfaye et al., 2011) as this is a yearly phenomenon with the period generally known as the biomass burning season. August to October AOD_{550} is generally above 0.2 while for the other months is lower than 0.16.

3.3 Comparison between Terra/Aqua MODIS AOD_{550}

The comparison between Terra/Aqua MODIS AOD_{550} values is given for the whole period in Fig. 6. The number of available daily data used for SKZ and RBAY are 2544 and 2897, respectively. In the earlier section, we show that the two products of MODIS did not have equal performance in each location. In this section, we want to look at the performance of the two sensors more closely. The annual scatter plot between the two sensors showed a linear regression with slope of about 0.6 and intercept of about 0.07 for both the locations, SKZ and RBAY. The coefficient of determination for the two locations are SKZ (R^2= 0.59) and RBAY (R^2= 0.66). For AOD_{550} < 0.2, points lie close to the 1:1 line in both locations but for AOD_{550}> 0.2, majority of the points make significant scatter thereby reducing the correlation.

The mean AOD_{550} (2004 – 2013) Terra/Aqua for SKZ are 0.175±0.131/(0.172±0.134) for RBAY are 0.172±0.134/(0.177±0.125) respectively. When the monthly data was used the coefficient of determination for SKZ was noticed to be R^2= 0.68 and for RBAY it is R^2= 0.87. For SKZ, the slope of the linear regression for all the seasons ~ 0.8 and coefficient of determination for summer (R^2=0.44), autumn (R^2 = 0.59), winter (R^2 =0.72) and spring (R^2 =0.58). At RBAY the slope of the linear regression for all seasons ~0.7 and the coefficient of determination for summer (R^2= 0.45), autumn (R^2= 0.63), winter (R^2= 0.82) and spring (R^2= 0.62) (see Fig. 7). In both locations the correlation is found to be highest in winter as the aerosol loading is lowest during this season. But in spring and in summer when there is high aerosol loading and variation in AOD, the correlation is lowered.

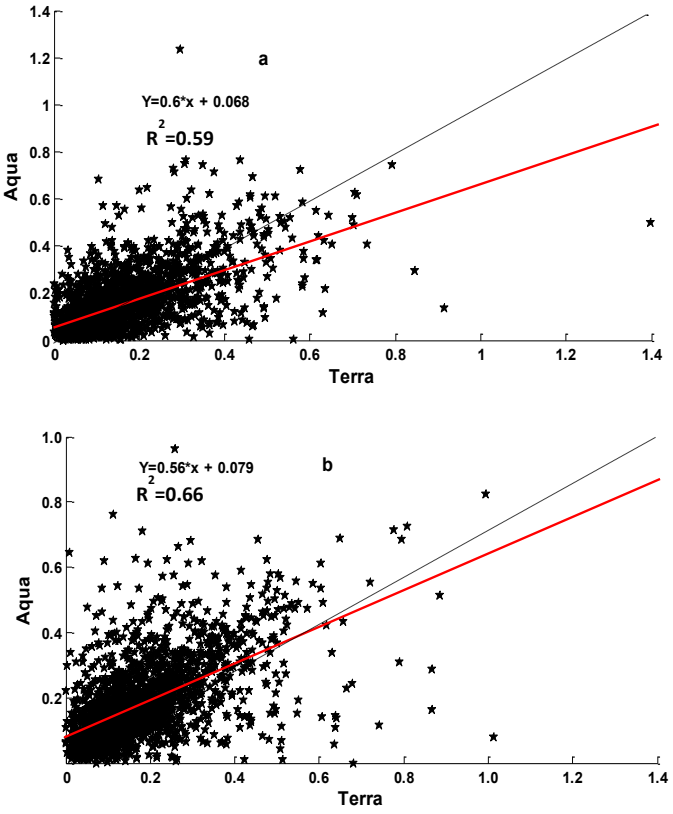

Fig 6: Correlation between Aqua and Terra MODIS for the whole dataset (2004 – 2013) over (a) Skukuza and (b) Richards Bay where the red solid line is the regression line and the black dashed line is the 1:1 line.

In the frequency table (Table 1), the seasonal AOD_{550} frequency distribution shows that the AOD_{550}bin 0.1 has the highest occurrence in all the seasons for both sensors apart from the spring season. The values range between 40 and 52% at RBAY and between 39-50% at SKZ. During the spring season the AOD bin 0.2 has maxima at both locations (~ 25-30% at RBAY and ~ 28-30% at SKZ) for both sensors. AOD_{550} is generally higher during the spring in SA as this is the period with frequent biomass burning activities.

The performance of each sensor seems to depend on season. At RBAY during the summer the AOD bin ≤0.1 have Terra overestimating Aqua while in autumn and winter, Terra underestimated Aqua. But for bins 0.2≤ AOD≤ 0.3, Terra underestimated Aqua in summer but overestimated Aqua in autumn and winter. The trend is reversed at SKZ for similar bins. At both locations, the spring seems not to follow any particular pattern but have the highest percentage for AOD bin > 0.3. The performance of the sensors seems affected therefore, by climatological and geographical features of a location.

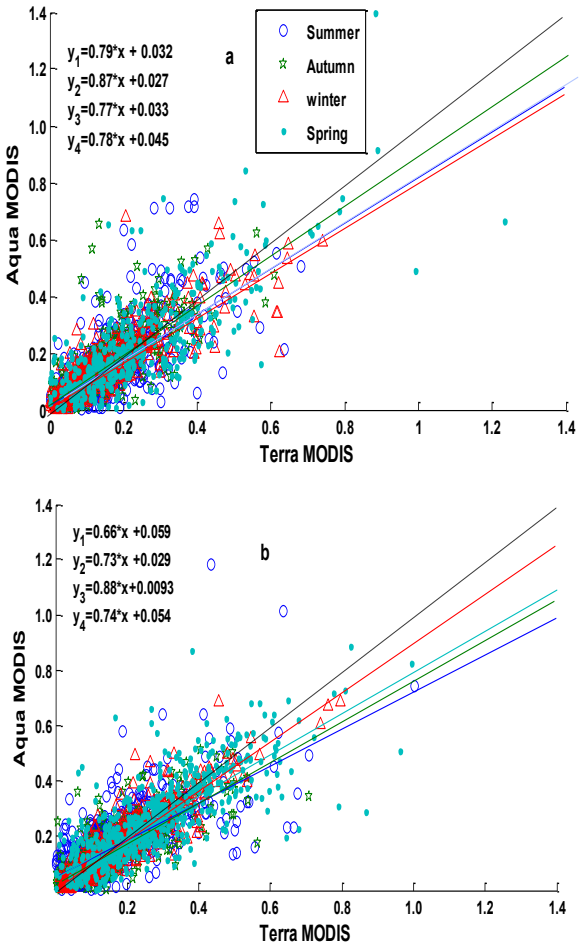

Fig 7: Same as Fig. 6 but for different seasons.

Table 1 Seasonal frequency of occurrence of Terra and Aqua MODIS AOD_{550} over SKZ and RBAY for the period 2004-2013 with the number (N) and percentage of occurrence (%).

		Summer				Autumn				Winter				Spring			
		Terra		Aqua		Terra		Aqua		Terra		Aqua		Terra		Aqua	
	AOD Bin	N	%	N	%	N	%	N	%	N	%	N	%	N	%	N	%
RBay	< 0.1	56	8.90	48	7.63	62	9.86	87	13.83	62	9.86	75	11.92	24	3.81	32	5.09
	0.1	272	43.24	264	41.97	316	50.24	324	51.51	257	40.86	283	44.99	145	23.05	143	22.73
	0.2	176	27.98	194	30.84	167	26.55	141	22.42	198	31.48	170	27.03	160	25.44	187	29.73
	0.3	74	11.76	85	13.51	54	8.58	52	8.27	70	11.13	64	10.17	138	21.94	118	18.76
	0.4	26	4.13	23	3.66	16	2.54	20	3.18	28	4.45	24	3.81	79	12.56	79	12.56
	> 0.4	25	3.97	15	2.38	14	2.22	5	0.79	14	2.22	13	2.07	83	13.19	70	11.13
SKZ	< 0.1	31	7.62	48	11.79	57	14	58	14.25	62	15.23	65	15.97	30	7.37	30	7.37
	0.1	159	39.07	165	40.54	204	50.12	198	48.65	180	44.23	180	44.23	112	27.52	115	28.25
	0.2	122	29.97	99	24.32	86	21.13	85	20.88	96	23.59	99	24.32	115	28.25	123	30.22
	0.3	61	14.99	52	12.78	43	10.56	36	8.84	34	8.35	36	8.84	63	15.48	67	16.46
	0.4	21	5.16	19	4.67	14	3.44	20	4.91	16	3.93	14	3.44	48	11.79	32	7.86
	> 0.4	13	3.19	24	5.9	3	0.74	10	2.46	19	4.67	13	3.19	39	9.58	40	9.28

3.4 Aerosol absorption characteristics

The annual variability in OMI retrieved UV aerosol index (UVAI) for the two study regions are shown in Fig. 8. It is clear from the figure that during the period 2005-2013 the interannual variability of UVAI in both the locations shows an increasing trend, with SKZ having increment of +0.0089/yr and RBAY with +0.0022/yr. SKZ experienced generally a higher UVAI than RBAY with the highest value occurring during the year 2008 (1.03) followed by 2013 (0.98). The highest UVAI recorded at RBAY was in 2010 (0.87) and followed by 2005 (0.86). SKZ's proximity to the highly industrialized Highveld area of the country on the one hand (Kumar et al., 2013) and Mozambique with high biomass burning on the other hand (Adesina et al., 2014) might have contributed to the high UVAI. The seasonal variation in UVAI at the two locations as shown in Fig. 9 indicated a low UVAI in summer and autumn but high values in winter and spring. In winter, the AOD is generally lowest in most part of SA.

During this period, the air transport pathway is more of African transport which may carry pollutants from central-southern Africa with advection of dust from Kalahari Desert (Freiman & Piketh, 2003) as UVAI is known to be sensitive to desert dust (Habib et al., 2006; Satheesh & Srinivasan, 2002). High UVAI values in spring may be associated with high intensity of biomass burning as UVAI is also sensitive to emissions of black carbon. The factors affecting UVAI seems to be regional and local, regional in the sense that there appears to be a seasonal effect and local in the sense that both locations experienced annual peak of UVAI at different years.

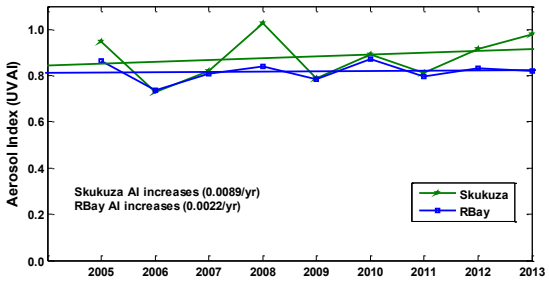

Fig 8: Annual trends in aerosol index over Skukuza and Richards Bay

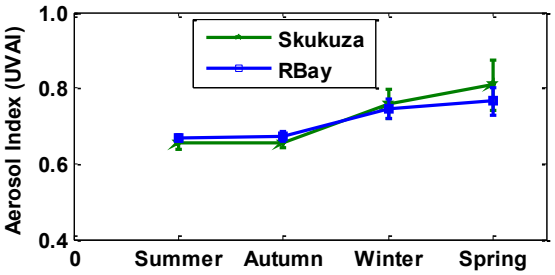

Fig 9: Averaged seasonal aerosol index (2005 – 2013) over Skukuza and Richards Bay.

4.0 CONCLUSIONS

The present study which was based on long term satellite aerosol measurements using MISR, MODIS and OMI instruments has demonstrated the variability of aerosol loading over the two selected locations. The performance of MISR and MODIS instruments based on the validation showed the MISR is better correlated with AERONET than the MODIS products at SKZ. The study reveals that as aerosols variation depends on geographical location and seasonal effects so also do the satellite measurements. The MODIS products (Terra and Aqua) were better correlated at coastland than at hinterland. The analysis of Terra and Aqua MODIS AOD_{550} over the two locations further demonstrates that the two sensors though having different overpass time generally have a good agreement based on the monthly mean data for entire study period.

The monthly mean instead of the daily mean of MODIS when used produces better correlation results. This is because the geometrical view of MODIS with its scattering angles exhibit an overlapping broad distribution capable of alleviating the errors introduced by the equator crossing times and the assumed phase function (Kharol et al., 2011; Remer & Kaufman, 2006). Though diurnal variation exists, but when long term statistics differences is used, the temporal variation becomes negligible as temporal average smoothens out between the two sensors. The UVAI over the two locations shows that aerosol absorption characteristics have been increasing over the decade and it is particularly higher over Skukuza.

REFERENCES

Adesina, A. J., Kumar, K. R., & Sivakumar, V. (2014). Variability in aerosol optical properties and radiative forcing over Gorongosa (18.97^{o} S, 34.35^{o} E) in Mozambique. *Meteorology and Atmospheric Physics*, 1-12.

Alam, K., Khan, R., Blaschke, T., & Mukhtiar, A. (2014). Variability of aerosol optical depth and their impact on cloud properties in Pakistan. *Journal of Atmospheric and Solar-Terrestrial Physics, 107*, 104-112.

Alam, K., Qureshi, S., & Blaschke, T. (2011). Monitoring spatio-temporal aerosol patterns over Pakistan based on MODIS, TOMS and MISR satellite data and a HYSPLIT model. *Atmospheric Environment, 45*(27), 4641-4651.

Andreae, M. O., Fishman, J., & Lindesay, J. (1996). The Southern Tropical Atlantic Region Experiment (STARE): Transport and Atmospheric Chemistry near the Equator-Atlantic (TRACE A) and Southern African Fire-Atmosphere Research Initiative (SAFARI): An introduction. *Journal of Geophysical Research: Atmospheres (1984–2012), 101*(D19), 23519-23520.

Cheng, T., Chen, H., Gu, X., Yu, T., Guo, J., & Guo, H. (2012). The inter-comparison of MODIS, MISR and GOCART aerosol products against AERONET data over China. *Journal of Quantitative Spectroscopy and Radiative Transfer, 113*(16), 2135-2145.

Chu, D., Kaufman, Y., Ichoku, C., Remer, L., Tanré, D., & Holben, B. (2002). Validation of MODIS aerosol optical depth retrieval over land. *Geophysical Research Letters, 29*(12), MOD2-1-MOD2-4.

Diner, D., Abdou, W., Bruegge, C., Conel, J., Crean, K., Gaitley, B., . . . Pilorz, S. (2001). MISR aerosol optical depth retrievals over southern Africa during the SAFARI-2000 dry season campaign. *Geophysical Research Letters, 28*(16), 3127-3130.

Diner, D. J., Beckert, J. C., Reilly, T. H., Bruegge, C. J., Conel, J. E., Kahn, R. A., . . . Gerstl, S. A. (1998). Multi-angle Imaging SpectroRadiometer (MISR) instrument description and experiment overview. *Geoscience and Remote Sensing, IEEE Transactions on, 36*(4), 1072-1087.

Freiman, M., & Piketh, S. (2003). Air transport into and out of the industrial Highveld region of South Africa. *Journal of Applied Meteorology, 42*(7), 994-1002.

Habib, G., Venkataraman, C., Chiapello, I., Ramachandran, S., Boucher, O., & Shekar Reddy, M. (2006). Seasonal and interannual variability in absorbing aerosols over India derived from TOMS: relationship to regional meteorology and emissions. *Atmospheric Environment, 40*(11), 1909-1921.

Hansen, J., Sato, M., & Ruedy, R. (1997). Radiative forcing and climate response. *Journal of Geophysical Research: Atmospheres (1984–2012), 102*(D6), 6831-6864.

Hersey, S., Garland, R., Crosbie, E., Shingler, T., Sorooshian, A., Piketh, S., & Burger, R. (2014). An overview of regional and local characteristics of aerosols in South Africa using satellite, ground, and modeling data. *Atmospheric chemistry and physics discussions, 14*(17), 24701-24752.

Ichoku, C., Chu, D. A., Mattoo, S., Kaufman, Y. J., Remer, L. A., Tanré, D., . . . Holben, B. N. (2002). A spatio-temporal approach for global validation and analysis of MODIS aerosol products. *Geophysical Research Letters, 29*(12), MOD1-1-MOD1-4.

Ichoku, C., Remer, L. A., & Eck, T. F. (2005). Quantitative evaluation and intercomparison of morning and afternoon Moderate Resolution Imaging Spectroradiometer (MODIS) aerosol measurements from Terra and Aqua. *Journal of Geophysical Research: Atmospheres (1984–2012), 110*(D10).

Ichoku, C., Remer, L. A., Kaufman, Y. J., Levy, R., Chu, D. A., Tanré, D., & Holben, B. N. (2003). MODIS observation of aerosols and estimation of aerosol radiative forcing over southern Africa during SAFARI 2000. *Journal of Geophysical Research: Atmospheres (1984–2012), 108*(D13).

Kahn, R. A., Gaitley, B. J., Garay, M. J., Diner, D. J., Eck, T. F., Smirnov, A., & Holben, B. N. (2010). Multiangle Imaging SpectroRadiometer global aerosol product assessment by comparison with the Aerosol Robotic Network. *Journal of Geophysical Research: Atmospheres (1984–2012), 115*(D23).

Kahn, R. A., Gaitley, B. J., Martonchik, J. V., Diner, D. J., Crean, K. A., & Holben, B. (2005). Multiangle Imaging Spectroradiometer (MISR) global aerosol optical depth validation based

on 2 years of coincident Aerosol Robotic Network (AERONET) observations. *Journal of Geophysical Research: Atmospheres (1984–2012), 110*(D10).

Kahn, R. A., Garay, M. J., Nelson, D. L., Yau, K. K., Bull, M. A., Gaitley, B. J., . . . Levy, R. C. (2007). Satellite-derived aerosol optical depth over dark water from MISR and MODIS: Comparisons with AERONET and implications for climatological studies. *Journal of Geophysical Research: Atmospheres (1984–2012), 112*(D18).

Kaufman, Y. J., Herring, D. D., Ranson, K. J., & Collatz, G. J. (1998). Earth Observing System AM1 mission to earth. *Geoscience and Remote Sensing, IEEE Transactions on, 36*(4), 1045-1055.

Kaufman, Y. J., Koren, I., Remer, L. A., Rosenfeld, D., & Rudich, Y. (2005). The effect of smoke, dust, and pollution aerosol on shallow cloud development over the Atlantic Ocean. *Proceedings of the National Academy of Sciences of the United States of America, 102*(32), 11207-11212.

Kaufman, Y. J., Tanré, D., & Boucher, O. (2002). A satellite view of aerosols in the climate system. *Nature, 419*(6903), 215-223.

Kharol, S. K., Badarinath, K., Sharma, A. R., Kaskaoutis, D., & Kambezidis, H. (2011). Multiyear analysis of Terra/Aqua MODIS aerosol optical depth and ground observations over tropical urban region of Hyderabad, India. *Atmospheric Environment, 45*(8), 1532-1542.

Kiran Kumar, T., Gadhavi, H., Jayaraman, A., Sai Suman, M., & Vijaya Bhaskara Rao, S. (2013). Temporal and spatial variability of aerosol optical depth over South India as inferred from MODIS. *Journal of Atmospheric and Solar-Terrestrial Physics, 94*, 71-80.

Kokhanovsky, A., Breon, F.-M., Cacciari, A., Carboni, E., Diner, D., Di Nicolantonio, W., . . . Lee, K.-H. (2007). Aerosol remote sensing over land: A comparison of satellite retrievals using different algorithms and instruments. *Atmospheric Research, 85*(3), 372-394.

Kumar, K. R., Sivakumar, V., Reddy, R., Gopal, K. R., & Adesina, A. J. (2013). Inferring wavelength dependence of AOD and Ångström exponent over a sub-tropical station in South Africa using AERONET data: Influence of meteorology, long-range transport and curvature effect. *Science of The Total Environment, 461*, 397-408.

Kumar, K. R., Sivakumar, V., Yin, Y., Reddy, R., Kang, N., Diao, Y., . . . Yu, X. (2014). Long-term (2003–2013) climatological trends and variations in aerosol optical parameters retrieved from MODIS over three stations in South Africa. *Atmospheric Environment, 95*, 400-408.

Levy, R. C., Remer, L. A., Kleidman, R. G., Mattoo, S., Ichoku, C., Kahn, R., & Eck, T. (2010). Global evaluation of the Collection 5 MODIS dark-target aerosol products over land. *Atmospheric Chemistry and Physics, 10*(21), 10399-10420.

Martonchik, J. V., Diner, D. J., Kahn, R. A., Ackerman, T. P., Verstraete, M. M., Pinty, B., & Gordon, H. R. (1998). Techniques for the retrieval of aerosol properties over land and ocean using multiangle imaging. *Geoscience and Remote Sensing, IEEE Transactions on, 36*(4), 1212-1227.

Mishchenko, M. I., Geogdzhayev, I. V., Liu, L., Lacis, A. A., Cairns, B., & Travis, L. D. (2009). Toward unified satellite climatology of aerosol properties: What do fully compatible MODIS and MISR aerosol pixels tell us? *Journal of Quantitative Spectroscopy and Radiative Transfer, 110*(6), 402-408.

Mishchenko, M. I., Geogdzhayev, I. V., Liu, L., Ogren, J. A., Lacis, A. A., Rossow, W. B., . . . Muñoz, O. (2003). Aerosol retrievals from AVHRR radiances: effects of particle nonsphericity and absorption and an updated long-term global climatology of aerosol properties. *Journal of Quantitative Spectroscopy and Radiative Transfer, 79*, 953-972.

More, S., Kumar, P. P., Gupta, P., Devara, P., & Aher, G. (2013). Comparison of aerosol products retrieved from AERONET, MICROTOPS and MODIS over a tropical urban city, Pune, India. *Aerosol and Air Quality Research, 13*(1), 107-121.

Petrenko, M., & Ichoku, C. (2013). Coherent uncertainty analysis of aerosol measurements from multiple satellite sensors. *Atmos. Chem. Phys, 13*, 6777-6805.

Petrenko, M., Ichoku, C., & Leptoukh, G. (2012). Multi-sensor aerosol products sampling system (MAPSS). *Atmospheric Measurement Techniques, 5*(5), 913-926.

Prasad, A. K., & Singh, R. P. (2007). Comparison of MISR-MODIS aerosol optical depth over the

Indo-Gangetic basin during the winter and summer seasons (2000–2005). *Remote sensing of environment, 107*(1), 109-119.

Queface, A. J., Piketh, S. J., Eck, T. F., Tsay, S.-C., & Mavume, A. F. (2011). Climatology of aerosol optical properties in Southern Africa. *Atmospheric Environment, 45*(17), 2910-2921.

Remer, L. A., Kaufman, Y., Tanré, D., Mattoo, S., Chu, D., Martins, J. V., . . . Kleidman, R. (2005). The MODIS aerosol algorithm, products, and validation. *Journal of the atmospheric sciences, 62*(4), 947-973.

Remer, L. A., & Kaufman, Y. J. (2006). Aerosol direct radiative effect at the top of the atmosphere over cloud free ocean derived from four years of MODIS data. *Atmospheric Chemistry and Physics, 6*(1), 237-253.

Rotstayn, L. D., Ryan, B. F., & Penner, J. E. (2000). Precipitation changes in a GCM resulting from the indirect effects of anthropogenic aerosols. *Geophysical Research Letters, 27*(19), 3045-3048.

Satheesh, S., & Srinivasan, J. (2002). Enhanced aerosol loading over Arabian Sea during the pre-monsoon season: Natural or anthropogenic? *Geophysical Research Letters, 29*(18), 21-21-21-24.

Tesfaye, M., Sivakumar, V., Botai, J., & Mengistu Tsidu, G. (2011). Aerosol climatology over South Africa based on 10 years of Multiangle Imaging Spectroradiometer (MISR) data. *Journal of Geophysical Research: Atmospheres (1984–2012), 116*(D20).

Torres, O., Bhartia, P., Herman, J., Ahmad, Z., & Gleason, J. (1998). Derivation of aerosol properties from satellite measurements of backscattered ultraviolet radiation: Theoretical basis. *Journal of Geophysical Research: Atmospheres (1984–2012), 103*(D14), 17099-17110.

Torres, O., Tanskanen, A., Veihelmann, B., Ahn, C., Braak, R., Bhartia, P. K., . . . Levelt, P. (2007). Aerosols and surface UV products from Ozone Monitoring Instrument observations: An overview. *Journal of Geophysical Research: Atmospheres (1984–2012), 112*(D24).

Tripathi, S., Dey, S., Chandel, A., Srivastava, S., Singh, R. P., & Holben, B. (2005). *Comparison of MODIS and AERONET derived aerosol optical depth over the Ganga Basin, India.* Paper presented at the Annales Geophysicae.

Vermote, E. F., Roger, J.-C., Sinyuk, A., Saleous, N., & Dubovik, O. (2007). Fusion of MODIS-MISR aerosol inversion for estimation of aerosol absorption. *Remote sensing of environment, 107*(1), 81-89.

Zhao, T. X., Stowe, L. L., Smirnov, A., Crosby, D., Sapper, J., & McClain, C. R. (2002). Development of a global validation package for satellite oceanic aerosol optical thickness retrieval based on AERONET observations and its application to NOAA/NESDIS operational aerosol retrievals. *Journal of the atmospheric sciences, 59*(3), 294-312.

CHAPTER SIX

Spatio-temporal heterogeneity in AOD and its impact on cloud properties over major cities in South Africa as retrieved from MODIS

This chapter to be cited as:

Adesina, A. J., Kumar, K. R., Sivakumar, V. (2014) Spatio-temporal heterogeneity in AOD and its impact on cloud properties over major cities in South Africa as retrieved from MODIS (To be submitted for review – Aerosol and Air Quality Research).

Spatio-temporal heterogeneity in AOD and its impact on cloud properties over major cities in South Africa as retrieved from MODIS

A Joseph Adesina[1], K. Raghavendra Kumar[2], V. Sivakumar[1]

[1]*Discipline of Physics, School of Chemistry and Physics, University of KwaZulu-Natal, Durban 4000, South Africa*
[2]*Key Laboratory for Aerosol-Cloud-Precipitation of China Meteorological Administration, School of Atmospheric Physics, Nanjing University of Information Science and Technology, Nanjing 210044, Jiangsu Province, China*

ABSTRACT

Aerosols constitute a significant component of air pollution and may lead to an increase in cloud optical thickness due to a combination of reduction in cloud droplet radius and increased water content. It can sometimes inhibit cloud formation and evaporation so that aerosol – cloud interaction presents a major research area in atmospheric science. We have used the Terra Satellite onboard of the Moderate Resolution Imaging Spectroradiometer (MODIS) to investigate the spatial and temporal relationship between aerosol optical depth (AOD) and cloud parameters namely, water vapor (WV), cloud optical depth (COD), cloud fraction (CF), cloud top pressure (CTP) and cloud top temperature (CTT) based on 5 years (January 2008 to December 2012) of dataset over six locations in South Africa. AOD has high values during spring (September to November) but low values in winter (June to August) in all locations. In terms of temporal variation AOD was lowest at Bloemfontein 0.06±0.04 followed by Cape Town 0.08±0.02, then Potchefstroom 0.09±0.05, Pretoria and Skukuza had 0.11±0.05 each and Durban 0.13±0.05. The mean Angstrom exponent values for each location shows a general prevalence of fine particles for most parts of the year. Our analysis of AOD and WV showed both quantities only co-vary at the beginning of the year but later in the year they tend to have opposite trend over all the locations. AOD and CF showed negative correlation for most of the locations while AOD and COD were positive over three of the locations. AOD and CTT, CTP showed similar variations in almost all the locations. The co-variation of CTT and CTP may be due to large scale meteorological variation.
Key words: South Africa, MODIS, COD, WV, CTP

1. INTRODUCTION

Aerosols are emitted into the atmosphere through either natural or anthropogenic origin. Consequently they then interact with solar radiation by causing absorption or scattering, this is being referred to as direct effect (Ichoku et al., 2004; Satheesh and Krishna Moorthy, 2005; Wright et al., 2010) in addition to it, they also interact with clouds by serving as cloud condensation nuclei (CCN) and ice nuclei (IN) making it possible for the formation of cloud droplets and ice crystals. Aerosol and clouds are both variable in space and time thereby, sometimes leading to ambiguity in making a distinction between them as they interact (Charlson et al., 2007; Koren et al., 2007; Stocker et al., 2013). The uncertainties in quantifying radiative forcing due to anthropogenic aerosols and non-greenhouse gas arise from the complex interactions between aerosols and cloud (Ackerman et al. (2000); (Alam et al., 2010; Alam et al., 2014; Andreae et al., 2005; Haywood & Boucher, 2000).

The indirect effects of aerosol on cloud includes increment in reduced sized water cloud droplets resulting from CCN (Feingold et al., 2003; Kaufman & Fraser, 1997; Myhre et al., 2007) and this in turn can impede precipitation (Albrecht, 1989; Quaas et al., 2008 and 2010; Rosenfeld, 2000). When this happens, the life time of cloud is thus prolonged and cloud may then grow into top height (Khain et al., 2005; Rosenfeld, 2007; Williams et al., 2002) with increase in liquid water path. Aerosols are also known to change the optical properties of cloud (Balakrishnaiah et al., 2012; Kim et al., 2003; Koren et al., 2004). Myhre et al., (2007) pointed out that aerosol-cloud process goes beyond physical interactions especially in the presence of large scale meteorological conditions.

Although many researchers have carried out investigations on the aerosol optical depth (AOD) over some parts or over all South Africa (SA) using both ground-based instruments (Adesina et al., 2014;

Eck et al., 2003; Kumar et al., 2013; Queface et al., 2011) and satellite-based instruments (Ichoku et al., 2003; Sivakumar et al., 2010; Tesfaye et al., 2011), but aerosol-cloud investigations has not been reported to the best of our knowledge. Aerosol-cloud interaction studies has been reported in India (Balakrishnaiah et al., 2012; Kumar, 2013), in Pakistan (Alam et al., 2014), in China (Guo et al., 2014; Tang et al., 2014) and other countries using long-term Moderate Resolution Imaging Spectroradiometer (MODIS) remote sensing satellite data for distinct stations to show the impact of AOD on cloud properties and its relationship in climate change. The cloud parameters used in this study are Water vapor (WV), Cloud fraction (CF), Cloud optical depth (COD), Cloud top pressure (CTP) and Cloud top temperature (CTT). This study is hoped to complement research effort in understanding aerosol effects on clouds, in particular climate change in SA. The study is discussed in the following way: a general outline of study locations, database used for the present study, results and discussion then concluding with brief summary of results.

2. STUDY LOCATIONS

The study was carried out over six important locations with different contribution for aerosol sources from six different provinces out of nine covering all portions in South Africa. The provinces and locations are summarized as Gauteng–Pretoria (PTR; 25.57^{o}S, 28.18^{o}E), Mpumalanga–Skukuza (SKZ; 24.98^{o}S, 31.60^{o}E), North West–Potchefstroom (PCS; 26.71^{o}S, 27.10^{o}E), Free State–Bloemfontein (BFN; 29.12^{o}S, 26.21^{o}E), KwaZulu-Natal–Durban (DBN; 29.88^{o}S, 31.05^{o}E) and Western Cape–Cape Town (CPT; 33.92^{o}E, 18.42^{o}E). These locations are diverse in population, climate and geographical features (refer to Table 1 for complete information).

3. MODIS DATA

MODIS is a satellite-based instrument that was launched since December 1999 (Terra) and May 2002 (Aqua). The description, algorithm, products and retrieval method has been discussed by earlier researchers (Levy et al., 2010; Remer et al., 2005; Tanré et al., 1997). Monthly dataset of Level-3 MODIS at 1^{o}x1^{o} grid resolution were downloaded from GIOVANNI (http://disc.sci.gsfc.nasa.gov/giovanni) for 5-year period (January 2008–December 2013). These values were obtained using Lat-Lon map, time series and correlation maps to generate the data for the study locations. The data was processed and analyzed according to combined months and seasons. The AOD used in this study is obtained at 550 nm and the Angstrom exponent (AE) used is $\alpha_{470\text{-}660}$ for land only (Terra). The cloud parameters though available for daytime, nighttime and combined, the daytime data was used in this study and the water vapor was retrieved for clear sky.

4. RESULTS AND DISCUSSION

4.1. Spatial and temporal variations of AOD and AE

AOD is the measure of transparency of aerosol to solar radiation and has to do with the degree to which it prevents the radiation through scattering and absorption. It is been defined as the integration of the extinction coefficient over a vertical column of unit cross section. It is a major property of aerosol by which its environmental effect is being measured. Fig 1 and Table 2 shows both the temporal and spatial variation of AOD_{550} over six selected cities of SA. The lowest value (AOD_{550} < 0.1) of the spatial variation of AOD_{550} (2008-2012) was observed over Bloemfontein. The location which is in the Free State province lies is in the heart of SA. It lies between the Vaal River towards the North and Orange Rivers towards the south. It is a region of grassland, crop fields and Sandstone Mountains hosting the country largest gold mining complex. AOD_{550} ranging between 0.10 and 0.13 is found over four locations; Potchefstroom in the North-West province with mostly flat areas of scattered trees and grassland, Skukuza in the Mpumalanga province with high altitude grassland and accounting for about 83% of SA's coal production, Cape Town in the Western Cape Province having an exceptional topographical and vegetation diversity and Pretoria in the Gauteng Province containing the country's largest city making it the province with the highest population density and urbanization while Durban in the Kwazulu-Natal Province having three geographical regions of lowland, midland and plateau with the coastal region having subtropical forest has the highest AOD close to 0.2. In terms of temporal variation, the mean AOD_{550} for the study period (2008-2012) was lowest at Bloemfontein 0.06±0.04 followed by Cape Town 0.08±0.02, then Potchefstroom 0.09±0.05, Pretoria and Skukuza had 0.11±0.05 each and Durban 0.13±0.05. We noticed a good agreement between the temporal and spatial aerosol distribution over SA. The combined (2008–2012) month to month variation shows that four of the locations experience

Table1: Geographical information about the six locations of study in South Africa [Wikipedia and Köppen-Geiger climate classification system].

Province	Location	Latitude (S)	Longitude (E)	Altitude (m)	Population (million)	Area (km^2)	Climate (subtropical)
Gauteng	Pretoria	25^o 44′	28^o 11′	1339	2.9	6,298	Urban; Semi-Arid
Mpumalanga	Skukuza	24^o 59′	31^o 35′	260	0.0016	4.9	Rural; Hot semi-arid
KwaZulu-Natal	Durban	30^o 57′	29^o 58′	8	3.5	2,292	Urban; Coastal
Free State	Bloemfontein	29^o 07′	26^o 13′	1400	0.0063	6,283	Suburban; Semi-Arid
North West	Potchefstroom	26^o 42′	27^o 06′	1350	0.149	185	Urban; Semi-Arid
Western Cape	Cape Town	33^o 55′	18^o 25′	50	3.74	2,444	Urban; Coastal; Mediterranean

maximum AOD during September (Bloemfontein and Durban) with Pretoria and Potchefstroom having double maxima one in February and the other in September also, Skukuza with double maxima corresponding to September and October. These two maxima when considered along with the AE show that the aerosol may not be of the same types during these two different periods. All locations have their minimum AOD in June which appears to be more of a seasonal effect. Seasonal variation of AOD_{550} is seen in all the six locations (Table 2). All locations apart from Pretoria have maximum seasonal AOD

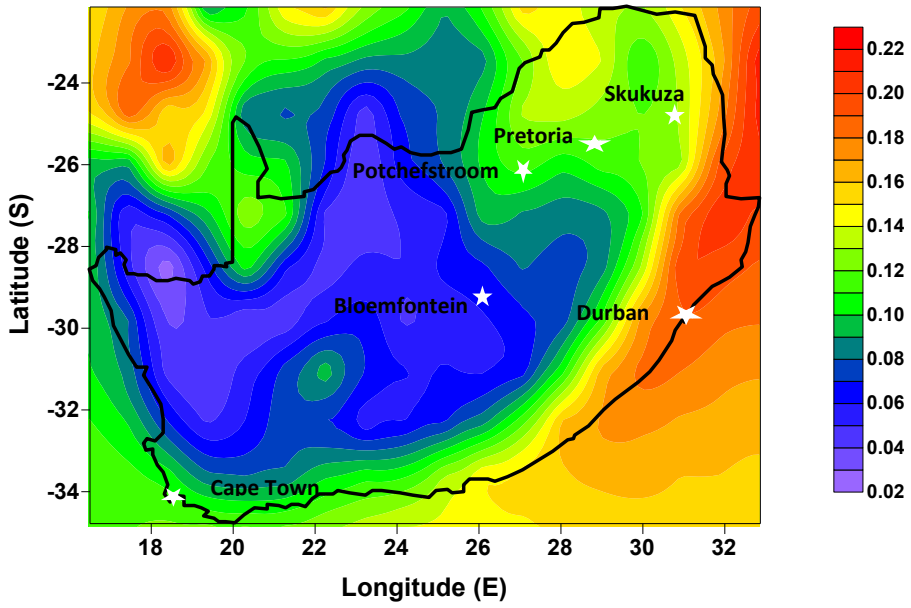

Fig 1 Monthly mean (2008 -2012) value of AOD_{550} Terra MODIS over six locations in SA

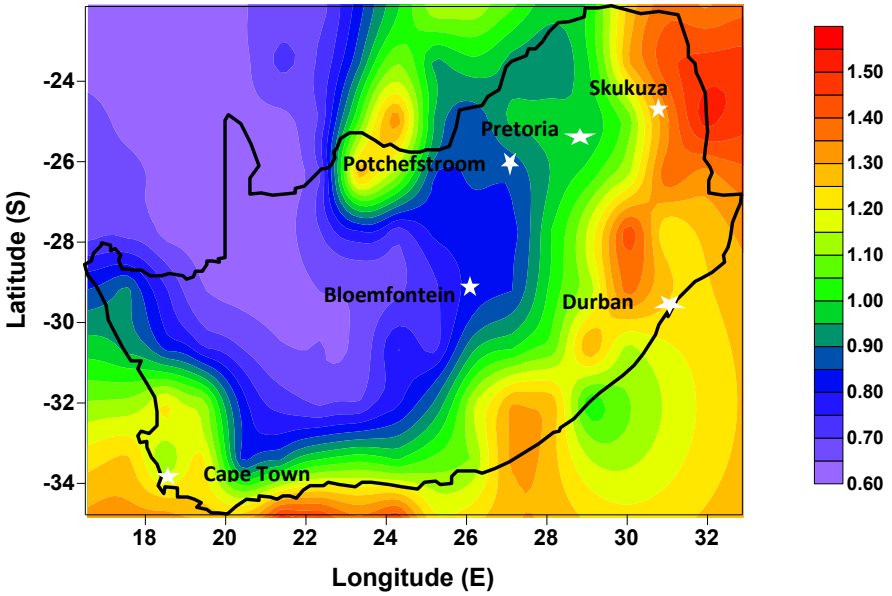

Fig 2 Monthly mean (2008 – 2012) value of $AE_{470\text{-}660}$ (2008-2012) over six locations in SA

during the spring season. This season corresponds to agricultural activities and known for biomass burning as agreed upon by a number of researchers (Adesina et al., 2014; Kumar et al., 2014; Queface et al., 2011; Tesfaye et al., 2011). Durban has AOD > 0.1 in all seasons while Skukuza and Pretoria have AOD > 0.1 only during the spring and summer. Bloemfontein and Cape Town have AOD < 0.1 for all seasons and so also in the case of Potchefstroom except for the spring season. The high aerosol loading in Pretoria, Skukuza and Potchefstroom occurring in summer and spring was explained by Freiman and Piketh (2003) as an effect of air transport over that region. In summer air transport comes from over Atlantic and Indian Oceans consisting more of sea salt and other anthropogenic aerosols while in spring transport is from hinterland originated from Zambia (Queface et al., 2011) and Mozambique (Adesina et al., 2014b) and causing the advection of biomass burning aerosol. Aerosol loading over SA is generally lower during autumn and winter compared to the other seasons. The Angstrom Exponent (AE) which is a parameter that determines aerosol particle-size with lower values indicating a larger size and higher values indicating a smaller size varies significantly over the locations. MODIS annual mean spatial distribution for the period (2008-2012) is shown in Fig 2. Durban and Skukuza have the highest with AE about 1.2; this is followed by Pretoria and Cape Town with AE of about 1.0 and then Bloemfontein and Potchefstroom where the AE is less than 1.0 being areas of less vegetation and might have more of dust particles. The temporal variation from Table 2 shows that Durban and Skukuza have AE > 1.0 throughout all the months of the year while Cape Town has AE >1.0 in all the months except in January when it is a little bit less. Bloemfontein, Potchefstroom and Pretoria have AE < 1.0 for most part of the year except for some few months. For seasonal averages Cape Town, Durban and Skukuza have average AE > 1.0 in all seasons, while Potchefstroom and Pretoria have AE > 1.0 in summer and spring but Bloemfontein has mean AE < 1.0 for all seasons.

4.2. *Relationship between AOD and AE*

The spatial correlation of Terra MODIS of AOD_{550} and AE (Fig 3a) shows that there is a positive correlation over Durban and Skukuza > 0.2 but we observed a negative correlation over Cape Town, Pretoria, Skukuza and Bloemfontein. When AOD has

positive correlation with AE, it implies that the particles do not undergo corresponding hydroscopic growth in the region of the clouds (Balakrishnaiah et al., 2012) but this trend normally changes when the ratio of coarse and fine particles changes in the aerosol loading (Myhre et al., 2007). The temporal correlation (Fig 3b) for Bloemfontein, Durban, Potchefstroom and Pretoria shows that AOD and AE follow same trend except for the last months of the year but for Skukuza the opposite trend was found at the beginning of the year. Cape Town has opposite trend through most part of the year. The correlation coefficients between AOD and AE for the locations are -0.022, -0.658, 0.208, 0.007, 0.155 and 0.633 for Bloemfontein, Cape Town, Durban, Potchefstroom, Pretoria and Skukuza respectively.

4.3. Relationship between AOD and Water Vapor

There are five near-infrared bands in MODIS just around 940 nm water vapor band for remote sensing clear sky column water vapour amount. It is so designed to observe water vapor absorption by solar radiation reflected by bottom surface at near-infrared. Through the use of the ratios of water absorbing bands with atmospheric window bands, the variation of surface reflectance with wavelength for most land surfaces is being removed (King et al., 2003). Different types of aerosols exhibit various degrees of absorbing water (Alam et al., 2010; Li & Shao, 2009; Shi et al., 2008).

Coarse mode aerosol can be hygroscopic when mixed with sulphate or other soluble inorganic aerosol during advection. When mineral dusts are coated with nitrate, they become hydrophilic but when uncoated, they are hydrophobic (Li and Shao, 2009).

A factor that affects the hygroscopic nature of aerosols therefore includes both meteorological parameters and particular mixing of different types of particles (Aloysius et al., 2009). The spatial correlation of AOD_{550} with water vapor (WV) during clear sky (Fig 4a) is found to be positive over Skukuza and Durban but negative over rest of the other locations. The temporal correlation (Fig 4b) between AOD_{550} and WV show that both quantities only co-vary at the beginning of the year but later in the year they tend to have opposite trend over all the locations. The correlation coefficients between AOD_{550} and WV for the locations are, -0.463, 0.254, -0.464, 0.123, 0.461 and 0.024 for Bloemfontein, Cape Town, Durban, Potchefstroom, Pretoria and Skukuza respectively. Since Pretoria has the highest correlation and the series plot indicates that summer months has higher correspondence between AOD_{550} and WV, it may be due to the fact that aerosol influence the cloud formation over Pretoria as the location experiences higher rainfall during that season (Adesina et al., 2014).

Table 2: Inter-annual monthly/seasonal variations in AOD_{550} and $\alpha_{470-660}$ with standard deviations over six locations in South Africa for the period of 2008-2013

Month/ Seasons	BFN		CPT		DBN		PCS		PTR		SKZ	
	AOD±SD	α ±SD	AOD±SD	α ±SD	AOD±SD	α ±SD	AOD±SD	α ±SD	AOD±SD	α ±SD	AOD±SD	α ±SD
Jan	0.03±0.02	0.94±0.11	0.09±0.01	0.99±0.12	0.10±0.02	1.24±0.07	0.09±0.03	1.19±0.12	0.15±0.06	1.10±0.07	0.10±0.05	1.21±0.18
Feb	0.06±0.02	0.99±0.25	0.08±0.02	1.12±0.05	0.11±0.01	1.27±0.14	0.12±0.01	1.08±0.15	0.17±0.03	0.95±0.08	0.13±0.04	1.03±0.12
Mar	0.06±0.02	0.89±0.15	0.09±0.02	1.17±0.10	0.12±0.03	1.22±0.11	0.10±0.03	0.91±0.09	0.12±0.03	0.81±0.05	0.11±0.04	1.05±0.19
Apr	0.04±0.03	0.77±0.17	0.08±0.01	1.28±0.08	0.09±0.02	1.17±0.09	0.05±0.02	0.82±0.12	0.08±0.01	0.86±0.08	0.08±0.04	1.15±0.14
May	0.04±0.01	0.77±0.19	0.07±0.02	1.20±0.10	0.11±0.03	1.22±0.08	0.04±0.02	0.79±0.13	0.07±0.02	0.87±0.13	0.10±0.01	1.26±0.17
Jun	0.04±0.01	0.76±0.14	0.06±0.01	1.24±0.16	0.09±0.01	1.18±0.12	0.04±0.00	0.76±0.02	0.06±0.01	0.84±0.06	0.07±0.01	1.18±0.16
Jul	0.06±0.03	0.86±0.30	0.07±0.01	1.33±0.04	0.13±0.01	1.15±0.13	0.07±0.02	0.75±0.04	0.09±0.03	0.82±0.07	0.09±0.03	1.20±0.20
Aug	0.10±0.02	0.88±0.38	0.08±0.02	1.23±0.07	0.20±0.04	1.21±0.14	0.10±0.03	0.75±0.06	0.11±0.03	0.84±0.09	0.11±0.03	1.23±0.19
Sep	0.11±0.05	0.85±0.33	0.10±0.02	1.20±0.05	0.21±0.03	1.36±0.14	0.15±0.03	0.78±0.11	0.15±0.01	0.89±0.13	0.17±0.04	1.45±0.08
Oct	0.09±0.04	0.92±0.36	0.10±0.00	1.08±0.08	0.15±0.03	1.61±0.15	0.14±0.07	0.97±0.28	0.16±0.07	1.04±0.24	0.17±0.08	1.67±0.05
Nov	0.04±0.01	1.03±0.37	0.09±0.08	1.05±0.12	0.12±0.02	1.62±0.12	0.06±0.01	1.27±0.28	0.09±0.02	1.35±0.19	0.15±0.05	1.68±0.12
Dec	0.04±0.02	1.02±0.30	0.09±0.02	1.01±0.06	0.10±0.01	1.40±0.16	0.07±0.03	1.29±0.09	0.11±0.04	1.29±0.08	0.09±0.02	1.44±0.17
Autumn	0.05±0.02	0.81±0.18	0.08±0.02	1.22±0.11	0.11±0.03	1.21±0.10	0.06±0.04	0.84±0.12	0.09±0.03	0.85±0.10	0.10±0.04	1.15±0.19
Winter	0.07±0.03	0.84±0.30	0.08±0.02	1.27±0.11	0.14±0.05	1.18±0.13	0.07±0.03	0.75±0.05	0.08±0.03	0.83±0.08	0.09±0.03	1.21±0.19
Spring	0.08±0.05	0.93±0.36	0.10±0.01	1.11±0.11	0.16±0.05	1.53±0.18	0.12±0.06	1.01±0.31	0.14±0.05	1.09±0.27	0.16±0.06	1.60±0.14
Summer	0.04±0.02	0.98±0.23	0.09±0.01	1.04±0.10	0.10±0.01	1.30±0.15	0.09±0.03	1.19±0.15	0.14±0.05	1.11±0.16	0.11±0.04	1.23±0.23

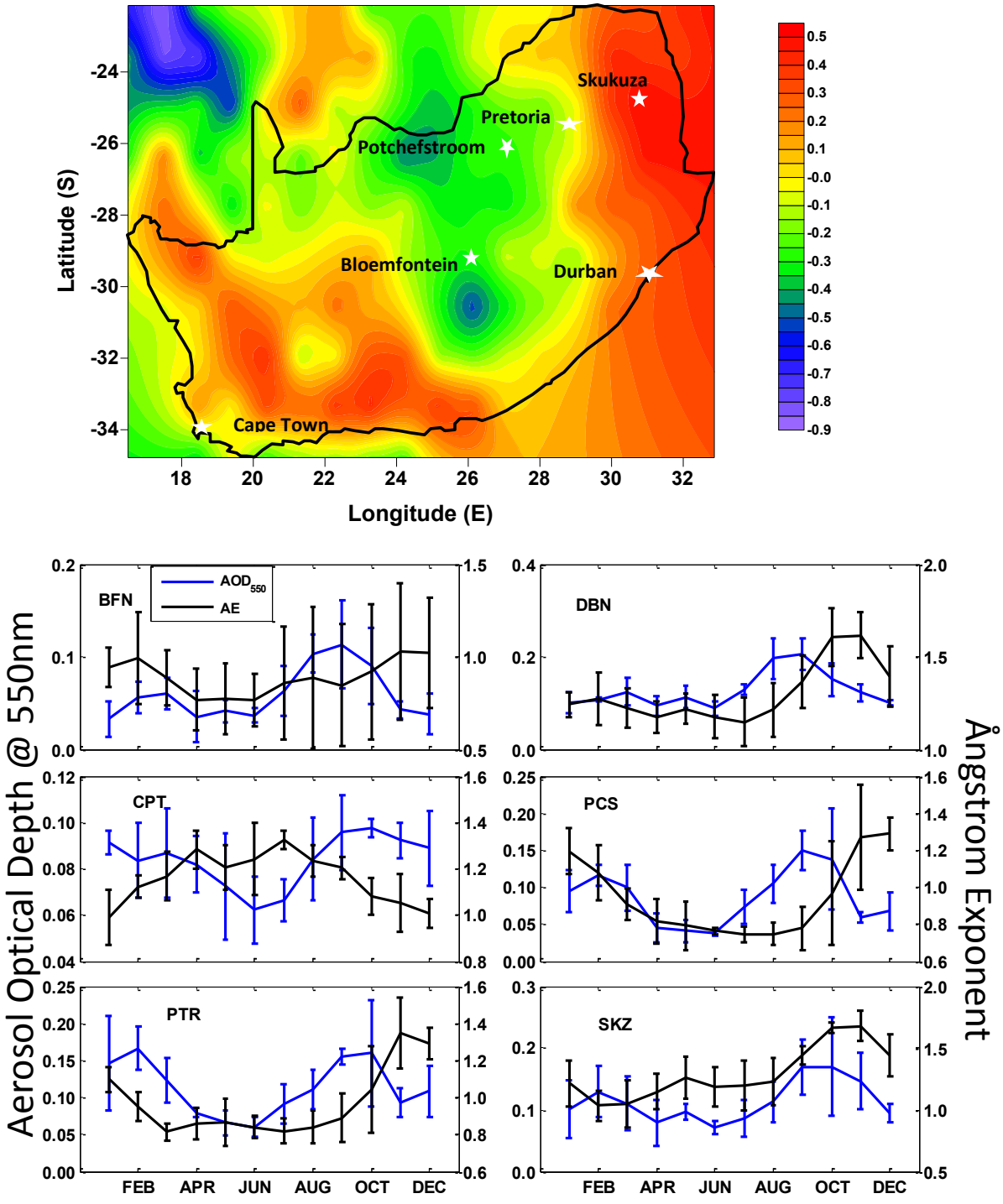

Fig 3 (a) Spatial correlation between AE and AOD (2008 -2012) over six locations in SA and (b) Combined monthly mean (2008 – 2012) plots with standard deviation between AOD and AE over six locations in SA.

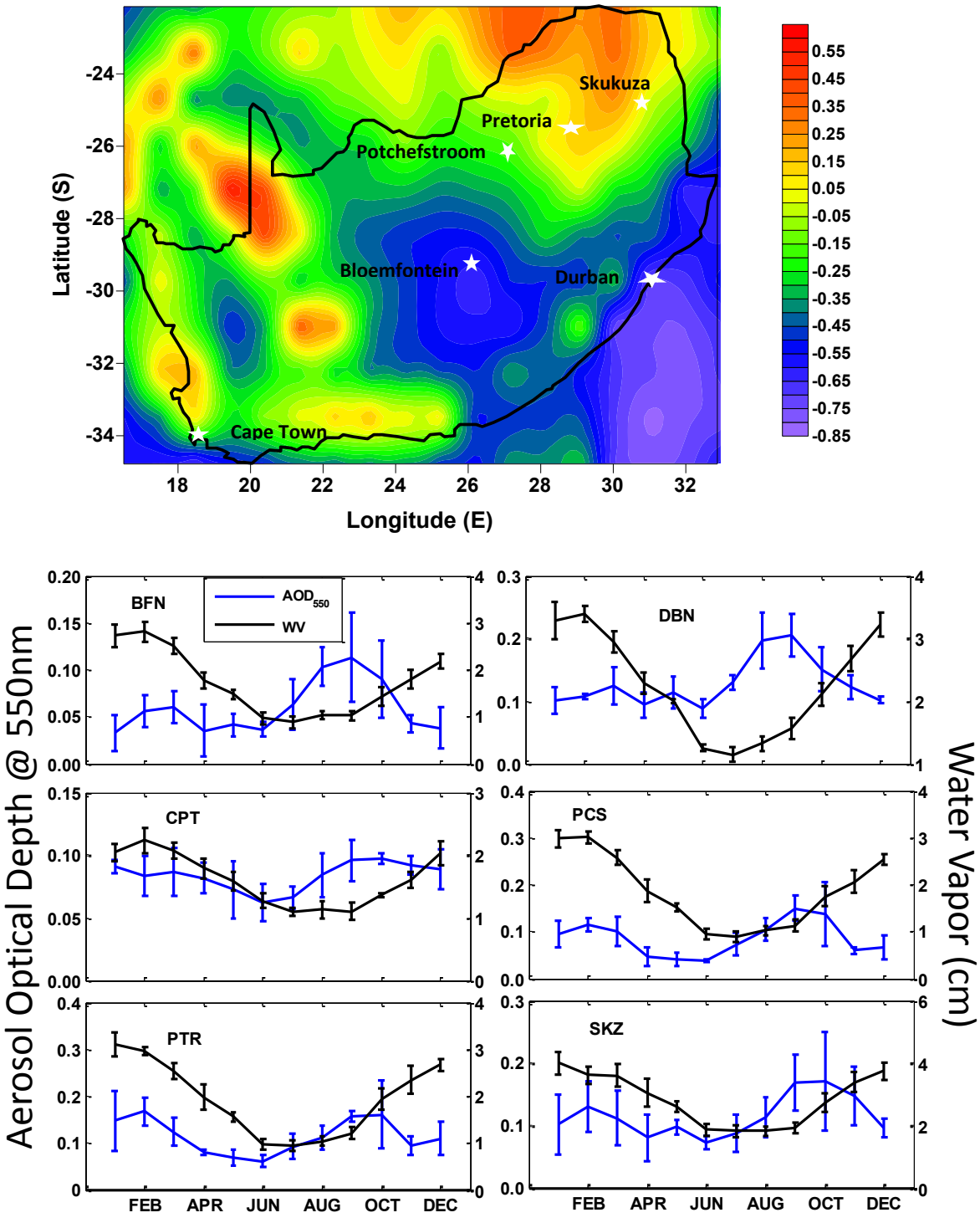

Fig 4 (a) Same as Fig. 3a but for AOD versus WV and (b) Same as Fig. 3b but for AOD and WV

It is possible that aerosol loading over Cape Town is coated with sulphate from sea salts thereby making it hygroscopic and hence enhancing the positive correlation. Aerosol may not be playing a significant role in cloud formation over Bloemfontein, Durban and Skukuza.

4.4 *Relationship between AOD and CF*

Fig 5a shows the spatial correlation between AOD_{550} and CF for the various selected locations. The data used for this analysis was that of MODIS combined data for both day and night for the years from 2008 to 2012. The spatial correlation is positive at Skukuza, Durban, Cape Town and Pretoria but negative for the other locations. Although Balakrishnaiah et al. (2012) found that AOD and CF have higher correlation at continental than coastal locations it seems that they may not always be the case as other factors like the AOD values might also contribute (Alam et al., 2014; Kang et al.; Ten Hoeve et al., 2011). Regions close to the coastal areas have equally been found to exhibit positive correlation between AOD and CF (Nakajima et al., 2001). Other factors that affect AOD and CF correlation includes high biomass activities, industrial or vehicular emission like the case of Pretoria and Skukuza (Alam et al., 2010; Balakrishnaiah et al., 2012; Kumar et al., 2014) Though Potchefstroom is in the high latitude, the aerosol loading is influenced more by the Kalahari desert dust.

The time series plots (Fig 5b) showed a similar pattern of CF having its minimum value in either July or August beginning with high values in January and decreasing to a minimum and subsequently rising to a peak in December apart from Cape Town where double maxima is seeing occurring in May and September and starts with low values in January ending with low values in December and also a low value in July in between the two maxima. The respective correlation coefficients for Bloemfontein, Cape Town, Durban, Potchefstroom, Durban and Skukuza are -0.606, -0.384, -0.148, -0.036, 0.357 and -0.504.

4.5. *Relationship between AOD and COD*

Cloud optical depth (COD) is a measure of the light passing through the cloud after absorption and scattering from the cloud droplets. It is an important factor affecting earth radiation budget both at atmosphere and surface. Ordinarily cloud optical depth ought to show increase with AOD while the cloud effective radius show a decrease according to Twomey effect (Twomey, 1977). Marshak et al. (2006) suggested that caution must be taken in using these two MODIS products. The spatial correlation of AOD with COD in Fig 6a showed a positive correlation over Durban, Pretoria and Skukuza, while negative at Cape Town, Potchefstroom and Bloemfontein. It is noticed that COD increases with increase of moisture in the atmosphere and correlates negatively with increasing AOD (Alam et al., 2010; Hoeve et al., 2011).

In the time series plots (Fig 6b) for the spatial averages, Bloemfontein and Pretoria experience minimum COD values in July, Potchefstroom and Durban in May and Skukuza in June while Cape Town was generally low throughout the year but experiences a maximum in June. Durban and Skukuza had COD increasing through July. The correlation coefficients between COD and AOD for the locations are 0.606, -0.802, 0.274, -0.169, -0.005 and 0.684 for Bloemfontein, Cape Town, Durban, Potchefstroom, Pretoria, and Skukuza respectively.

4.6. *Relationship between AOD and CTP*

The spatial correlation between AOD and CTP in Fig 7a shows that Durban, Potchefstroom and Bloemfontein have positive correlations > 0.1 while the other locations have observed negative correlation. CTP tends to have higher negative correlation at higher latitude as reported by earlier studies (Kaufman et al., 2005; Myhre et al., 2007; Sekiguchi et al., 2003) as in the case of Pretoria and Skukuza. In the time series plot for the spatial averages (Fig 7b), we can see same pattern of CTP increase to a maximum value from January to July in all stations except Cape Town where it first decreased to a minimum value in May then increased to July before it started to decreasing to the end of the year. The correlation coefficients between AOD and CTP for the locations are 0.260, 0.182, 0.203, -0.225, -0.452 and -0.327 for Bloemfontein, Cape Town, Durban, Potchefstroom, Pretoria and Skukuza respectively.

4.7. *Relationship between AOD and CTT*

Figure 8 shows the AOD variation with CTT. The spatial correlation of AOD with CTT in Fig 8a

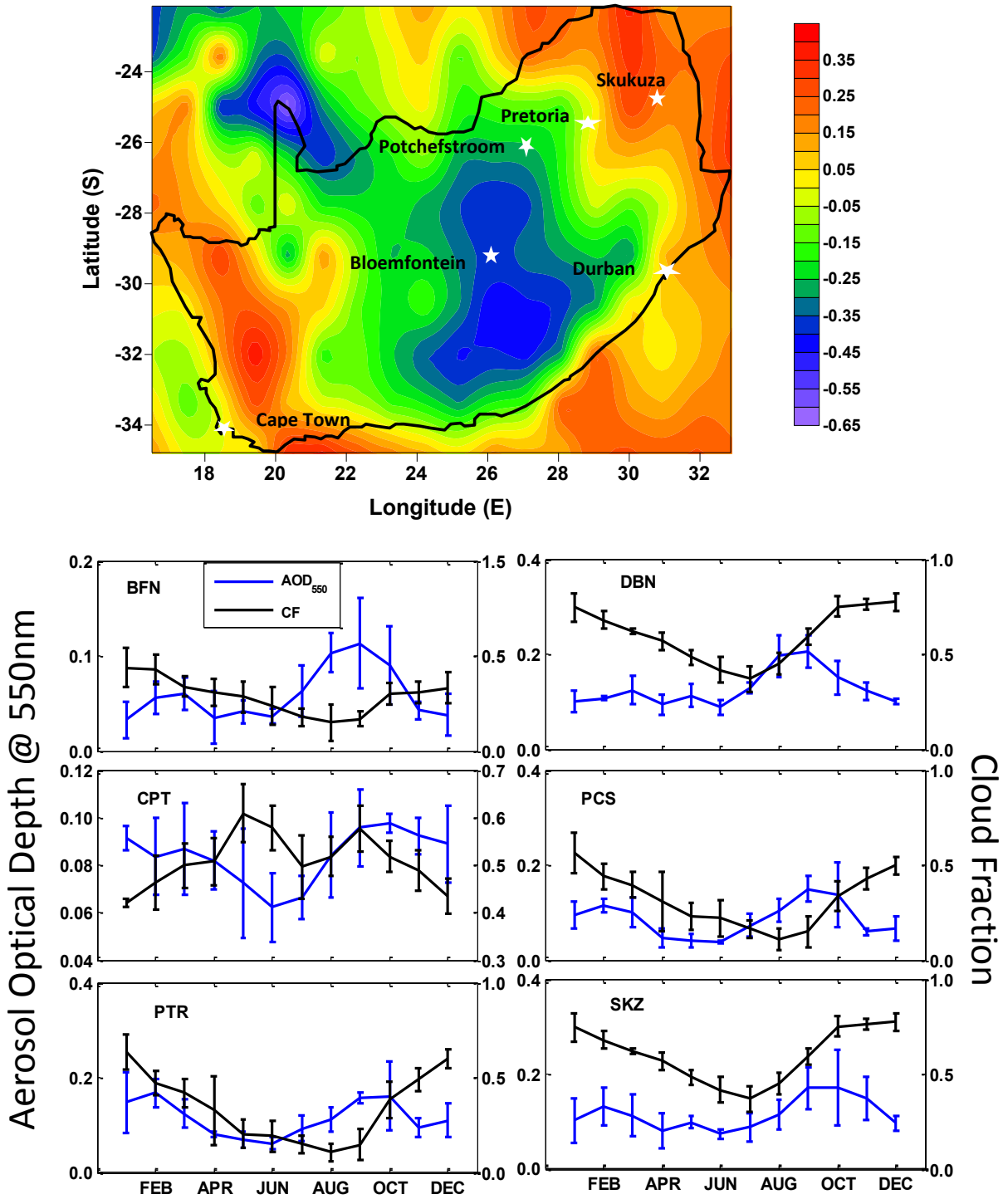

Fig 5 (a) Same as Fig. 3a but for AOD versus CF (b) Same as Fig. 3b but for AOD and CF

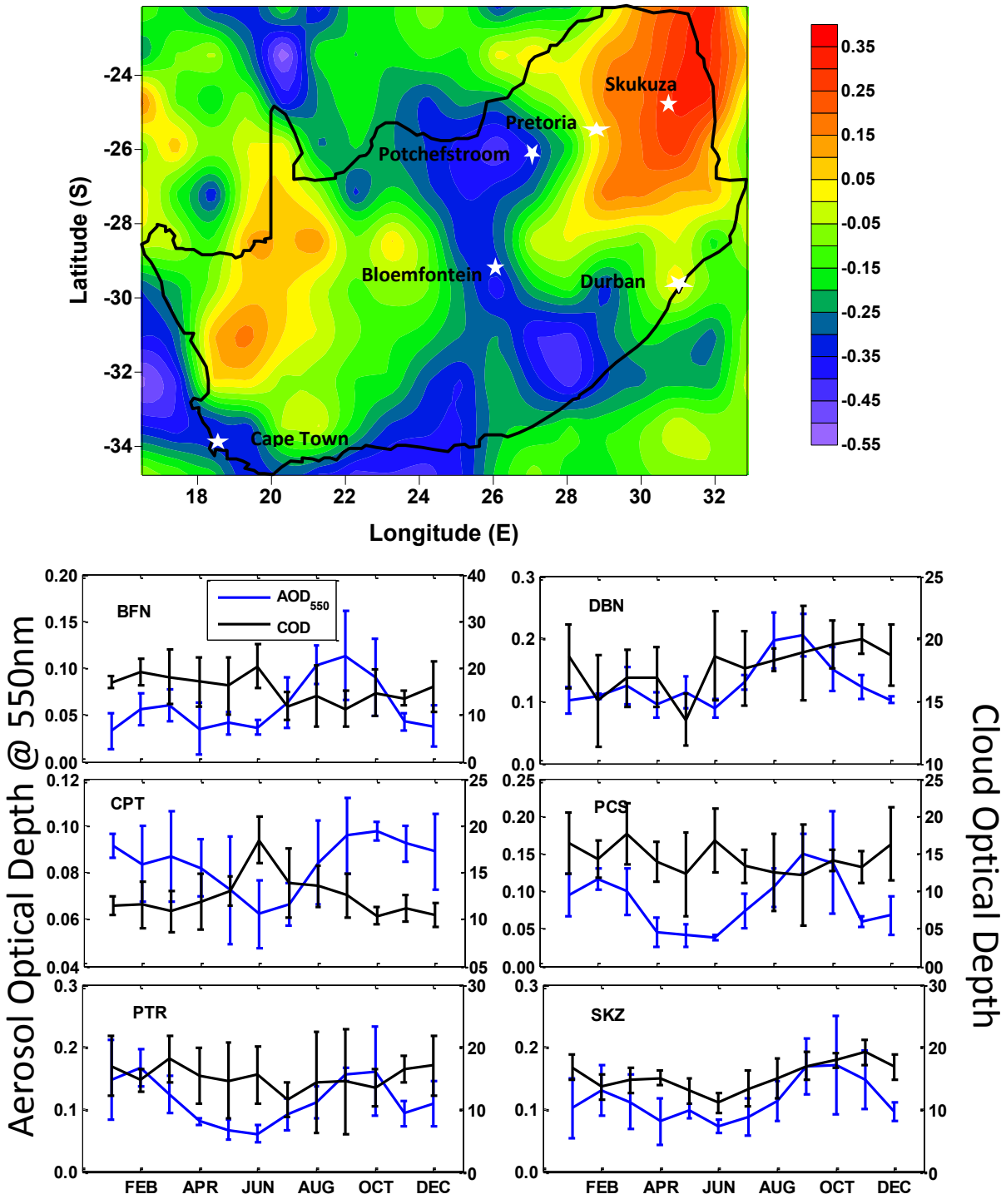

Fig 6 (a) Same as Fig. 3a but for AOD versus COD and (b) Same as Fig. 3b but for AOD and COD

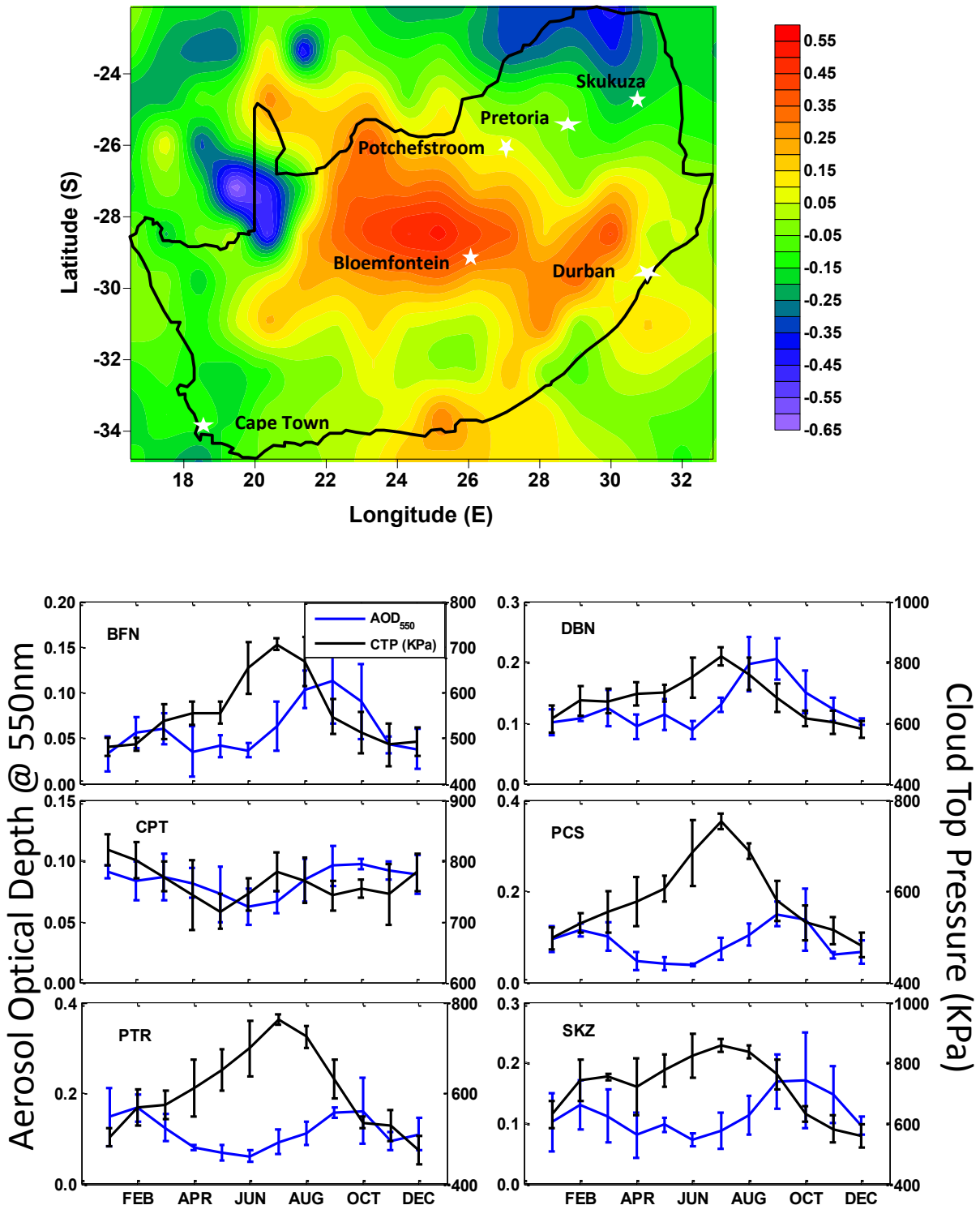

Fig 7 (a) Same as Fig. 3a but for AOD versus CTP (b) Same as Fig. 3b but for AOD and CTP

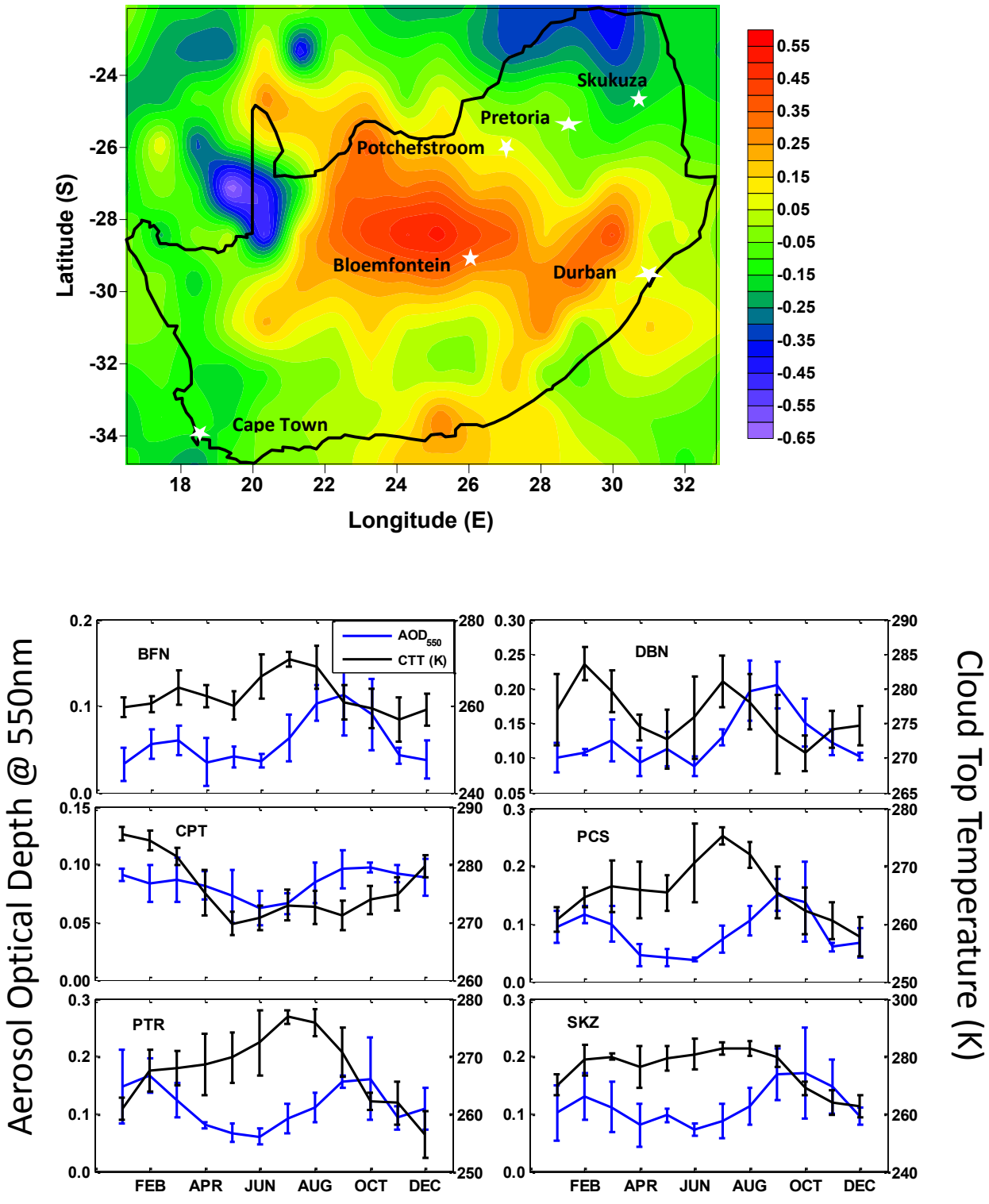

Fig 8 (a) Same as Fig. 3a but for AOD versus CTT (b) Same as Fig. 3b but for AOD and CTT

showed positive correlation with CTT at Pretoria, Durban and particularly high value at Skukuza > 0.25 but it is correlated negatively over Bloemfontein, Cape Town and Potchefstroom. Sekiguchi et al. (2003) showed that CTT really does not change but stated that aerosol affects only COD and CF. Also, CTT and humidity profile can be modified if there is such an increase in anthropogenic aerosol such that it sets up a secondary circulation (Santer et al., 1996). Time series plots (Fig 8b) for monthly averages of AOD and CTT showed a similar pattern as that of CTP in all the locations this may be due to large scale meteorological conditions(Alam et al., 2010). The correlation coefficients between AOD and CTT are found to be 0.244, 0.370, -0.128, -0.095, -0.310 and -0.252 for Bloemfontein, Cape Town, Durban, Potchefstroom, Pretoria, and Skukuza respectively.

5.0. CONCLUSIONS

The study has been conducted using the MODIS satellite data for addressing the impact of aerosol optical depth on cloud parameters over six locations in South Africa. To the best of our knowledge, it is the first attempt over Southern Africa region. Our report therefore stands to fill a scientific gap in our knowledge of aerosol-cloud interaction studies. Though the work did not include details of the aerosol types and their source regions, we nevertheless were able to make the following findings:

1. The spatial AOD_{550} over the selected cities were generally not too high. Apart from Durban where average value approaches 0.2, other locations were either less than 0.1 or very close to it. The temporal variation shows that the mean AOD_{550} ranges between 0.06±0.04 at Bloemfontein to 0.13±0.05 at Durban. While all locations have the minimum AOD_{550} during the winter (June), most have their maximum during the spring except Pretoria which has its maximum in summer (February).

2. The Angstrom exponent indicated that all the locations except Bloemfontein has predominance of fine particles for most part of the year. Only two of the locations have their AOD correlating positively with Angstrom exponent in terms of spatial correlation.

3. The spatial correlation of water vapor with AOD was similar to that of the Angstrom exponent showing that aerosol do not undergo hygroscopic growth in these locations.

4. The cloud fraction correlates negatively for most locations under study while the cloud optical depth correlates positively with aerosol optical depth for three locations but the correlation does not particularly depend on aerosol optical depth of the location.

5. Cloud top temperature and cloud top pressure have similar trend suggesting the influence of large scale meteorological conditions.

REFERENCES

Ackerman, A. S., Toon, O., Stevens, D., Heymsfield, A., Ramanathan, V., & Welton, E. (2000). Reduction of tropical cloudiness by soot. *Science, 288*(5468), 1042-1047.

Adesina, A. J., Kumar, K. R., Sivakumar, V., & Griffith, D. (2014). Direct radiative forcing of urban aerosols over Pretoria (25.75° S, 28.28° E) using AERONET Sunphotometer data: First scientific results and environmental impact. *Journal of Environmental Sciences*.

Alam, K., Iqbal, M. J., Blaschke, T., Qureshi, S., & Khan, G. (2010). Monitoring spatio-temporal variations in aerosols and aerosol–cloud interactions over Pakistan using MODIS data. *Advances in Space Research, 46*(9), 1162-1176.

Alam, K., Khan, R., Blaschke, T., & Mukhtiar, A. (2014). Variability of aerosol optical depth and their impact on cloud properties in Pakistan. *Journal of Atmospheric and Solar-Terrestrial Physics, 107*, 104-112.

Albrecht, B. A. (1989). Aerosols, cloud microphysics, and fractional cloudiness. *Science, 245*(4923), 1227-1230.

Aloysius, M., Mohan, M., Suresh Babu, S., Parameswaran, K., & Krishna Moorthy, K. (2009). *Validation of MODIS derived aerosol optical depth and an investigation on aerosol transport over the South East Arabian Sea during ARMEX-II.* Paper presented at the Annales Geophysicae.

Andreae, M. O., Jones, C. D., & Cox, P. M. (2005). Strong present-day aerosol cooling implies a hot future. *Nature, 435*(7046), 1187-1190.

Balakrishnaiah, G., Suresh Kumar Reddy, B., Rama Gopal, K., Reddy, R., Reddy, L., Swamulu, C., . . . Suresh Babu, S. (2012). Spatio-temporal variations in aerosol optical and cloud parameters over Southern India retrieved from MODIS satellite data. *Atmospheric Environment, 47*, 435-445.

Charlson, R. J., Ackerman, A. S., BENDER, F. A. M., Anderson, T. L., & Liu, Z. (2007). On the climate forcing consequences of the albedo continuum between cloudy and clear air. *Tellus B, 59*(4), 715-727.

Eck, T., Holben, B., Ward, D., Mukelabai, M., Dubovik, O., Smirnov, A., . . . Queface, A. (2003). Variability of biomass burning aerosol optical characteristics in southern Africa during the SAFARI 2000 dry season campaign and a comparison of single scattering albedo estimates from radiometric measurements. *Journal of Geophysical Research: Atmospheres (1984–2012), 108*(D13).

Feingold, G., Eberhard, W. L., Veron, D. E., & Previdi, M. (2003). First measurements of the Twomey indirect effect using ground-based remote sensors. *Geophysical Research Letters, 30*(6).

Freiman, M., & Piketh, S. (2003). Air transport into and out of the industrial Highveld region of South Africa. *Journal of Applied Meteorology, 42*(7), 994-1002.

Guo, X., Fu, D., Guo, X., & Zhang, C. (2014). A case study of aerosol impacts on summer convective clouds and precipitation over northern China. *Atmospheric Research, 142*, 142-157.

Haywood, J., & Boucher, O. (2000). Estimates of the direct and indirect radiative forcing due to tropospheric aerosols: A review. *Reviews of Geophysics, 38*(4), 513-543.

Ichoku, C., Kaufman, Y. J., Remer, L. A., & Levy, R. (2004). Global aerosol remote sensing from MODIS. *Advances in Space Research, 34*(4), 820-827.

Ichoku, C., Remer, L. A., Kaufman, Y. J., Levy, R., Chu, D. A., Tanré, D., & Holben, B. N. (2003). MODIS observation of aerosols and estimation of aerosol radiative forcing over southern Africa during SAFARI 2000. *Journal of Geophysical Research: Atmospheres (1984–2012), 108*(D13).

Kang, N., Kanike Raghavendra Kumar, Y. Y., Diao, Y., & Yu, X. Correlation Analysis between AOD and Cloud Parameters to Study Their Relationship over China Using MODIS Data (2003–2013): Impact on Cloud Formation and Climate Change.

Kaufman, Y. J., & Fraser, R. S. (1997). The effect of smoke particles on clouds and climate forcing. *Science, 277*(5332), 1636-1639.

Kaufman, Y. J., Koren, I., Remer, L. A., Rosenfeld, D., & Rudich, Y. (2005). The effect of smoke, dust, and pollution aerosol on shallow cloud development over the Atlantic Ocean. *Proceedings of the National Academy of Sciences of the United States of America, 102*(32), 11207-11212.

Khain, A., Rosenfeld, D., & Pokrovsky, A. (2005). Aerosol impact on the dynamics and microphysics of deep convective clouds. *Quarterly Journal of the Royal Meteorological Society, 131*(611), 2639-2663.

Kim, B. G., Schwartz, S. E., Miller, M. A., & Min, Q. (2003). Effective radius of cloud droplets by ground-based remote sensing: Relationship to aerosol. *Journal of Geophysical Research: Atmospheres (1984–2012), 108*(D23).

Koren, I., Kaufman, Y. J., Remer, L. A., & Martins, J. V. (2004). Measurement of the effect of Amazon smoke on inhibition of cloud formation. *Science, 303*(5662), 1342-1345.

Koren, I., Remer, L. A., Kaufman, Y. J., Rudich, Y., & Martins, J. V. (2007). On the twilight zone between clouds and aerosols. *Geophysical Research Letters, 34*(8).

Kumar, A. (2013). Variability of aerosol optical depth and cloud parameters over North Eastern regions of India retrieved from MODIS satellite data. *Journal of Atmospheric and Solar-Terrestrial Physics, 100*, 34-49.

Kumar, K. R., Sivakumar, V., Reddy, R., Gopal, K. R., & Adesina, A. J. (2013). Inferring wavelength dependence of AOD and Ångström exponent over a sub-tropical station in South Africa using AERONET data: Influence of meteorology, long-range transport and curvature effect. *Science of The Total Environment, 461*, 397-408.

Kumar, K. R., Sivakumar, V., Yin, Y., Reddy, R., Kang, N., Diao, Y., . . . Yu, X. (2014). Long-term (2003–2013) climatological trends and variations in aerosol optical parameters retrieved from MODIS over three stations in South Africa. *Atmospheric Environment, 95*, 400-408.

Levy, R. C., Remer, L. A., Kleidman, R. G., Mattoo, S., Ichoku, C., Kahn, R., & Eck, T. (2010). Global evaluation of the Collection 5 MODIS dark-target aerosol products over land. *Atmospheric Chemistry and Physics, 10*(21), 10399-10420.

Li, W., & Shao, L. (2009). Observation of nitrate coatings on atmospheric mineral dust particles. *Atmospheric Chemistry and Physics, 9*(6), 1863-1871.

Marshak, A., Platnick, S., Várnai, T., Wen, G., & Cahalan, R. F. (2006). Impact of three-dimensional radiative effects on satellite retrievals of cloud droplet sizes. *Journal of Geophysical Research: Atmospheres (1984–2012), 111*(D9).

Myhre, G., Stordal, F., Johnsrud, M., Kaufman, Y., Rosenfeld, D., Storelvmo, T., . . . Isaksen, I. (2007). Aerosol-cloud interaction inferred from MODIS satellite data and global aerosol models. *Atmospheric Chemistry and Physics, 7*(12), 3081-3101.

Nakajima, T., Higurashi, A., Kawamoto, K., & Penner, J. E. (2001). A possible correlation between satellite-derived cloud and aerosol microphysical parameters. *Geophysical Research Letters, 28*(7), 1171-1174.

Quaas, J., Boucher, O., Bellouin, N., & Kinne, S. (2008). Satellite-based estimate of the direct and indirect aerosol climate forcing. *Journal of Geophysical Research: Atmospheres (1984–2012), 113*(D5).

Quaas, J., Stevens, B., Stier, P., & Lohmann, U. (2010). Interpreting the cloud cover–aerosol optical depth relationship found in satellite data using a general circulation model. *Atmospheric Chemistry and Physics, 10*(13), 6129-6135.

Queface, A. J., Piketh, S. J., Eck, T. F., Tsay, S.-C., & Mavume, A. F. (2011). Climatology of aerosol optical properties in Southern Africa. *Atmospheric Environment, 45*(17), 2910-2921.

Remer, L. A., Kaufman, Y., Tanré, D., Mattoo, S., Chu, D., Martins, J. V., . . . Kleidman, R. (2005). The MODIS aerosol algorithm, products, and validation. *Journal of the atmospheric sciences, 62*(4), 947-973.

Rosenfeld, D. (2000). Suppression of rain and snow by urban and industrial air pollution. *Science, 287*(5459), 1793-1796.

Rosenfeld, D. (2007). Aerosol-cloud interactions control of earth radiation and latent heat release budgets *Solar Variability and Planetary Climates* (pp. 149-157): Springer.

Santer, B., Taylor, K., Wigleyi, T., Johns, T., & Jones, P. (1996). structure of the atmosphere. *Nature, 382*, 4.

Satheesh, S., & Krishna Moorthy, K. (2005). Radiative effects of natural aerosols: A review. *Atmospheric Environment, 39*(11), 2089-2110.

Sekiguchi, M., Nakajima, T., Suzuki, K., Kawamoto, K., Higurashi, A., Rosenfeld, D., . . . Mukai, S. (2003). A study of the direct and indirect effects of aerosols using global satellite data sets of aerosol and cloud parameters. *Journal of Geophysical Research: Atmospheres (1984–2012), 108*(D22).

Shi, Z., Zhang, D., Hayashi, M., Ogata, H., Ji, H., & Fujiie, W. (2008). Influences of sulfate and nitrate on the hygroscopic behaviour of coarse dust particles. *Atmospheric Environment, 42*(4), 822-827.

Sivakumar, V., Tesfaye, M., Alemu, W., Sharma, A., Bollig, C., & Mengistu, G. (2010). Aerosol measurements over South Africa using satellite, Sun-photometer and LIDAR. *Advances in Geosciences, Volume 16: Atmospheric Science (AS), 16*, 253.

Stocker, T. F., Qin, D., Plattner, G.-K., Tignor, M., Allen, S. K., Boschung, J., . . . Midgley, P. M. (2013). Climate change 2013: The physical science basis. *Intergovernmental Panel on Climate Change, Working Group I Contribution to the IPCC Fifth Assessment Report (AR5)(Cambridge Univ Press, New York)*.

Tang, J., Wang, P., Mickley, L. J., Xia, X., Liao, H., Yue, X., . . . Xia, J. (2014). Positive relationship between liquid cloud droplet effective radius and aerosol optical depth over Eastern China from satellite data. *Atmospheric Environment, 84*, 244-253.

Tanré, D., Kaufman, Y., Herman, M., & Mattoo, S. (1997). Remote sensing of aerosol properties over oceans using the MODIS/EOS spectral radiances. *Journal of Geophysical Research: Atmospheres (1984–2012), 102*(D14), 16971-16988.

Ten Hoeve, J., Remer, L., & Jacobson, M. (2011). Microphysical and radiative effects of aerosols on warm clouds during the Amazon biomass burning season as observed by MODIS: impacts of water vapor and land cover. *Atmospheric Chemistry and Physics, 11*(7), 3021-3036.

Tesfaye, M., Sivakumar, V., Botai, J., & Mengistu Tsidu, G. (2011). Aerosol climatology over South Africa based on 10 years of Multiangle Imaging Spectroradiometer (MISR) data. *Journal of Geophysical Research: Atmospheres (1984–2012), 116*(D20).

Twomey, S. (1977). The influence of pollution on the shortwave albedo of clouds. *Journal of the atmospheric sciences, 34*(7), 1149-1152.

Williams, E., Rosenfeld, D., Madden, N., Gerlach, J., Gears, N., Atkinson, L., . . . Biazon, B. (2002). Contrasting convective regimes over the Amazon: Implications for cloud electrification. *Journal of Geophysical Research: Atmospheres (1984–2012), 107*(D20), LBA 50-51-LBA 50-19.

Wright, M. E., Atkinson, D. B., Ziemba, L., Griffin, R., Hiranuma, N., Brooks, S., . . . Rappenglück, B. (2010). Extensive aerosol optical properties and aerosol mass related measurements during TRAMP/TexAQS 2006–Implications for PM compliance and planning. *Atmospheric Environment, 44*(33), 4035-4044.

CHAPTER SEVEN

7. SUMMARY AND FUTURE WORK

7.1 Summary

Most of the studies relating to aerosols in Southern Africa were conducted in three major countries; South Africa, Mozambique and Zambia. Reports from Southern African Regional Initiative (SAFARI) 2000 showed that Zambia is dominated by biomass burning aerosol while South Africa and Mozambique is dominated by aerosol mixture of aeolian coarse mode, fossil fuel burning and other industrial aerosol types while other related work showed that the biomass burning impacting South Africa mostly originates from Mozambique. South Africa was divided into three parts according to aerosol loading and that sulphate is the most important contributor to this loading over South Africa for all other months outside the biomass season. These results are complemented by this research work by focusing on aerosol properties and climate impacts on specific of places of interest.

The places of interest covered six out of the nine provinces in South Africa. Pretoria, the administrative capital of South Africa was one of major focus of the study. Through the study it was discovered that the aerosol loading is characterized by a double maxima with the highest occurring in summer (February). The single scattering albedo being greater than 0.9 at lower wavelength shows the season was filled with urban-industrial aerosols. The radiative forcing over Pretoria was positive throughout the year indicating aerosol having a warming effect with the highest average heating rate of 0.81 K/day in September (spring season) falling into the peak

of biomass burning period. The radiative forcing was not proportional to AOD unlike some other places.

The study of Skukuza and Richards Bay from a long term satellite data from MODIS and MISR showed that high aerosol loading occurs from August to November and low loading from April to July. The high loading corresponds to the biomass season when biomass aerosol is being advected from neighboring countries. The MODIS sensor underestimates the MISR in both of these locations but there seems to be a general decreasing trend in aerosol loading over these locations with the UVAI for both locations showing a general increase; this shows the presence of significant soot aerosols. Out of the six locations selected for aerosol-cloud interaction study Bloemfontein has the lowest AOD value followed by Cape Town while Durban has the highest.

In overall, the major aims of this work were realized. Through this study, we were able to characterize aerosols by their optical, microphysical and radiative properties. We run some web-based models to determine the radiative forcing of aerosols and determine the long transport regions of aerosols. Through multiplication of coordinated platforms, we were able both to validate satellite instruments and find trend in aerosol optical depth. Satellite instrument was used to study aerosol-cloud interaction with clear understanding of how they interact.

7.2 Future Work

In summary, aerosol research is still at the infant stage over South Africa as there are only very few reports on use of measuring instruments like sunphotometer (AERONET), Microtops II

sunphotometer, Aetholometer, Multiwavelength solar radiometer, and very few reports based on the use of LIDAR. In future, we shall embark upon a multi-platform approach to the study of aerosol which will help in effective monitoring of our environment and complement the model/simulation based studies.